Theoretical Calculations of Magnetic Hysteresis and Critical Sizes For Transitions Between Single-domain and Multi-domain Properties in Titanomagnetites

by

Andrew James Newell

A dissertation submitted in partial fulfillment of
the requirements for the degree of

Doctor of Philosophy

University of Washington

1997

Approved by Ronald T. Merrill

(Chairperson of Supervisory Committee)

Program Authorized
to Offer Degree Geophysics Program

Date October 28, 1997

In presenting this dissertation in partial fulfillment of the requirements for the Doctoral degree at the University of Washington, I agree that the Library shall make its copies freely available for inspection. I further agree that extensive copying of this dissertation is allowable only for scholarly purposes, consistent with "fair use" as prescribed in the U.S. Copyright Law. Requests for copying or reproduction of this dissertation may be referred to University Microfilms, 1490 Eisenhower Place, P.O. Box 975, Ann Arbor, MI 48106 to whom the author has granted "the right to reproduce and sell (a) copies of the manuscript in microform and/or (b) printed copies of the manuscript made from microform."

Signature Andrew Newell

Date October 28, 1997

University of Washington

Abstract

Theoretical Calculations of Magnetic Hysteresis and Critical Sizes For Transitions Between Single-domain and Multi-domain Properties in Titanomagnetites

by Andrew James Newell

Chairperson of Supervisory Committee: *Professor Ronald T. Merrill*
Geophysics Program

In this dissertation, I develop some theoretical tools to interpret measurements of magnetization in rocks, sediments and soils. I show that the magnetization curve for an ensemble of superparamagnetic particles depends only on odd moments of the volume distribution $(\langle V\rangle, \langle V^3\rangle, ...)$. As long as the ensemble is isotropic, the magnetic anisotropies of individual particles do not affect the curve. I derive analytical expressions for acquisition and loss of isothermal remanent magnetization in single-domain (SD) particles with uniaxial anisotropy. These curves depend only on the volume-average anisotropy. Plots of acquisition against loss of remanence can be used to distinguish uniaxial anisotropy from cubic anisotropy. I show that existing multi-domain (MD) hysteresis models, including the theory of Néel [1955] for thermoremanent magnetization, are internally inconsistent. I develop a simple self-consistent two-domain model and show that the slope of the hysteresis curve is always $1/N$, where N is the demagnetizing factor for a two-domain particle.

Using micromagnetic theory, I derive analytical expressions for the critical sizes L_{sw}, the upper limit for SD hysteresis, and L_{n}, the upper limit for stability of the SD

remanent state. L_{sw} depends weakly on elongation and not at all on magnetocrystalline anisotropy, but

$$L_n = L_{sw}\left(\frac{N_b}{N_a}\right)^{1/2}\left(1-\frac{2\kappa}{\mu_0 M_s^2 N_a}\right)^{-1/2}$$

where $N_a > N_b$ are demagnetizing factors and κ depends on the combined magnetocrystalline and magnetoelastic anisotropy. Mainly because of the the difference in Ms, L_n is orders of magnitude larger for a particle of $Fe_{2.4}Ti_{0.6}O_4$ than for a particle of magnetite with the same aspect ratio.

I develop a technique for eliminating unstable solutions of three-dimensional numerical micromagnetic models. I show that nucleation theory can be extended to non-ellipsoidal particles. The nucleation field H_n for a cuboid can be precisely located by a change in slope dM/dH and the appearance of curl in the magnetization. For a cube with $K_1 = 0$, the plot of H_n against $1/L^2$ has the same slope as for a sphere, but the intercept is lower, reflecting a smaller average demagnetizing field. H_n is not affected by the demagnetizing field in the corners of the particle.

TABLE OF CONTENTS

List of Figures iv

List of Tables viii

Acronyms ix

Symbols xi

Chapter 1: Introduction 1

1.1 Hysteresis 3

1.2 Interpreting Remanence in Rocks 5

1.3 Proxies for Particle Size 16

1.4 Summary 21

Chapter 2: Hysteresis Theories 23

2.1 Thermodynamic Fundamentals 23

2.2 Superparamagnetic Grains 27

2.3 Single-Domain Theory 29

2.4 MD Theory 48

2.5 Summary 67

Chapter 3: Single-Domain Critical Sizes and Nucleation 70

3.1 Critical Sizes in Rock Magnetism 72

3.2 Rigorous Micromagnetic Calculations 75

3.3 A Reassessment of Critical Sizes in Rock Magnetism 81
3.4 Summary 89

Chapter 4: The Numerical Model **90**
4.1 Solving the Micromagnetic Equations 91
4.2 Numerical Implementation 92
4.3 Strategic Considerations 93
4.4 Comparison with Fukuma and Dunlop 100
4.5 Controversy Over the Number of Domains 103
4.6 Summary 106

Chapter 5: Nucleation in Magnetically Isotropic Cuboids **107**
5.1 The SD (Flower) State in the Cube 111
5.2 Nucleation in the Cube 114
5.3 SD States and Nucleation in a Triaxial Cuboid 121
5.4 Nucleation and Curling 127
5.5 Transitions in Remanent States 129
5.6 Nucleation and Bifurcations 133
5.7 Summary 138

Chapter 6: Hysteresis Properties Above the Critical Sizes **141**
6.1 The Magnetically Isotropic Sphere and Cube 142
6.2 Hysteresis Curves for the Triaxial Particle 145
6.3 Critical Sizes 148
6.4 Size Dependence of Hysteresis Properties 151
6.5 Summary 155

Chapter 7: Conclusions **156**

7.1 SP and SD Hysteresis Theories 156

7.2 MD Hysteresis Theories 158

7.3 Micromagnetics 159

7.4 Possible Implications for Paleomagnetism 163

Appendix A: SD Calculations Using Lagrange Multipliers **184**

A.1 Calculating Stationary Points 184

A.2 Using Perturbation Theory to Calculate Susceptibility 186

LIST OF FIGURES

1.1 An example of a magnetic hysteresis loop (after Tauxe *et al.* [1996], Figure 4). 4

1.2 An illustration of thermal blocking for a SD particle. 7

1.3 Classification of hysteresis parameters, after Day *et al.* [1977]. 17

2.1 Energy surface for a SD particle in zero field. 31

2.2 Energy surface for a SD particle exposed to a field along the easy axis. 32

2.3 Examples of hysteresis curves for a triaxial SD particle. 33

2.4 Plots of IRM acquisition against (a) DC demagnetization and (b) AF demagnetization. 39

2.5 The geometry of the Stoner-Wohlfarth model. 40

2.6 Dependence of the reduced coercivity h_c and the switching field h_c on the angle θ between the field and the easy axis. 41

2.7 Acquisition and loss of IRM, as a function of field, for non-interacting SD particles with uniaxial anisotropy. 43

2.8 Relationship between acquisition and destructive fields for IRM in non-interacting, uniaxial SD particles. 44

2.9 The model of Landau and Lifshitz. 50

2.10 The two-domain model. 51

2.11 A MD hysteresis model with a sinusoidal wall energy. 53

2.12 Néel's MD hysteresis model. 54

2.13 The remanence curves for Néel's MD hysteresis model. 55

2.14 An example of a wall pinning model proposed by Néel. 59
2.15 Hysteresis predictions for the same wall energy $E_w(M)$ based on (a) the internal field approximation and (b) the correct equations. 62
2.16 The effect of spacing of maxima on hysteresis properties in the two-domain model. 64

3.1 A curling state and a closure domain state. 73
3.2 Critical sizes as a function of elongation for (a) magnetite (b) TM60. 87

4.1 A hysteresis loop for a particle with $X = 1.5Y = 1.4Z$ and volume $(0.084\mu\text{m})^3$ in a field with direction $(8, 1, 4)$. 96
4.2 An example of the procedure for identifying the true instability field. 99
4.3 The remanent state for the two-dimensional model of a one micron cube in a field parallel to $(1, 7, 4)$. 102

5.1 The curling state: magnetization vectors for a particle with $L = 12.4L_{\text{ex}}$ (0.084μm in magnetite). 108
5.2 The flower state: magnetization vectors for a cube with $L = 9.03L_{\text{ex}}$ (0.061μm in magnetite). 109
5.3 The demagnetizing field for uniform magnetization. 112
5.4 The approach to saturation for a particle with $L = 9.03L_{\text{ex}}$ (0.061μm in magnetite). 115
5.5 A plot of nucleation field as a function of particle size for an isotropic cube. 116
5.6 The extrema of the demagnetizing field for a uniformly magnetized cube, as a function of grid size. 118
5.7 The nucleation field for a 0.084 micron cube as a function of grid size. 120
5.8 The difference between magnetization vectors before and after nucleation. 122

5.9 Volume-average magnetizations of the remanent states in the region where nucleation occurs. 124
5.10 A magnetic state for $L = 0.084\mu$m, just above the nucleation size. . . 125
5.11 A magnetic state for $L = 0.09\mu$m: a flower state with second order curl added. 126
5.12 The difference between the magnetic state in Figure 5.11 and the pure flower state for the same particle size. 128
5.13 The intermediate axis curling state at 0.112μm, just before a transition occurs. 130
5.14 The intermediate axis curling state at 0.113μm, just after the transition occurs. 131
5.15 An illustration of the calculation of the x component of the normalized curl parameter $\mathbf{\Lambda}$. 132
5.16 Components of normalized volume-average magnetization $\mathbf{M}/M_s$ and normalized volume-average curl $\mathbf{\Lambda}$ for the intermediate-axis curling state. 134
5.17 Components of normalized volume-average magnetization $\mathbf{M}/M_s$ and normalized volume-average curl $\mathbf{\Lambda}$ for the short-axis curling state. . . 135
5.18 Components of normalized volume-average magnetization $\mathbf{M}/M_s$ and normalized volume-average curl $\mathbf{\Lambda}$ for the long-axis curling state. . . . 136
5.19 Models of bifurcation, after Nicolis and Prigogine [1989]. 137

6.1 Comparison of the magnetization curves for magnetically isotropic cubes and spheres. 144
6.2 Two hysteresis curves for a magnetically isotropic cube in the SD size range ($L = 0.05\mu$m for magnetite). 146
6.3 A sequence of nested hysteresis curves for triaxial cuboids of varying sizes in a field with direction $\mathbf{H}||(8,1,4)$. 147

6.4 A hysteresis curve for a magnetically isotropic triaxial cuboid with size 0.09μm in a field with direction $(0.22, 0.96, 0.19)$. 149
6.5 The normalized energy density for each stable remanent state of the magnetically isotropic triaxial cuboid. 152
6.6 The total moment of each remanent state for the magnetically isotropic triaxial cuboid. 153

LIST OF TABLES

2.1 Some hysteresis parameters for SD particles. 48

ACRONYMS

AF: alternating field

ARM: anhysteretic remanent magnetization

CRM: chemical remanent magnetization

DRM: depositional remanent magnetization

IRM: isothermal remanent magnetization

MD: multi-domain

NRM: natural remanent magnetization

PSD: pseudo-single-domain

SD: single-domain

SEM: scanning electron microscope

SIRM: saturation IRM (same as M_{rs})

SP: superparamagnetic

TEM: transmission electron microscope

TMXX: titanomagnetite containing xx mol% titanium

TRM: thermal remanent magnetization

VRM: viscous remanent magnetization

SYMBOLS

α, β, γ: direction cosines for magnetization $\mathbf{M}$

A: exchange constant

χ_0: initial susceptibility

$\mathbf{H}$: applied field

$\mathbf{H_a}$: anisotropy field

H_c: coercivity

H_{cr}: coercivity of remanence

$\mathbf{H_d}$: demagnetizing field

$\mathbf{H_{ex}}$: exchange field

$\mathbf{H_{eff}}$: total effective field

$\tilde{H}_{1/2}$: median destructive field

$H^+_{1/2}$: acquisition field for half the saturation remanence

H_n: nucleation field

H_r: critical field for reversal by uniform rotation

H_s: switching field

k_B: Boltzmann constant

K_1: first order magnetocrystalline anisotropy constant

L_0: global critical length (cube root of the volume), below which the SD state has a lower energy than any non-uniform state

L_{ex}: exchange length $(A/\mu_0 M_s^2)^{1/2}$

L_n: nucleation critical length (cube root of the volume), or upper limit for stability of the SD remanent state

L_{sp}: critical size for superparamagnetic-SD transition

L_{sw}: uniform critical length (cube root of the volume), below which magnetization only changes by uniform rotation

$\mathbf{m}$: magnetic moment

$\mathbf{M}$: magnetization (a function of position)

$\hat{\mathbf{m}}$: unit vector (α, β, γ) along $\mathbf{M}$

M_H: volume-average magnetization in the direction of the applied field

M_r: isothermal remanence

M_r^{AF}: remanence after AF demagnetization of an IRM

M_r^{DC}: remanence after DC demagnetization of an IRM

M_{rs}: saturation isothermal remanence

M_s: saturation magnetization

N: demagnetizing tensor

N_a,N_b: demagnetizing factors for long axis and short axis of a prolate ellipsoid of rotation

T_B: blocking temperature

T_{UB}: unblocking temperature

T_c: Curie temperature

ACKNOWLEDGMENTS

I would like to thank Ron Merrill for his generosity and his enthusiasm - and also for repeatedly reminding me to think of the relevance of my work to geophysics. And I would like to thank my wife Cynthia for her patience as I used up the summer hours writing. I would also like to thank her for making many of the transparencies for my defense and helping me in so many other ways. Without her love and support I might not have made it.

Chapter 1

INTRODUCTION

> *When I last did a magnetic experiment (about 1909) we were warned against careless handling of permanent magnets, and the magnetism was liable to change without much carelessness. In studying the magnetism of rocks the specimen has to be broken off with a geological hammer and then carried to the laboratory. It is supposed that in the process its magnetism does not change to any important extent, and though I have often asked how this comes to be the case I have never received any answer. In fact the modern study started with the announcement that many old rocks showed magnetism in opposite directions to the present field, but later work appeared to show that the magnetism at neighboring geological dates appeared to concentrate about a direction and its opposite; since then reversals have been ignored, it being usually assumed that the Earth's general field is liable to sudden reversal but not to intermediate shifts. The reason for the reversal, it being supposed genuine, remains unknown.* [Jeffreys, 1962]

As the above quote suggests, in its early days paleomagnetism was viewed with skepticism by many reputable scientists. Today, it is well established that the Earth's field reverses and that paleomagnetism works - although we still don't fully understand how. Since the early contributions that helped establish plate tectonics, paleomagnetism has expanded into a major discipline with applications in many branches of the earth sciences.

At first, earth scientists were mainly interested in magnetic minerals for their remanence, or magnetization in the absence of an inducing field. This remanence carried information on the field in which the remanence was acquired. The Earth's field in the past is an interesting subject in its own right, but the direction of the ancient field is also used in tectonic reconstructions, and the polarity (normal or reversed) is used in magnetostratigraphy. In addition, there is increasing interest in the use of magnetic "proxies" for size, composition and concentration of magnetic minerals. This information is used to deduce paleoclimate and other environmental processes. Also, anisotropies in magnetic properties are used to infer the direction of flow of lavas that formed volcanic rocks or the strain in rocks.

Ferromagnetic behavior can be roughly classified into three types. If a ferromagnet is small enough, its magnetization is uniform but the direction of the moment is constantly buffeted around by thermal fluctuations. In analogy to paramagnetism, this phenomenon is called superparamagnetism and the particle is called superparamagnetic (SP). A single-domain (SD) is uniformly magnetized and the magnetization changes by uniform rotation. A multi-domain (MD) particle is divided into magnetic domains and the magnetization changes by translation of domain walls. As a particle increases in size, it goes from SP to SD to MD, but the transitions are not abrupt. Thermal fluctuations gradually decrease in importance. Many particles are considered to have both SD-like and MD-like properties. Verhoogen [1959] proposed that there were small regions within MD particles that acted like SD particles. Stacey [1963] called such behavior "pseudo-single-domain (PSD)", although he proposed a mechanism related to domain wall movement.

The size range for the different kinds of behavior depends on the composition and shape of the particles. For a magnetite particle with nearly equal dimensions, the SP-SD and SD-PSD transitions both occur between about 0.01μm and 0.1μm, so the size range for SD behavior is quite narrow. Estimates of the PSD-MD transition in magnetite depend on the criterion and range from 3μm [Worm and Markert, 1987a]

to 100μm [Heider *et al.*, 1992].

If particle size were the only factor that affected magnetic properties, it would probably be easy to interpret magnetic measurements. The properties also depend on particle shape, composition and concentration, and they are affected by inhomogeneities in particles. Unraveling the different effects is a major challenge for rock magnetism.

In this chapter I will look at some applications of rock magnetism with emphasis on particle size. In later chapters I develop theories for different particle sizes in an effort to improve our understanding of magnetic properties in rocks.

1.1 Hysteresis

A system has hysteresis if its state depends on what has happened to it in the past. For hysteresis to occur, there must be at least two possible states for a given set of conditions and there must be points at which irreversible transitions between states occur. For example, a ferromagnet[1] has a magnetization **M** that resides primarily in electron spins. Interactions between spins tends to make them parallel or antiparallel, and this gives rise to magnetic hysteresis. As the temperature of a ferromagnet increases, thermal fluctuations decrease the alignment between spins, until at the Curie temperature[2] T_c there is no hysteresis. The solid is then paramagnetic, and changes in magnetization are reversible.

The magnetization **M** changes in response to an applied field **H**. Both are vector quantities, but in samples with a large number of randomly oriented particles **M** is

---

[1] Various kinds of magnetic order (ferrimagnetism, canted antiferromagnetism) exist in minerals of interest to earth scientists, but the differences do not affect the work in this dissertation. I will refer to them collectively as ferromagnets.

[2] Strictly speaking, the critical temperature for ferromagnets is the Curie temperature while that for ferrimagnets and antiferromagnets is the Néel temperature, but it is common to call both the Curie temperature.

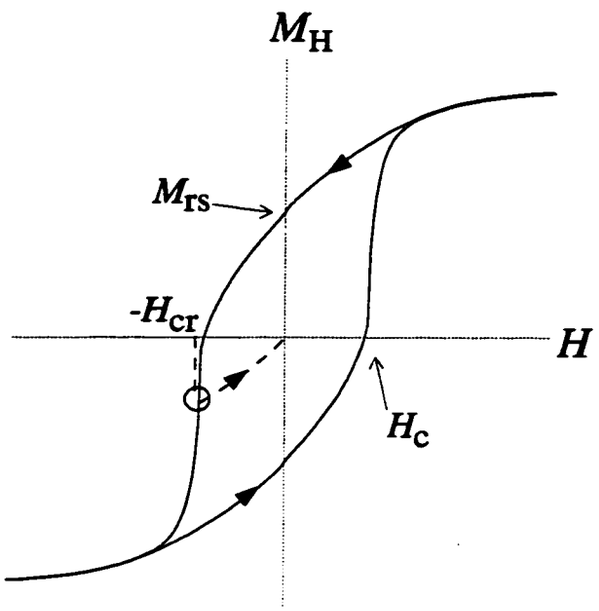

Figure 1.1: An example of a magnetic hysteresis loop (after Tauxe *et al.* [1996], Figure 4).

usually parallel to **H**. Often the only component of magnetization that is measured is M_H, the component of **M** in the direction of **H**.

An example of magnetic hysteresis at a fixed temperature is shown in Figure 1.1. The arrows indicate the direction of change. If the sample is initially demagnetized ($M_H = \mathbf{H} = 0$) and **H** is increased, the magnetization follows the curve that starts at the origin. The initial susceptibility is defined as

$$\chi_0 \equiv \left.\frac{dM_H}{d\mathbf{H}}\right|_{M_H=0,\mathbf{H}=0} \tag{1.1}$$

When **H** gets large enough, the curve levels off and M_H approaches the saturation magnetization M_s. If the field is then decreased to zero, the magnetization follows the upper curve and the magnetization in zero field is a positive quantity called the

saturation remanence.[3] If the field goes negative (that is, **H** is now in the opposite direction), the magnetization continues to decrease. The coercivity H_c is defined by $M_H(-H_c) = 0$. If **H** continues to large negative values, M_H approaches negative saturation.

The sequence from positive to negative saturation can be reversed, tracing out the bottom curve in Figure 1.1. The upper and lower curves form a closed loop called the major hysteresis loop, and they are called the ascending and descending branches of the major loop. The major loop is unchanged if the variables M_H and **H** are replaced by $-M_H$ and $-\mathbf{H}$.

If the field decreases to a minimum and then increases, the magnetization for the increasing field moves along a new curve called the first order reversal curve. If the minimum field is negative, the remanence M_r on this curve is in general less than M_{rs}. The coercivity of remanence H_{cr} is the field at which the first order reversal curve for $M_r = 0$ meets the major loop.

1.2 Interpreting Remanence in Rocks

1.2.1 Thermoremanent Magnetization

When an igneous rock cools from above the Curie temperature, it acquires a thermoremanent magnetization (TRM). If the TRM is not altered, it provides information on the direction and intensity of the Earth's field at the time of cooling.

Néel [1949, 1955] proposed two mechanisms for acquisition of TRM, referred to as the Néel SD and MD theories. In the SD theory, the remanence is determined by a transition from reversible to irreversible behavior, with an equilibrium distribution "frozen in" at the transition. In the MD theory, the remanence is determined by hysteresis.

In his SD theory, Néel [1949] assumes that at high temperatures a particle is

[3] A remanence is a magnetization in zero field.

superparamagnetic. At any given time, the moment can point in any direction with a reasonable probability. Néel assumes a rotationally symmetric configuration for which the energy depends only on the angle θ of the moment with respect to the easy axis. The directions $\theta = 0$ and $\theta = \pi$ have the lowest energy (Figure 1.2).

If there is a field of magnitude H aligned with the easy axis, the probability density $p(\theta, H) \sin\theta d\theta$ of the angle being in a range $[\theta, \theta + d\theta]$ is determined by the Boltzmann distribution:

$$p(\theta, H) \propto \exp\left(\frac{-E(\theta, H)}{k_B T}\right) \tag{1.2}$$

where k_B is the Boltzmann constant.

At higher temperatures, the moment can wander freely from one minimum to the other. As the temperature decreases, the probable states become clustered near the minima, and transitions between energy wells become unlikely. To a good approximation, the magnetization is either "up" or "down" with respect to the easy axis and the distribution of up and down is "blocked". The temperature at which this occurs is called the blocking temperature T_B.

Of course, the energy (and therefore the probability distribution) depends on the applied field. Paleomagnetists are also interested in the *un*blocking temperature T_{UB} at which a particle becomes superparamagnetic as it is heated in zero field. In general, $T_{UB} > T_B$ [Enkin and Dunlop, 1988], but the Earth's field is small enough that $T_{UB} \approx T_B$ because the magnetostatic energy is a small portion of the energy barrier.

In the MD theory, the magnetization is proportional to the displacement of the domain wall from the center of the particle (chapter 2), which in turn is determined by the balance between the magnetic field pushing the wall inwards and "pinning" forces that resist the movement. At first, as the temperature decreases the magnetic force increases faster than the pinning force, and the wall moves inward; if the push from the field exceeds the local pinning force, the wall jumps to a new site where

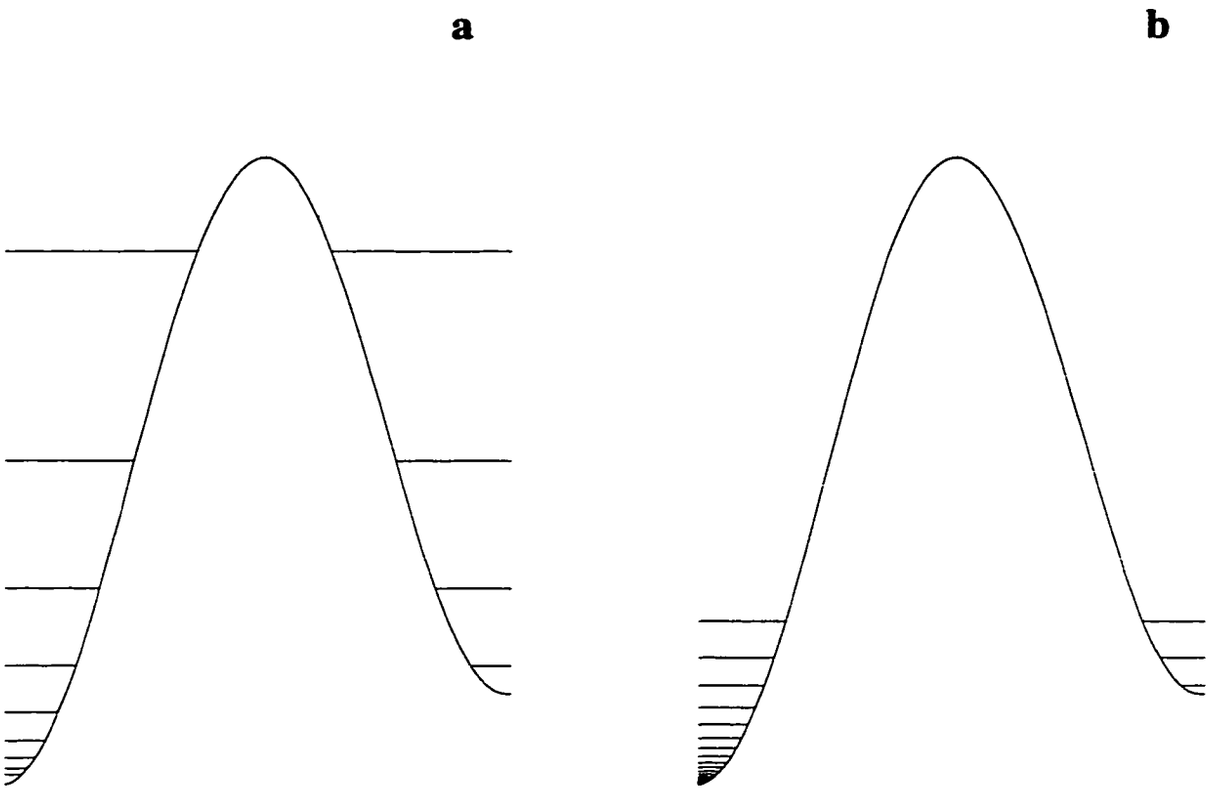

Figure 1.2: An illustration of thermal blocking for a SD particle. The curve is a profile of the energy as a function of the angle θ between the magnetization and the easy axis. The horizontal lines illustrate the probability density. (a) Above the blocking temperature, any angle has a reasonable probability and the moment wanders from one well to the other. (b) Below the blocking temperature, the moment is confined to directions near the minima, and transitions between minima are rare.

the pinning force is greater. The temperature at which the last jump occurs during cooling to room temperature is called the blocking temperature.

In the SD theory, the blocking temperature marks the transition from equilibrium to non-equilibrium conditions. The transition can be reversed by re-heating the particle. In the MD theory, there is a series of irreversible jumps as the temperature decreases, and the blocking temperature merely marks the last such jump. Furthermore, the jumps are irreversible: if the temperature increases, a different series of jumps at different temperatures occurs. In other words, there is hysteresis. It is therefore misleading to use the term "blocking temperature" with MD grains.

1.2.2 Other Kinds of Remanence

In sediments, the remanence is called detrital remanent magnetization (DRM) if it is acquired during deposition, and post-depositional remanent magnetization (pDRM) if it is acquired afterwards during the complex process of consolidation and compaction. In any kind of rock, some of the remanence may be chemical remanent magnetization (CRM). This may be either grain-growth CRM, formed when small ferromagnetic particles become large enough to hold a remanence, or a change in remanence during chemical alteration of a magnetic mineral. Another source of remagnetization is viscous remanent magnetization (VRM), which is acquired gradually when a particle is exposed for a long time to a weak field.

In the laboratory, two other kinds of remanence are commonly encountered. Isothermal remanent magnetization (IRM) is the kind of remanence discussed in the introduction to hysteresis. Anhysteretic remanent magnetization (ARM) is acquired in a field with a DC component that is fixed and an alternating field (AF) with a peak amplitude that is initially large enough to saturate the magnetization and decays to zero. ARM has many similarities to TRM, and it is often used as a proxy for it because it does not involve heating (which may cause chemical alteration).

1.2.3 Paleomagnetic Poles

As paleomagnetic techniques improve and the number of paleomagnetic poles in the literature increases, authors compiling lists of paleomagnetic poles for interpretation are using increasingly stringent criteria for including a pole. Still, even in the most recent compilations [Van der Voo, 1993; McElhinny *et al.*, 1996], the only rock magnetic criterion is that the remanence in each sample must be fully demagnetized and separated into vector components.

The remanence in a sample is rarely the pure, unaltered original component that was acquired when the sample was formed. There are often secondary components that were acquired later; generally each component is in a different direction, since the Earth's field and the location of the rock changed between acquisition events. Two methods are commonly used to separate the components. Thermal demagnetization involves heating the sample step by step in zero field, cooling it and measuring the remanence after each step. Alternating field (AF) demagnetization uses an alternating field with an amplitude that decays to zero; the peak amplitude is increased in steps.

If there is only one component, it can be represented by a vector **A** that is in the direction the field was in relative to the rock; as demagnetization progresses, the magnitude of **A** decreases. If there is a secondary component **B**, the total remanence is **A** + **B**; as demagnetization progresses, the proportions of **A** and **B** will usually change, so the direction of the sum will change. The components can be separated if all of **B** is demagnetized before **A**, so that the direction of the combined remanence approaches **A**.[4]

It was once assumed that secondary components were inherently easier to demagnetize than the primary component. Paleomagnetists used a "blanket step" demag-

[4] Examples of demagnetization and vector decomposition can be found in any book on paleomagnetism, for example Butler [1992].

netization, exposing the sample to a temperature or peak alternating field that they considered enough to "clean" the sample of its secondary remanence. This does not always work. In the 1980's, paleomagnetists discovered that most Paleozoic rocks were remagnetized, and the original remanence had not been isolated by blanket step methods. Many paleomagnetic poles determined before the 1980's are now considered unreliable [McCabe and Elmore, 1989; Van der Voo, 1993].

The primary remanence can often be isolated in a remagnetized sample if the demagnetization is carried far enough to remove all the remanence. This does not always work either: the secondary component can be more resistant to AF demagnetization, thermal demagnetization or both [O'Reilly, 1984, page 196].

It would be easier to interpret the components of the remanence if each component were associated with a distinct size or composition of magnetic mineral. Paleomagnetists often carry out rock magnetic and petrographic analyses to identify the carriers. Stable magnetization in a variety of igneous rocks has been linked to the presence of small, often submicron, magnetite grains [Strangway *et al.*, 1968; Evans and McElhinny, 1969; Larson *et al.*, 1969; Hargraves and Young, 1969; Wu *et al.*, 1974; Morgan and Smith, 1981; Xu *et al.*, 1997].[5]

It is generally agreed that the main carriers of stable remanence are SD and PSD grains, but it is not clear what one can do with this information. The relevance of rock magnetic measurements is aptly summarized by Van der Voo [1993], page 65:

> This information is, obviously, of importance, but in general it does not contribute to our knowledge about the reliability of a paleomagnetic pole ... any magnetic mineral can be primary or secondary and remagnetization can be carried by all grain sizes.

[5] Often a very small volume fraction of SD magnetite can produce the observed remanence, and SD-size minerals are easily missed in petrographic studies; for example, the magnetic carriers in Banded Series rocks of the Stillwater Complex were not found until electron microscopy was used [Bergh, 1970; Xu *et al.*, 1997].

Stability of Remanence

The stability of magnetic remanence is a major concern of rock magnetists and much of the work on size dependence of magnetic properties is related to stability. Stability can be defined in many ways. In the field, stability is the resistance to remagnetization by such processes as CRM and VRM, and field tests are commonly employed to check whether remagnetization has occurred.

In the laboratory, the primary measures of stability are resistance to AF and thermal demagnetization. The shape of the demagnetization curve tends to be different for SD and MD grains, with the SD grains showing little loss in small fields while the MD grains show a large initial loss. A commonly used measure of stability is the median destructive field $\tilde{H}_{1/2}$, the peak alternating field required to remove half the remanence; this appears to decrease rapidly as grain size increases [Bailey and Dunlop, 1983; Levi and Merrill, 1978]. An analogous parameter for thermal demagnetization, the average blocking temperature $\langle T_{UB} \rangle$, does not have a clear size dependence [Levi and Merrill, 1978].

Because the initial loss of remanence is usually greater in MD grains than in SD grains, MD grains are considered less stable than SD grains; but it has long been known that there tends to be a fraction of remanence in MD grains that is much harder to remove. This inspired Verhoogen [1959] to propose that hysteresis properties in MD grains are controlled by SD-like regions around defects. Ironically, the samples he was interested in (titanomagnetites in basalts) may not have been MD: many particles that appear to be MD-size high-Ti titanomagnetites are really networks of SD-size magnetite particles separated by ilmenite lamellae [Strangway *et al.*, 1968; Evans and McElhinny, 1969; Larson *et al.*, 1969].

The coercivity of remanence H_{cr} is a measure of how difficult it is to remove *all* the remanence. This has been measured for magnetites up to millimeters in size, and it does not depend strongly on particle size [Heider *et al.*, 1996].

Another measure of stability involves low temperature demagnetization (LTD). Magnetite has an isotropic temperature $T_I \approx 130$K at which the magnetocrystalline anisotropy disappears. If a bulk sample is cooled below T_I and heated back to room temperature, up to 90% of the remanence is lost; SD particles have little or no loss, and the loss tends to increase with particle size [Heider *et al.*, 1992].

Based on the stability of states after low-temperature demagnetization (LTD), Dunlop and Argyle [1991] revived the idea of SD-like regions in MD grains. After LTD, the AF demagnetization spectrum is SD-like (there is little loss in remanence for small fields). The remanence has other properties, however, that are considered MD-like, such as $T_{\mathrm{UB}} > T_{\mathrm{B}}$ [McClelland *et al.*, 1996].

This raises an important point. We must be careful when we interpret measures of stability for a remanence, because the stability of the remanence depends very much on how the remanence was acquired. A simple example makes this clear: suppose we demagnetize a saturation IRM in an alternating field with peak amplitude H_1. The new remanence should be resistant to demagnetization in any field $H < H_1$ (although there will probably be some loss), so this remanence is much "harder" than the SIRM. This is true whether the sample is SD or MD. If a process such as low-temperature demagnetization has a similar effect to AF demagnetization, we can expect the remanence after LTD to have a "SD-like" AF demagnetization curve whether or not there are SD-like regions in the particle.

A remanence can be stable by one measure and unstable by another. If a sample is easily AF demagnetized, for example, it might seem reasonable to assume it can be easily remagnetized, so it should not retain reliable field directions. Some such samples do, however [Grommé and Merrill, 1965].

If a sample is easily remagnetized, one would think that the remagnetization would be easy to remove. If this were true, and the primary magnetization was carried by SD grains while the secondary remanence was carrier by MD grains, it would be easy to separate them. It is increasingly apparent, however, that remagnetization in MD

grains can be very hard to remove. Even a VRM acquired at room temperature in a small field may not be thermally demagnetized until the temperature is nearly equal to the Curie temperature [Dunlop, 1983b; Halgedahl, 1993].

1.2.4 Paleointensity in Igneous Rocks

If we are trying to use a remanence to deduce the intensity of the Earth's at the time of acquisition, our criteria for a good sample are more restrictive than for paleomagnetic poles. Any isotropic sample will acquire a remanence in the direction of the inducing field, but the intensity of the remanence varies greatly with composition and grain size. To deduce the paleointensity, one must make some assumptions about the acquisition of remanence. The two most commonly used methods are the modified Thellier-Thellier method and the Shaw method.

Thellier-Thellier Method

The modified Thellier-Thellier method [Thellier and Thellier, 1959; Coe, 1967a,b] is considered by most practitioners to be the most reliable way of deriving a paleointensity a from lava flow or an archaeological artifact. The method involves two sequences of heating and cooling:

1. In zero field, heat the sample to a temperature T_i. Cool to room temperature T_0 and measure the residual remanence NRM(T_i, T_c). Repeat for a sequence of temperatures T_i up to the Curie temperature. The sample should then be completely demagnetized.

2. Expose the sample to a laboratory field and heat it to the same series of temperatures T_i; measure the partial thermoremanent magnetization pTRM(T_0, T_i) after each step.

Now plot the pairs (pTRM(T_0, T_i), NRM(T_i, T_c)) against each other. If they form a straight line, the slope gives the ratio of the Earth's field at the time of NRM acquisition to the laboratory field.

Conditions for a successful paleointensity determination using the Thellier-Thellier method are:

1. The NRM is a pure, unaltered TRM.

2. The pTRM acquired in one temperature interval is independent of the pTRM acquired in a non-overlapping temperature interval (the Thellier additivity law).

3. TRM(H) $\propto H$ for small fields.

4. A pTRM acquired at a given temperature can be removed by heating in zero field to the same temperature.

Most samples fail at least one of the criteria and have a nonlinear Thellier plot. The second criterion, the Thellier additivity law, works fairly well for small particles or low fields [Levi, 1979], but gets progressively worse for larger fields and larger particles [McClelland and Sugiura, 1987; Tucker and O'Reilly, 1980].

The fourth criterion is often stated in terms of the blocking and unblocking temperatures: $T_B = T_{UB}$. This appears to be satisfied by SD grains [Dunlop and West, 1969; Day, 1977; Hartstra, 1983], but $T_{UB} > T_B$ in large MD particles [Bol'shakov and Shcherbakova, 1979; McClelland and Sugiura, 1987]. Numerous authors have developed theories for the "anomalous" unblocking temperatures in MD grains [Halgedahl, 1993; Dunlop and Xu, 1994; Xu and Dunlop, 1994; McClelland and Shcherbakov, 1995; McClelland *et al.*, 1996]. However, as I mentioned earlier, blocking and unblocking (in the sense of transitions from superparamagnetism to hysteresis and back) do not occur in MD particles. TRM acquisition in MD particles is a hysteresis phe-

nomenon, so it is not surprising there should be an asymmetry between acquisition and destruction of remanence. No special mechanism is required.

This implies that the Thellier-Thellier method will not work once remanence is acquired by a hysteresis mechanism. As the particle size increases, the blocking temperature rapidly approaches the Curie temperature (e.g. [Dunlop *et al.*, 1994]). Levi [1977] found that sized magnetites with $\langle L \rangle \leq 0.25\mu$m had linear Thellier plots, while larger particles did not. By most estimates, the SD critical size is under 0.1μm, so thermal blocking may occur in non-SD particles.

Shaw's Method

If there is hysteresis in the acquisition and destruction of TRM, we cannot use demagnetization to reverse the process of acquisition. Instead, we must compare parallel processes of acquisition and demagnetization. This is the essence of Shaw's method [Smith, 1967; Shaw, 1974]. First, the NRM is demagnetized in an alternating field. Then a TRM is acquired in a laboratory field, and it is demagnetized in an alternating field. As in the Thellier-Thellier method, the partially demagnetized NRM and TRM are plotted against each other and the slope gives the field the NRM was acquired in.

In principle, Shaw's method may work for MD grains. The criteria for success are analogous to those for the Thellier-Thellier method:

1. The remanence is a pure, unaltered TRM.

2. The remanence lost in an interval (H_1, H_2) of peak alternating fields is independent of the remanence lost in a non-overlapping interval.

3. If H is the acquisition field, $\Delta M_r \propto H$ in each interval.

The third criterion can be put another way: the normalized AF demagnetization curve has a shape that is independent of the acquisition field (at least for small fields).

This is certainly not true for all kinds of remanence (for example, IRM in SD grains - see chapter 2), so it would be useful to know when this condition is satisfied.

One concern about a method involving acquisition of TRM is that the chemical properties of the rock may change when it is heated. Shaw [1974] introduced a consistency check: before heating and after, give the sample an ARM and demagnetize it, and plot the partial ARMs against each other. If any chemical change has occurred, the curve should be nonlinear.

1.3 Proxies for Particle Size

At first, paleomagnetists were interested in the size of ferromagnetic grains because size was correlated with stability of remanence; but they gradually realized that the size, composition and concentration of ferromagnetic particles carried information on the processes that gave rise to them. Thus was born the field of environmental magnetism [Thompson and Oldfield, 1986].

Magnetic "proxies" for particle size take advantage of the strong dependence of some hysteresis parameters on particle size. It can be difficult, however, to deduce a size from hysteresis parameters because they also depend strongly on other factors including composition and elongation. This is usually handled by taking the ratios of parameters, or plotting one against the other, or both. A collection of SD particles of any composition and shape, with uniaxial anisotropy, will have $M_{rs}/M_s = 0.5$ and $H_{cr}/H_c = 1.09$ (chapter 2). Partly because of this, these parameters are widely used as indicators of particle size, and they are often combined on a single plot called the Day diagram (Figure 1.3).

The Day diagram developed the way many proxies do: various parameters were plotted against each other and a combination was chosen that showed a coherent trend with particle size. Day *et al.* [1977] measured M_{rs}/M_s and H_{cr}/H_c for titanomagnetites covering the normal span of compositions that paleomagnetists are

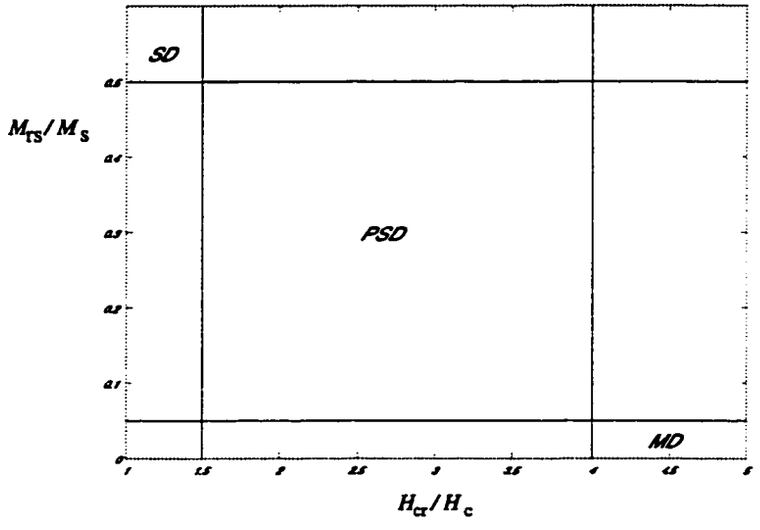

Figure 1.3: Classification of hysteresis parameters, after Day *et al.* [1977]. SD particles are in the upper left corner, PSD particles in the middle and MD in the lower right.

interested in; the points fell along roughly the same curve in the Day diagram. By contrast, a plot of M_{rs}/M_s against χ_0/M_s showed a dependence on composition.

In Figure 1.3, SD particles are shown occupying a region with $M_{rs}/M_s > 0.5$ and $H_{cr}/H_c < 1.5$. Uniaxial SD particles lie right on the boundary of this region. Various criteria for the PSD-MD transition have been suggested, but the choice is arbitrary; Day *et al.* [1977] use $M_{rs}/M_s < 0.05$ and $H_{cr}/H_c > 4$.

Other combinations of hysteresis parameters that have been suggested include χ_0 vs χ_{ARM} (susceptibility of ARM) [Banerjee *et al.*, 1981; King *et al.*, 1982]; M_{rs} vs χ_0 [Tauxe, 1993]; and the dependence of susceptibility on frequency [Bloemendal *et al.*, 1985].

Most of these plots are combinations of the familiar parameters M_s, M_{rs}, H_c, H_{cr} and χ_0. Why use more than one parameter? Why not, for example, use M_{rs}/M_s and leave it at that?

The reason for using multiple parameters is that there many other factors besides

particle size and composition that affect the hysteresis parameters. Elongation, for example, can be important. In SD particles, combinations of M_{rs}/M_s and H_{cr}/H_c eliminate the effect of elongation - but we don't know how these parameters depend on elongation in larger particles. Another problem is that there may be a broad range of particle sizes, and we wish to know something about the distribution. Each parameter may be more sensitive to a particular fraction. Large particles dominate M_s, for example, because of their volume; SD particles have the largest coercivities, so they dominate H_c and H_{cr}.

Unfortunately, unless we know how all the factors influence the hysteresis parameters, we cannot make much use of the extra information in plots such as the Day diagram. It is therefore crucial to have measurements of hysteresis parameters for well characterized samples with narrow size ranges. At present, there is still a large uncertainty even in the size dependence (see below).

If there are superparamagnetic particles in a sample, they can affect any parameter that is measured in a nonzero field: M_s, H_c and especially χ_0. Tauxe *et al.* [1996] showed that combinations of SP and SD particles can plot almost anywhere on a Day diagram. Thus, even if we knew how hysteresis parameters depended on all the factors mentioned above, the interpretation of a given set of parameters would probably not be unique.

Size Dependence: Measurements

Magnetic properties have been measured in sized samples of titanomagnetites, titanohematites, pyrrhotite, goethite and hematite (for references, see Hunt *et al.* [1995]). In all of these minerals, some magnetic properties are strongly dependent on particle size.

The most heavily studied mineral is magnetite. Compilations of M_{rs}/M_s and H_c show a power-law dependence above the SD size range; both scale as L^{-n}, where $n \approx 0.6 - 0.7$ [Heider *et al.*, 1987]. However, the hysteresis parameters also depend

strongly on the method of preparation of the magnetite particles. In most of the samples (e.g. Dunlop [1973]), the magnetite particles are precipitates from solution, and they remained clumped together even after they are mixed with a non-magnetic medium and stirred vigorously. Particle interactions can decrease M_{rs}/M_s and H_c and H_c considerably. Samples prepared by the glass ceramic method [Worm and Markert, 1987b] appear to be well dispersed, but they may be under considerable stress (Chapter 4). These samples have higher M_{rs}/M_s and H_c than the precipitates. In the earliest studies (e.g. [Parry, 1965]), magnetite was crushed and sieved in order to obtain the desired size range. These samples have even higher M_{rs}/M_s and H_c than the glass ceramics. The particles in these samples have a broad, bimodal size distribution [Heider *et al.*, 1987] and they are highly nonuniform internally [Brown and O'Reilly, 1996; Zitzelsberger and Schmidbauer, 1996], so they are probably not useful for understanding the size dependence of hysteresis parameters.

The size dependence for the coercivity of remanence is unclear [Heider *et al.*, 1996]: there appears to be some decrease with particle size, but the decrease is no larger than the scatter. On the other hand, there is a strong size dependence in many of the individual studies. Either way, H_{cr}/H_c tends to increase as particle size increases.

The median destructive field $\tilde{H}_{1/2}$ appears to have a strong size dependence [Bailey and Dunlop, 1983; Levi and Merrill, 1978], but there are only two studies. Perhaps with more measurements there would be a large scatter in this parameter as well.

The susceptibility χ_0 is essentially independent of size [Heider *et al.*, 1996]. This makes χ_0 useless as a particle size indicator, but all the more useful for determining concentration.

Tests Involving Demagnetization

Also in use are some particle size proxies involving AF demagnetization curves. These proxies are not affected by a superparamagnetic component (although they can be affected by thermal fluctuations: section 2.3.2). Tests of this sort, it is argued, provide

information on the distribution of particle sizes, but they have the disadvantage of being much more laborious than the hysteresis parameters.

The oldest such test is the Lowrie-Fuller test. Lowrie and Fuller [1971] compared AF demagnetization curves (normalized by the initial remanence) for TRM and SIRM and proposed the following test: if the TRM is "harder" than the SIRM (the AF curve decreases more slowly initially), the particles are SD; if the TRM is softer, the particles are MD.

The Lowrie-Fuller test soon ran into trouble. Schmidt [1976] calculated the AF demagnetization curves for Néel's SD and MD theories of TRM, and discovered that the theories predicted the opposite of what Lowrie and Fuller [1971] had obtained. No one has yet proposed any mechanism that would make SD particles "SD-like"; theoretical models have been proposed for MD particles [Bailey and Dunlop, 1983; Xu and Dunlop, 1995], but even these models reinterpret the Lowrie-Fuller test as a division between PSD and MD behavior. SD-like properties have been observed in magnetite particles as large as 100μm [Heider *et al.*, 1992].

A different test looks at the shape of the demagnetizing curve for SIRM alone: for SD particles, the curve has a plateau in small fields [Dunlop and West, 1969; Bailey and Dunlop, 1983]. Unlike the Lowrie-Fuller test, this does agree with theory (section 2.3.3). Bailey and Dunlop [1983] also argue that this test is correlated with the Stoner-Wohlfarth theory, however, and they propose a quantitative measure of the shape of the demagnetization curve that distinguishes between PSD and MD grains.

More recently, Cisowski [1981] suggested comparing IRM acquisition (as a function of applied field) with AF demagnetization of saturation IRM. He proposed a parameter R which is the remanence (as a fraction of SIRM) where the curves cross. For SD particles with uniaxial anisotropy, $R = 0.5$. This parameter can be justified by the Wohlfarth relations, which I will discuss in detail in section 2.3.2.

1.4 Summary

The dependence of magnetic properties on particle size is important both for magnetic proxies of size that are used in environmental magnetism and for paleomagnetic applications; for example, the mode of acquisition of TRM determines whether the Thellier-Thellier method will provide a reliable paleointensity, while the dependence of the AF demagnetization spectrum for TRM determines whether the Shaw method can be used.

Hysteresis properties depend on other factors besides size, such as composition, elongation and particle interactions. Some combinations of hysteresis parameters, such as M_{rs}/M_s and H_{cr}/H_c, cancel out the effect of composition and elongation in SD particles, but it is not known how they depend on elongation in larger particles.

Thermal fluctuations also affect hysteresis properties. Paramagnetic and superparamagnetic particles contribute to parameters such as M_{rs}, H_c and χ_0 that are measured in nonzero field, so these parameters can be misleading. Measurements of remanence acquisition and destruction (DC or AF) eliminate the (super)paramagnetic contribution, so they are potentially more reliable indicators of particle size. They must still be used with caution: the usefulness iof the Lowrie-Fuller test is questionable, the coercivity of remanence H_{cr} does not have a strong size dependence, and there are not many measurements of the median destructive field $\tilde{H}_{1/2}$ for samples with well defined particle sizes.

To understand how magnetic properties change with particle size, we must know how the magnetization changes within a particle. The two main models for change are the SD model (uniform rotation) and the MD model (domain wall motion). The SD model is well established, but the MD model is more controversial. Since Verhoogen [1959] observed that large particles appeared to have some "SD-like" properties (such as a remanence that requires large alternating fields to remove completely), rock magnetists have called particles with apparently mixed properties pseudo-single-domain

(PSD). It is supposed that there is a PSD size range where a transition occurs between the limiting cases of SD and MD behavior, but estimates of this size range vary by at least an order of magnitude and depend strongly on the criterion used.

In this dissertation, I re-examine SP, SD and MD models, looking for robust proerties that can be used to interpret magnetic measurements. I also use analytical and numerical micromagnetic theory in an effort to develop a unified picture of how magnetic properties change as particle size increases. The frame for this picture is nucleation theory, which I introduce in Chapter 3.

Chapter 2

HYSTERESIS THEORIES

The SD and MD models are the two main models for changes in magnetization. In the SD model, magnetization changes by uniform rotation. In the MD model, it changes by translation of domain walls. SD and MD models are often considered end members of the possible range of behavior, with PSD particles in between.

In this chapter, after reviewing the basic equations for all ferromagnets, I will explore the SD and MD models, looking for hysteresis properties that distinguish the two.

2.1 Thermodynamic Fundamentals

Magnetism is a quantum mechanical phenomenon. Niels Bohr proved that in a classical system at a finite temperature, in finite applied electric or magnetic fields, the magnetization induced by currents vanishes in equilibrium [Mattis, 1988]. The source of most of the magnetism in a ferromagnets is electron spin. Unfortunately, it is still beyond our resources to calculate all the quantum mechanical forces (including exchange coupling, magnetic dipole-dipole forces and spin-orbit coupling) in a ferromagnet. All the work in this dissertation is based on thermodynamic equations whose form is justified by quantum mechanics but which have parameters that must be measured for each substance. The thermodynamic theory is developed in numerous textbooks such as Brown [1963] or Chikazumi [1964]; for a more fundamental treatment, the reader should consult a book like Mattis [1988].

In a ferromagnet, the magnetization $\mathbf{M}$ has a direction which depends on position,

but a magnitude which is assumed to be equal to the saturation magnetization M_s. The equations can therefore be written in terms of the unit vector

$$\hat{\mathbf{m}} = \frac{\mathbf{M}}{M_s} = \alpha\hat{\mathbf{i}} + \beta\hat{\mathbf{j}} + \gamma\hat{\mathbf{k}} \tag{2.1}$$

The direction cosines satisfy $\alpha^2 + \beta^2 + \gamma^2 = 1$.

For a given temperature and external field $\mathbf{H}$, the free energy G is a minimum [Brown, 1963]. This energy is an integral over the volume of the ferromagnet:

$$G = \int \left\{ A\left[(\nabla\alpha)^2 + (\nabla\beta)^2 + (\nabla\gamma)^2\right] - \frac{\mu_0}{2}\mathbf{M}\cdot\mathbf{H}_d - \mu_0\mathbf{M}\cdot\mathbf{H} + g_a + g_\lambda \right\} dV \tag{2.2}$$

The first term is called the exchange energy density, and A is a temperature-dependent parameter called the exchange constant.[1] This term is minimized when the magnetization is uniform.

The second term is the magnetic self-energy density, or demagnetizing energy density. The demagnetizing field $\mathbf{H}_d$ has the magnetization as its source. If the contribution of currents to the magnetization is negligible compared to spins (a good approximation in ferromagnets), then $\nabla \times \mathbf{H}_d = 0$ and there is a magnetic scalar potential Φ_M such that

$$\mathbf{H}_d = -\nabla\Phi_M \tag{2.3}$$

From Maxwell's equations, Φ_M is the solution to Poisson's equation:

$$\nabla^2\Phi_M = -\nabla\cdot\mathbf{M} \tag{2.4}$$

Assuming $\mathbf{H}_d$ goes to zero at infinity, the solution can be expressed as an integral over the volume and surface of the particle [Jackson, 1975]:

$$\Phi_M(\mathbf{r}) = -\frac{1}{4\pi}\int \frac{\nabla'\cdot\mathbf{M}(\mathbf{r}')}{|\mathbf{r}-\mathbf{r}'|}dV' + \frac{1}{4\pi}\oint \frac{\mathbf{M}(\mathbf{r}')\cdot\hat{\mathbf{n}}'}{|\mathbf{r}-\mathbf{r}'|}dS' \tag{2.5}$$

The prime in ∇' indicates the derivatives are with respect to the dummy variable $\mathbf{r}'$; $\hat{\mathbf{n}}'$ is the outward normal to the surface.

---

[1] Many authors use $C/2$ instead of A.

$\mathbf{H_d}$ is called the demagnetizing field because the magnetic self-energy tends to be reduced if the magnetic moment is reduced. More precisely, Brown [1963] derives the "pole-reduction" principle, which states that the magnetic self-energy is minimized if the volume and surface pole densities $-\nabla \cdot \mathbf{M}$ and $\mathbf{M} \cdot \hat{\mathbf{n}}$ vanish.

The term g_a in equation 2.2 is called the magnetocrystalline energy density and depends on the direction of magnetization relative to the crystal lattice. It is derived by expanding the energy in powers of the direction cosines α, β, γ and keeping the lowest order terms. Many combinations of powers vanish because of the symmetry of the crystal. For hexagonal symmetry with γ the component of magnetization along the c axis,

$$g_a \approx K_1(1 - \gamma^2) \tag{2.6}$$

If $K_1 > 0$, g_a is minimized when the magnetization is along the c axis ($\alpha = \beta = 0, \gamma = 1$). The c axis is called the easy axis, and this type of magnetic anisotropy is called uniaxial. If $K_1 < 0$, the c axis is the hard direction (g_a is maximized), and the basal plane is an easy plane of magnetization However, if higher order terms are included there is a unique easy axis.

If the crystal has cubic symmetry,

$$g_a \approx K_1(\alpha^2\beta^2 + \beta^2\gamma^2 + \gamma^2\alpha^2) \tag{2.7}$$

If $K_1 > 0$ (iron or high-Ti titanomagnetites), the easy axes are the three crystallographic $\langle 100 \rangle$ directions and the hard axes are the four $\langle 111 \rangle$ directions. If $K_1 < 0$ (magnetite), the easy and hard axes are reversed.

Finally, if there is a stress σ_{ij} on the sample,[2] there is an inverse magnetostriction energy density:

$$g_\lambda = -\frac{3}{2}\lambda_{100}\left[\sigma_{11}\alpha^2 + \sigma_{22}\beta^2 + \sigma_{33}\gamma^2\right] - 3\lambda_{111}\left[\sigma_{12}\alpha\beta + \sigma_{23}\beta\gamma + \sigma_{31}\gamma\alpha\right] \tag{2.8}$$

[2] The sign of σ_{ij} is chosen so at the surface, $\sigma_{ij}n_j > 0$ indicates an outward traction or tension.

In general, σ_{ij} depends on position, and inverse magnetization can deflect the easy axes locally away from the magnetocrystalline easy axes. The magnetization itself strains the crystal, which contributes to the stresses in the above equation. This nonlinear effect, called magnetostriction, is usually expected to be small, and I will say little about it in this dissertation.

2.1.1 Micromagnetics

Brown [1963] defined micromagnetics as a model of magnetization on a scale where the magnetization can be approximated by a continuous function - well above the atomic scale but small enough to resolve the internal structure of domain walls.

Ideally, we would like to solve for the three-dimensional distribution of magnetization $\mathbf{M}(\mathbf{r})$ by minimizing the free energy (equation 2.2) with the appropriate constraints and boundary conditions. Using variational calculus, Brown [1963] obtained the equations

$$\hat{\mathbf{m}} \times \mathbf{H}_{\text{eff}} = 0 \tag{2.9}$$

with the surface condition

$$\frac{\partial \hat{\mathbf{m}}}{\partial n} = 0 \tag{2.10}$$

where (ignoring magnetostriction)

$$\mathbf{H}_{\text{eff}} = \mathbf{H} + \mathbf{H}_{\text{d}} + \frac{2A}{\mu_0 M_{\text{s}}} \nabla^2 \hat{\mathbf{m}} - \frac{\partial g_a}{\partial \hat{\mathbf{m}}} \tag{2.11}$$

These are called Brown's equations. The field $\mathbf{H}_{\text{eff}}$ is called the effective field and $\hat{\mathbf{m}} \times \mathbf{H}_{\text{eff}}$ is the local torque on the magnetization.

Brown [1963] shows that the hysteresis curves corresponding to equilibrium states always have positive slope:

$$\frac{\partial M_{\text{H}}}{\partial H} > 0 \tag{2.12}$$

The second half of this dissertation describes the results I obtain using a numerical algorithm to solve the micromagnetic equations. Much of the theory I describe

in this chapter is not micromagnetic. Strictly speaking, SD theory is not micromagnetic because it assumes the magnetization is uniform, but it can be shown using micromagnetics (chapter 3) that SD theory is correct for ellipsoidal particles within a certain size range. MD theory is not micromagnetic: the magnetization is not allowed to vary continuously within the particle. Nevertheless, MD theory is still widely used because the micromagnetic equations are very difficult to solve.

2.2 Superparamagnetic Grains

When the magnetic behavior in a particle is dominated by thermal fluctuations, and all directions of the moment are in equilibrium with each other, the particle is called superparamagnetic (SP). In an SP grain, changes in magnetization are reversible and the magnetization is determined by the Boltzmann distribution. If there is no intrinsic anisotropy, the energy is $-\mu_0 \mathbf{M} \cdot \mathbf{H} V$, where V is the volume of the particle. If we choose a set of polar coordinates so that $\mathbf{H}$ is along the polar axis, the probability density $P(\theta, \phi) \sin\theta d\theta d\phi$ for $\mathbf{M}$ to be at an angle (θ, ϕ) is given by

$$P(\theta, \phi) = Z^{-1} \exp\left(-\mu_0 \mathbf{M} \cdot \mathbf{H} V / k_B T\right) = Z^{-1} \exp\left(-a \cos\theta\right) \tag{2.13}$$

where $a = \mu_0 M_s H V / k_B T$ and Z is a normalizing factor:

$$Z = \int_0^{2\pi} \int_0^{\pi} \exp\left(-a \cos\theta\right) \sin\theta d\theta d\phi = 2a \sinh a \tag{2.14}$$

The average magnetization is therefore

$$M_H = \langle \cos\phi \rangle = \int_0^{2\pi} \int_0^{\pi} \cos\theta P(\theta, \phi) \sin\theta d\theta d\phi = M_s L(a) \tag{2.15}$$

where L is the Langevin function that appears in the classical theory for paramagnets [Cullity, 1972]:

$$L(a) = \coth(a) - \frac{1}{a} \tag{2.16}$$

Note that the result would be exactly the same if we fixed the direction of $\mathbf{M}$ and averaged over all orientations of $\mathbf{H}$.

[Asimow, 1965] and Tauxe *et al.* [1996] made numerical calculations of the magnetization for materials with anisotropy, and obtained a dependence of the curve on anisotropy. However, if the particles are randomly oriented and there is no net anisotropy for the ensemble, the anisotropy should not affect the magnetization. In general, the energy depends on the orientation (θ_M, ϕ_M) of the magnetization as well as the orientation of the field, but the term $-\mu_0 \mathbf{M} \cdot \mathbf{H} V$ is the only part of the energy that depends on the direction of the field. If we define $\tilde{G} \equiv G + \mu_0 \mathbf{M} \cdot \mathbf{H} V$, then the probability density can be written

$$P(\theta_M, \phi_M, \theta, \phi) = P_1(\theta_M, \phi_M) P_2(\theta, \phi) \tag{2.17}$$

where

$$P_1(\theta_M, \phi_M) \propto \exp(-\tilde{G}/k_B T) \tag{2.18}$$

and

$$P_2(\theta, \phi) \propto \exp(-a \cos\theta) \tag{2.19}$$

These are independent probabilities, and P_1 does not depend on the angle θ. Thus P_1 does not affect the average of $\cos\theta$, so the average magnetization is still given by the Langevin function.

Suppose an ensemble of SP particles has a distribution $\rho(V)$ of volumes. The average magnetization for the ensemble is

$$\frac{\langle M \rangle}{M_s} = \int_0^\infty L\left(\frac{\mu_0 M_s H V}{k_B T}\right) \rho(V) dV \tag{2.20}$$

The Taylor expansion of the Langevin function is

$$L(x) = \frac{x}{3} - \frac{x^3}{45} + O(x^5) \tag{2.21}$$

If we substitute this in the equation for the magnetization, we get

$$\frac{\langle M \rangle}{M_s} = \frac{1}{3}\left(\frac{\mu_0 M_s}{k_B T}\right) \langle V \rangle H - \frac{1}{3}\left(\frac{\mu_0 M_s}{k_B T}\right)^3 \langle V^3 \rangle H^3 + O(H^5) \tag{2.22}$$

Thus the initial susceptibility is

$$\chi_0 = (1/3)\mu_0 M_s^2 \langle V \rangle / k_B T \tag{2.23}$$

By fitting the magnetization curve to a polynomial in H we can determine the odd moments $\langle V^{2k+1} \rangle$ for the volume distribution. However, we cannot determine quantities such as the standard deviation $(\langle V^2 \rangle - \langle V \rangle^2)^{1/2}$.

2.3 Single-Domain Theory

In this section, I have three goals. The first is to describe SD hysteresis in a more three-dimensional and geometrical way than usual. Micromagnetic solutions are three-dimensional, so it may help us to understand them if we first look at the simplest three-dimensional ferromagnetic behavior. The second is to introduce the Wohlfarth relations and show that they are more robust indicators of SD remanence carriers than the usual parameters such as M_{rs}/M_s and H_{cr}/H_c. The third is to derive some analytical expressions for SD hysteresis that have only been derived numerically before.

2.3.1 Single SD Particle

The moment of a SD particle has a fixed magnitude and can only rotate in response to an applied field. Within the particle, the magnetization is uniform and its magnitude is the saturation magnetization M_s. The direction of the moment in an SD particle is determined by the applied field and the magnetic anisotropy of the particle. In an ellipsoidal particle, $\mathbf{H_d}$ is uniform and there is a demagnetizing tensor N such that

$$\mathbf{H_d} = -\mathsf{N} \cdot \mathbf{M} \tag{2.24}$$

If we include only magnetostatic terms, the energy density for a given external field $\mathbf{H}$ and magnetization $\mathbf{M}$ is

$$\mathrm{E} = \frac{1}{2}\mu_0 M_s^2 \hat{\mathbf{m}} \cdot \mathsf{N} \cdot \hat{\mathbf{m}} - \mu_0 M_s \hat{\mathbf{m}} \cdot \mathbf{H} \tag{2.25}$$

If uniaxial magnetocrystalline anisotropy (equation 2.6) or inverse magnetostriction (equation 2.8) are added, they can also be written in the form $(1/2)\mu_0 \hat{\mathbf{m}} \cdot \mathbf{N}' \cdot \hat{\mathbf{m}}$, so the total energy has the same form as for pure shape anisotropy.

Since $\hat{\mathbf{m}} \cdot \hat{\mathbf{m}} = 1$, the energy depends only on the direction of the magnetization. This energy can be represented by a closed surface (Figures 2.1 and 2.2) with the depressions corresponding to minima and the high points to maxima. Between any two minima or maxima are saddle points. If the magnetization is represented by polar angles (M_θ, M_ϕ), the minima, maxima and saddle points all have zero derivatives and thus are stationary points.[3] In a large field (Figure 2.2), there is one minimum in the direction of the field and one maximum in the opposite direction. In zero field, there are two minima for magnetization along the short (easy) axis, two maxima for magnetization along the long (hard) axis, and two saddle points for magnetization along the intermediate length axis.

Some examples of a set of solutions are shown in Figure 2.3. The solutions are for a particle with three unequal axes. In a large field, there are two solutions, a minimum and a maximum. The applied field is not aligned with the easy axis, so as the field decreases the minimum moves towards the easy axis and the maximum towards the hard axis. In addition, new stationary states appear. In Figure 2.3c, for example, there is a critical field (point A) where a second minimum appears. If there are two valleys, there must be a mountain pass connecting them, so a saddle point appears at the same field. Initially, the saddle point coincides with the new minimum, but as the field decreases it moves toward the intermediate axis. Then another maximum and saddle point appear (point B). In zero field there are six stationary states corresponding to those in Figure 2.1.

As the field continues to decrease, pairs of stationary points approach each other again, but the pairing is not the same as before. The saddle point that appeared

---

[3] The stationary points can also be obtained using Lagrange multipliers (Appendix A).

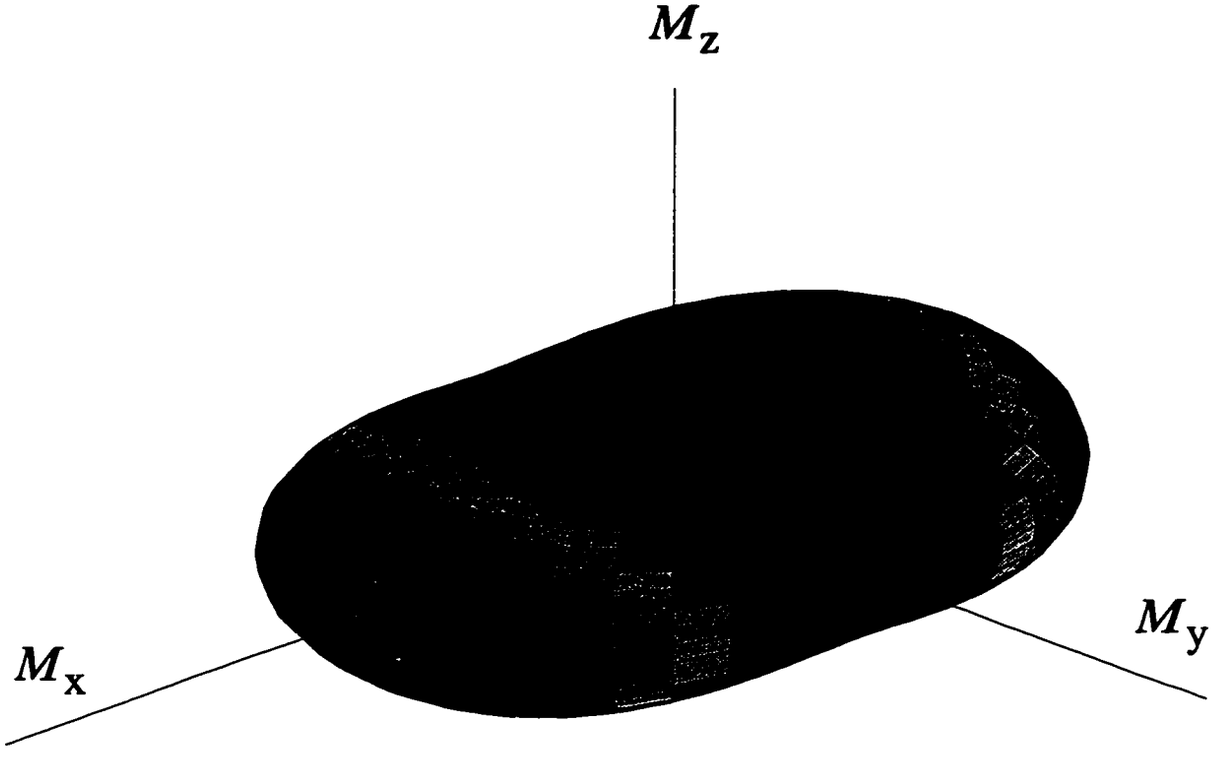

Figure 2.1: Energy surface for a SD particle in zero field. The particle is an ellipsoid with three unequal axes. The energy depends only on the direction of the magnetization and is proportional to the distance from the origin. The depressions in the $\pm z$ directions indicate minima. There are maxima in the $\pm x$ directions and saddle points in the $\pm y$ directions.

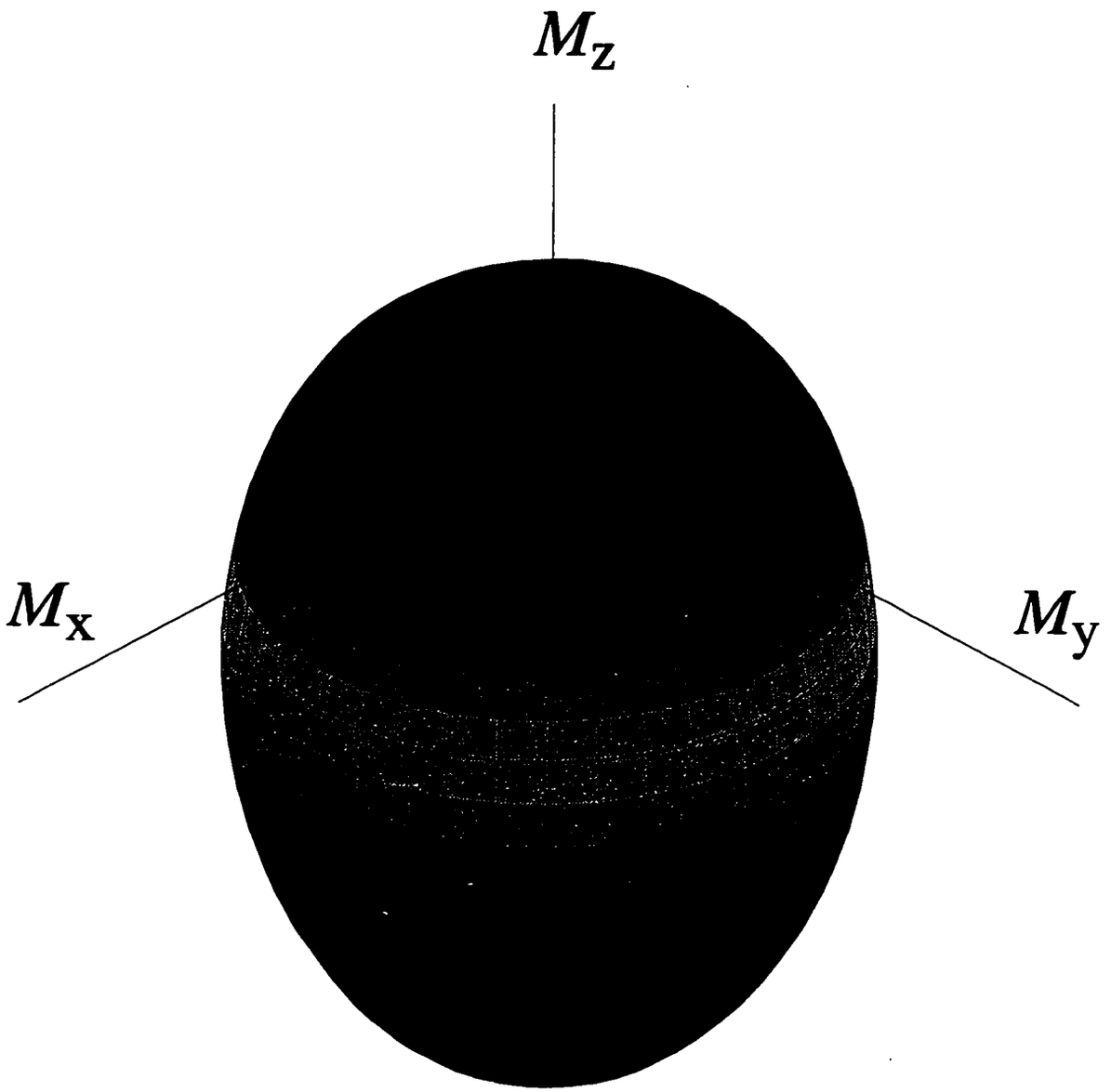

Figure 2.2: Energy surface for a SD particle exposed to a large field along the easy axis. The conventions are the same as in the previous figure. The field is above the switching field for the particle. The only minimum is in the $+z$ direction, and there is a maximum in the $-z$ direction.

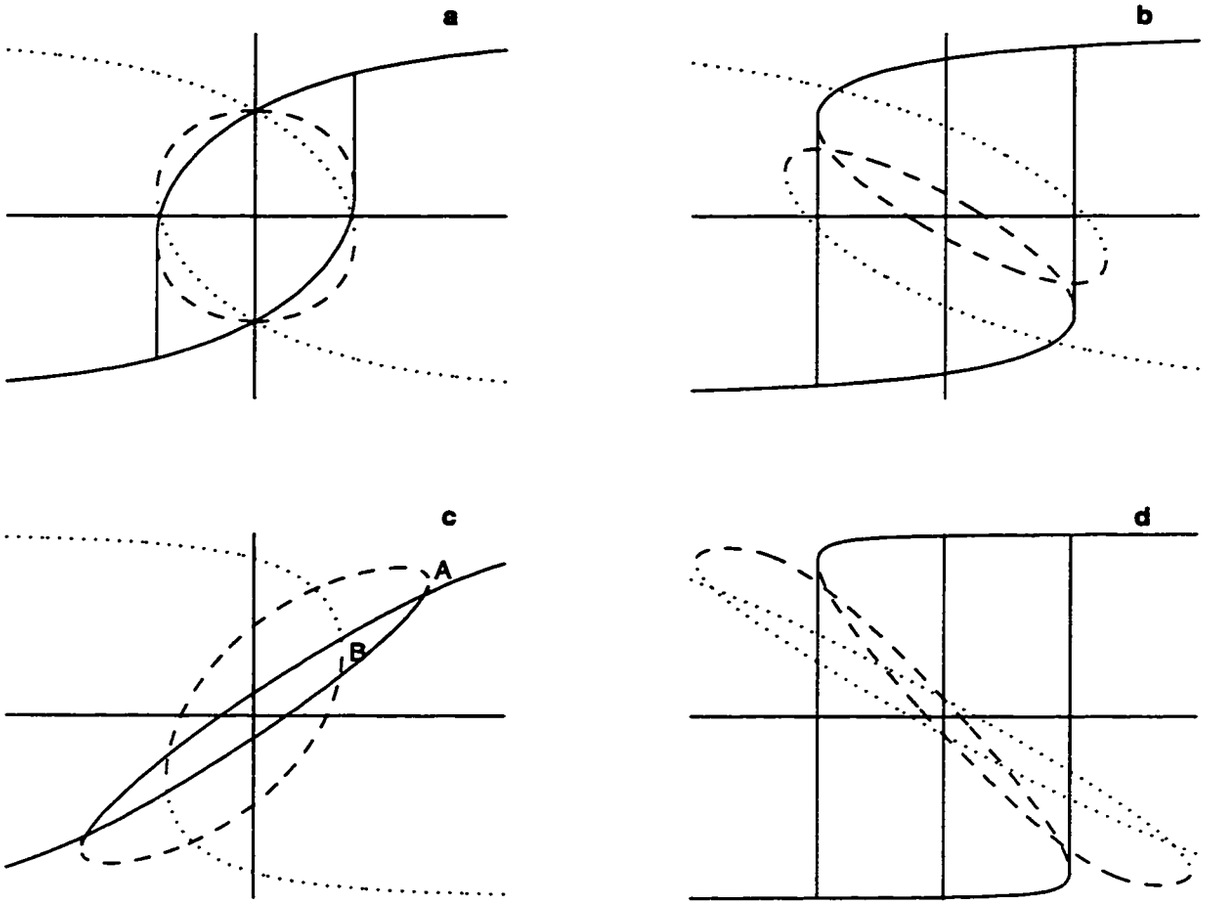

Figure 2.3: Examples of hysteresis curves for a triaxial SD particle which has a demagnetizing tensor with eigenvalues $[1/6, 1/3, 1/2]$. The vertical axis is the magnetization, the horizontal axis is the applied field. Minima are connected by solid lines, saddle points by dashed lines and maxima by dotted lines. Vertical solid lines indicate jumps when the minima become unstable. Points A and B are referred to in the text. The field directions are parallel to (a) (1,1,1) (b) (7,1,4) (c) (1,4,7) (d) (10, 1, 1).

with the minimum approaches the original maximum; when the pair meet they both disappear. The other saddle point disappears with the original minimum. Finally, in large negative fields there are just a minimum and maximum in directions opposite to the original directions.

When a minimum is annihilated, the magnetization must jump to the other minimum. The hysteresis curve is a combination of the reversible curves and the irreversible jumps. Where the magnetization changes are reversible, the slope of the curve dM_H/dH is always positive. This is an example of the more general theorem by Brown (section 2.1.1). There is one exception, however, that Brown overlooked. If an isolated, uniaxial SD particle is in a field that is parallel to the easy axis, M_H does not change until the state becomes unstable. Brown assumes in his proof that M_H can change continuously, but in this highly symmetric configuration the magnetization can only be up or down.

Note also that the maxima always have negative slope. A maximum for an energy functional E is a minimum for $-E$, so the same arguments that Brown used can be adapted to show that energy maxima satisfy $\partial M_H/\partial H \leq 0$. Saddle points can have positive or negative slope.

Where a minimum and a saddle point approach each other, the slope of the hysteresis curve approaches vertical ($dM_H/dH \to \infty$). It is likely that this is generally true (aside from special cases), but I have no proof of that. Schabes and Bertram [1988] called the field at which the jump occurs the switching field H_s.

2.3.2 Ensembles of Particles and the Wohlfarth Relations

In rock magnetism, we are interested in samples in which many grains contribute to the moment, and the grains usually have a nearly uniform distribution of orientations. There are some qualitative differences in magnetic behavior between single particles and multiple particles. The moment of a single particle can be in any direction, depending on the balance between the field and the internal anisotropy; the moment

of an isotropic ensemble of grains is in the direction of the field. The moment of the single particle has a fixed magnitude, but that of the ensemble can be anywhere from positive to negative saturation. A single SD particle cannot be demagnetized, but an ensemble can.

If particle interactions can be ignored, the bulk hysteresis properties can be obtained by summing the single-particle contributions. Some parameters are easy to derive: for example, the saturation magnetization for an isotropic ensemble of SD grains is $M_{rs}/M_s = 0.5$ (Appendix A). Other parameters, such as the coercivity H_c, have only been calculated numerically.

If we are interested in the remanence-carrying fraction of a sample, hysteresis parameters such as M_s, H_c and χ_0 can be misleading because they are affected by paramagnetic and superparamagnetic particles. It is better to concentrate on irreversible changes.

In this section, I look at three kinds of remanence. The first, isothermal remanence $M_r(H)$, is acquired after a sample is exposed to a field H; it is assumed the sample was previously demagnetized so the moments of individual particles are uniformly distributed in all directions. The saturation isothermal remanence (SIRM) is $M_{rs} \equiv M_r(\infty)$. The second remanence, $M_r^{DC}(\infty, H)$, is obtained after an SIRM is exposed to a negative DC field $-H$. The third remanence, $M_r^{AF}(\infty, H)$, is obtained after an SIRM is exposed to an alternating field with peak amplitude H.

Two common measures of the stability of a remanence are the coercivity of remanence H_{cr}, the DC field required to reduce the remanence to zero, and the median destructive field $\tilde{H}_{1/2}$, the peak alternating field that removes half the remanence. A third measure which is sometimes used is $H_{1/2}^{+}$, the acquisition field for a remanence of $M_{rs}/2$. In terms of the above remanences, these parameters are defined by

$$M_r^{DC}(\infty, H_{cr}) = 0 \tag{2.26}$$

$$M_r^{AF}(\infty, \tilde{H}_{1/2}) = M_{rs}/2 \tag{2.27}$$

$$M_r(H^+_{1/2}) = M_{rs}/2 \tag{2.28}$$

Wohlfarth [1958] derived some useful relations between the above three remanences for non-interacting, uniaxial SD particles:

$$M_r^{DC}(\infty, H) = M_{rs} - 2M_r(H) \tag{2.29}$$

$$M_r^{AF}(\infty, H) = M_{rs} - M_r(H) \tag{2.30}$$

The Wohlfarth relations hold for any mixture of uniaxial anisotropies and any arrangement of particles (random or ordered). Wohlfarth does not derive the equations, remarking that they are easy to show; but it is worth doing the derivation explicitly to gain some insight into them. The key is that the relations are additive, so if it works for each particle separately it works for them all together, as long as they are not interacting. Thus it is sufficient to show the relations work for an arbitrary SD particle.

Suppose we have such a particle and there is an initial field $\mathbf{H}_0$ at an angle θ with respect to the easy axis. The remanence has only two possible values $\pm M_0$, where $M_0 = M_s \cos\theta$. The saturation remanence is M_0. If the particle has a saturation remanence and it is exposed to a field $-H$, the new remanence is

$$M_r^{DC}(\infty, H) = \begin{cases} M_0 & \text{if } H < H_s \\ -M_0 & \text{if } H > H_s \end{cases}$$

An individual SD particle cannot be demagnetized. To simulate AF demagnetization we must assume that if the peak amplitude of the alternating field is greater than H_s, the remanence has an equal probability of being $\pm M_0$, so on average the remanence is zero. Thus

$$\langle M_r^{AF}(\infty, H)\rangle = \begin{cases} M_0 & \text{if } H < H_s \\ 0 & \text{if } H > H_s \end{cases}$$

The same argument in reverse gives

$$\langle M_r(\infty, H)\rangle = \begin{cases} 0 & \text{if } H < H_s \\ M_0 & \text{if } H > H_s \end{cases}$$

If we combine the above expressions for the two cases ($H < H_s$ and $H > H_s$), we get the Wohlfarth relations.

From the Wohlfarth relations, Cisowski [1981] derived a diagnostic parameter R for a SD source of remanence. From equation 2.30, if the IRM acquisition and AF demagnetization curves are plotted against the acquisition field H, they are symmetric about $M = M_{rs}/2$ (see Figure 2.7). Where they cross, $M_r^{AF}(\infty, H) = M_r(H) = M_{rs}/2$, so equation 2.30 gives $M_r^{DC}(\infty, H) = 0$. Thus the crossing point is $H = H_{cr}$, the coercivity of remanence. Cisowski [1981] defined $R \equiv M_r(\infty, H_{cr})/M_{rs}$. For non-interacting, uniaxial SD particles, $R = 0.5$. For most samples, R is well below 0.5; this is attributed to particle interactions or larger particles. This parameter has the advantage that it is not affected by a superparamagnetic component.

Another crossing point could be used in place of the R parameter. From equation 2.30, at the crossing point of the IRM curve and the DC demagnetization curve, $M = M_{rs}/3$. I will denote the field at this point by $H_=^{DC}$.

Wohlfarth [1958] also generalized his relations to the demagnetization of an IRM acquired in a field H_0. If we define $M_r^{DC}(H_0, H)$ as the remanence after $M_r(H_0)$ is exposed to a DC field $-H$ and $M_r^{AF}(H_0, H)$ as the remanence after $M_r(H_0)$ is exposed to an alternating field with peak amplitude H; then

$$M_r^{DC}(H_0, H) = \begin{cases} M_r(H_0) - 2M_r(H) & \text{if } H < H_0 \\ -M_r(H) & \text{if } H > H_0 \end{cases} \tag{2.31}$$

$$M_r^{AF}(H_0, H) = \begin{cases} M_r(H_0) - M_r(H) & \text{if } H < H_0 \\ 0 & \text{if } H > H_0 \end{cases} \tag{2.32}$$

From equation 2.32, an IRM acquired in a field H_0 is removed by a peak alternating field of the same magnitude. We can generalize the coercivity of remanence to $H_{cr}(H_0)$, the DC field that removes $M_r(H_0)$; similarly, we generalize $\tilde{H}_{1/2}$ to $\tilde{H}_{1/2}(H_0)$ and $H_{1/2}^+$ to $H_{1/2}^+(H_0)$ (the latter being the acquisition field for a remanence

$M_r(H_0)/2$). The above relations then give

$$H_{cr}(H_0) = \tilde{H}_{1/2}(H_0) = H^+_{1/2}(H_0) \tag{2.33}$$

for any H.

The stability of a remanence is often judged by plotting the demagnetizing curves with the remanence normalized by the initial remanence. From the above equations, the slopes are $-2M_r(H)/M_r(H_0)$ for DC and $-M_r(H)/M_r(H_0)$ for AF demagnetization. The slope decreases as $M_r(H_0)$ increases, and therefore as H_0 increases. Thus by this measure IRM in SD particles increases in stability as the acquisition field increases.

Thermal Fluctuations Affect Remanence

So far I have only mentioned thermal fluctuations in superparamagnetic particles, where they maintain equilibrium between remanent states. In SD particles, thermal fluctuations can still be important because as the field increases, the energy barrier between minima decreases and the relaxation time for a transition decreases. In section 2.3.3 I will describe the effect on remanence.

Thermal fluctuations do not affect the Wohlfarth relations, however. For a single particle (2.3.2), the relaxation time is the same for a transition from $-M_0$ to M_0 in a field $H > 0$ and for the reverse transition in a field $-H$. Thus the acquisition and destruction of remanence are affected equally.

Henkel [1964] introduced the idea of plotting the remanences against each other (Figure 2.4) using the more general version of the Wohlfarth relations (equations 2.32 and 2.32). This has not caught on in rock magnetism, but it has two advantages over plotting remanences against the field. First, although thermal fluctuations change the plots of remanence against field (Figure 2.7), they do not change the Henkel plots. Secondly, if there is a low-coercivity fraction that does not obey the Wohlfarth relations (for example, a cubic anisotropy), there may be a deviation from a straight

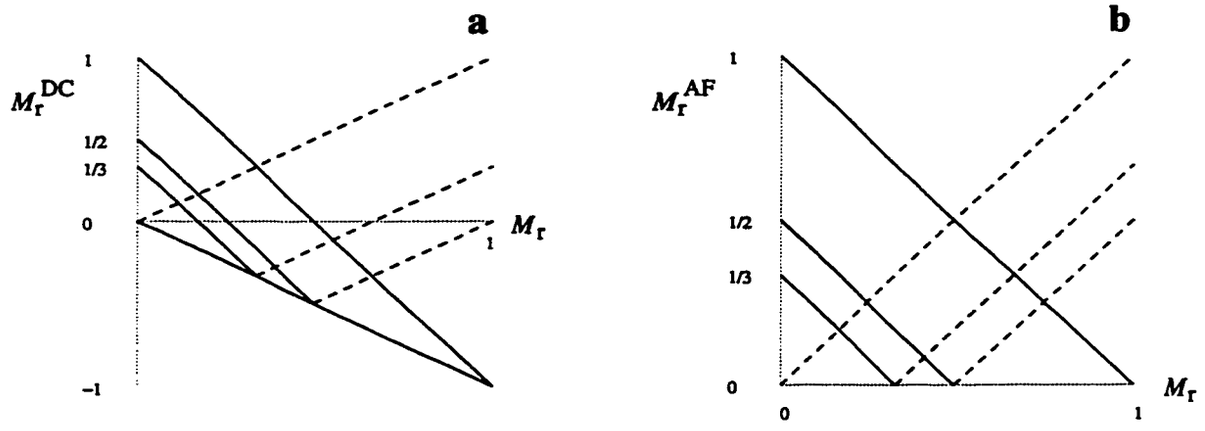

Figure 2.4: Plots of IRM acquisition against (a) DC demagnetization and (b) AF demagnetization; an augmented version of the plots in Henkel [1964]. Solid lines follow the demagnetization of a remanence acquired in a field H; dotted lines are for constant reverse or alternating field H.

line in small fields but a return to the line in larger fields. This would supplement the R parameter of Cisowski [1981].

2.3.3 Stoner-Wohlfarth Theory

It is much easier to derive the magnetic properties of ensembles if we simplify the problem as Stoner and Wohlfarth [1947] did, by assuming rotational symmetry about the long axis (or pure magnetocrystalline anisotropy): then $N_{11} = N_{22}$ and the demagnetizing tensor can be represented by a single demagnetizing factor $N = N_{11} - N_{33}$. The moment, the field and the easy axis all lie in the same plane, so the magnetization can be represented by a single angle ψ between it and the easy axis, and the field can be represented by the angle θ between it and the magnetization (Figure 2.5). The magnetization in the direction of the field is then $M_H = M_s \cos\phi$, where $\phi = \theta + \psi$. If we define a normalized field $h \equiv H/NM_s$, the reduced energy

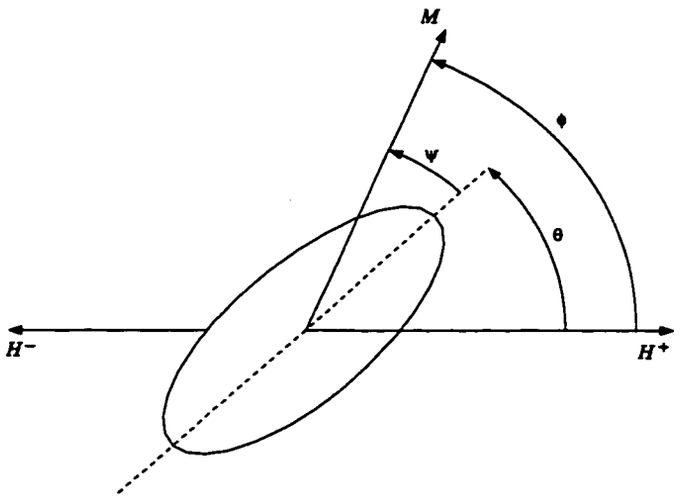

Figure 2.5: The geometry of the Stoner-Wohlfarth model. All the angles are with respect to the direction of the external field.

density is

$$\eta \equiv \frac{\mathrm{E}}{\mu_0 N M_s^2} = -\frac{1}{4}\cos 2(\phi - \theta) - h\cos\phi \tag{2.34}$$

so the magnetization is determined by just two parameters, the normalized field strength and the angle of the field θ. Stationary points satisfy

$$d\eta/d\phi = \frac{1}{2}\sin 2(\phi - \theta) + h\sin\phi = 0 \tag{2.35}$$

and minima satisfy the additional condition $d^2\eta/d\phi^2 > 0$.

If an increasing negative field is applied, the moment rotates until it reaches a critical angle $\psi_s(\theta)$ such that $d^2\eta/d\phi^2 = 0$, then it becomes unstable and jumps to a new direction. The switching field can be given in terms of the angle of the field [Stoner and Wohlfarth, 1947]:

$$h_s = \frac{\sqrt{1 - t^2 + t^4}}{1 + t^2} \tag{2.36}$$

where $t \equiv \tan^{1/3}\theta$. The critical angle ψ_s is always less than or equal to $\pi/4$.

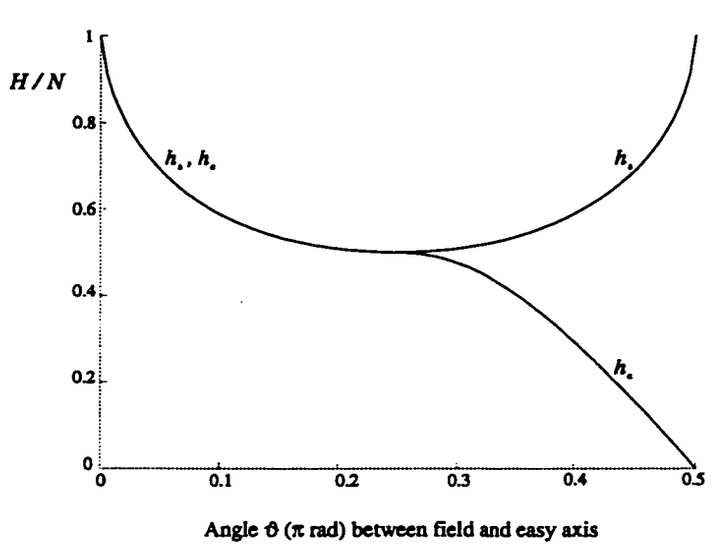

Figure 2.6: Dependence of the reduced coercivity h_c and the switching field h_c on the angle θ between the field and the easy axis. The curves coincide for $\theta \leq \pi/4$. The coercivity decreases monotonically from 1 to 0, but the switching field has a minimum of 0.5.

If $\theta < \pi/4$, the coercivity of a single particle is equal to the switching field. If $\theta > \pi/4$, the jump does not occur until $\cos\phi$ is already negative. The coercivity is then the solution of equation 2.35 for $\phi = \pi/2$ and is $h_c = (1/2)\sin 2\theta$. The dependence of h_s and h_c on θ are shown in Figure 2.6.

In a sample with many SD particles, the changes in remanence are determined by the switching field and they are straightforward to calculate (see below). To calculate the coercivity, the magnetization as a function of field must be summed up for all the particles and this has only been done numerically. For a uniform distribution of identical particles, Stoner and Wohlfarth [1947] obtained $h_c = 0.479$.

If thermal fluctuations are included, the saturation remanence is unchanged, but H_c and H_{cr} both decrease, and the ratio H_{cr}/H_c approaches unity [Joffe, 1969].

Remanence Calculations for Isotropically Oriented SD Particles

Remanence acquisition and destruction curves have been calculated before for the Stoner-Wohlfarth model [Chantrell *et al.*, 1985; Walker *et al.*, 1988], but the calculations have been numerical. In the simplest case, where thermal fluctuations are ignored, analytical expressions for the curves can be derived. I do that below.

Suppose we have an ensemble of identical particles with moments that are initially distributed uniformly in all directions. Using the Stoner-Wohlfarth notation, suppose a field $h = H/NM_s$ is applied to the sample. The magnetization is unchanged unless h exceeds the switching field h_s, in which case the particle acquires a remanence of $\cos\theta$. The remanence for the ensemble is

$$\frac{M_r(h)}{M_{rs}} = \frac{\langle\cos\theta\rangle}{0.5} = 2\int_0^{\pi/2} f(\theta,h)\cos\theta\sin\theta d\theta \tag{2.37}$$

where

$$f(\theta,h) = \begin{cases} 0 & \text{if } h \le h_s(\theta) \\ 1 & \text{otherwise} \end{cases} \tag{2.38}$$

When $h < 1/2$, the field is not large enough to reverse any particles (so $M_r = 0$); when $h \ge 1$, the magnetization is saturated ($M_r = M_{rs}$). For $1/2 \le h < 1$, it is convenient to use the inverse relation for the switching angle θ_s as a function of the field [Stoner and Wohlfarth, 1947]:

$$\tan^{1/3}\theta_s = \frac{\sqrt{3} \pm \sqrt{4h^2 - 1}}{2\sqrt{1-h^2}} \tag{2.39}$$

There are two solutions $\theta_s^{\pm}$, with the $\pm$ corresponding to the sign in equation 2.39; they are related by $\theta_s^+ + \theta_s^- = \pi/2$. For $\theta_s^- \le \theta \le \theta_s^+$, $f(\theta,h) = 1$. Thus for $1/2 \le h < 1$, using $\cos 2\theta = (1 - \tan^2\theta)\,/\,(1 + \tan^2\theta)$,

$$\frac{M_r(h)}{M_{rs}} = 2\int_{\theta_s^-}^{\pi/2-\theta_s^-} \cos\theta\sin\theta d\theta = \cos 2\theta_s^- = \frac{1 - t_s^6}{1 + t_s^6} \tag{2.40}$$

where

$$t_s = \tan^{1/3}\theta_s^- = \frac{\sqrt{3} - \sqrt{4h^2 - 1}}{2\sqrt{1-h^2}} \tag{2.41}$$

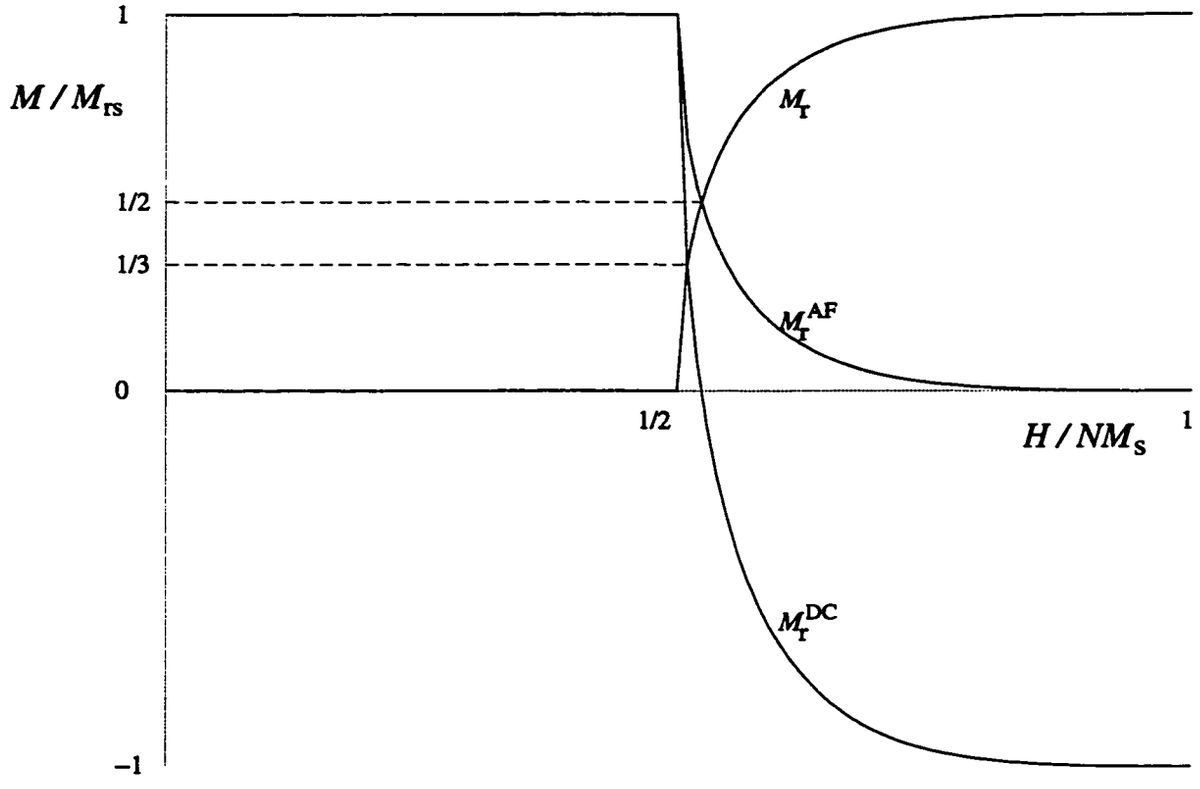

Figure 2.7: Acquisition and loss of IRM, as a function of field, for non-interacting SD particles with uniaxial anisotropy. The crossing point for IRM and AF demagnetization of SIRM is 1/2, while the crossing point for IRM and DC demagnetization of SIRM is 1/3.

In Figure 2.7, I plot the three kinds of remanence (with M_r^{AF} and M_r^{DC} obtained from M_r using the Wohlfarth relations). There is no change in remanence until $H = 0.5NM_s$.

The normalized median destructive field $\tilde{h}_{1/2}(h_0)$ can be calculated analytically using the above equations. From equation 2.32, if $M_r^{DC}(h_0, h_1) = 0$ then $M_r(h_1) = M_r(h_0)/2$. If $t_{s0} \equiv t_s(h_0)$ and $t_{s1} \equiv t_s(h_1)$, equation 2.40 implies

$$t_{s1}^6 = \frac{3 + t_{s0}^6}{1 + 3t_{s0}^6}$$

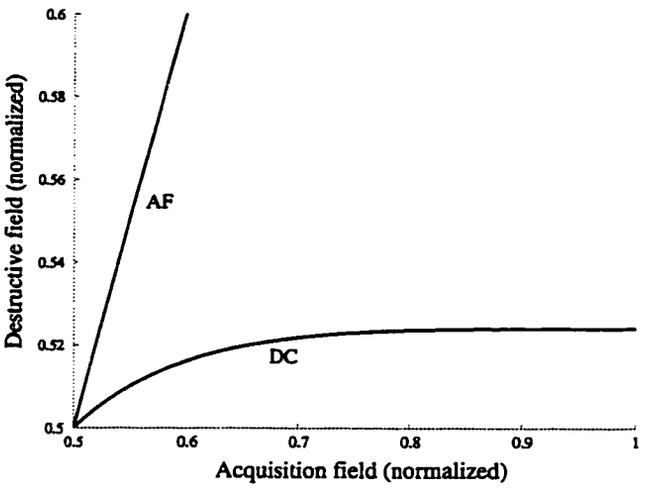

Figure 2.8: Relationship between acquisition and destructive fields for IRM in non-interacting, uniaxial SD particles. If the acquisition field is H, the peak alternating field (labeled AF) that removes it is also H, while the DC field is always between $0.5NM_s$ and $H_{cr} = 0.5240NM_s$.

The peak alternating field required to destroy this remanence is equal to the maximum switching field h_1, so from equation 2.36,

$$\tilde{h}_{1/2}(h_0) = \frac{\sqrt{1 - t_{s1}^2 + t_{s1}^4}}{1 + t_{s1}^2} \tag{2.42}$$

The other important field parameters immediately follow from the Wohlfarth relations (equation 2.33).

The relationship between acquisition and destructive fields is shown in Figure 2.8. If the initial state is one of saturation remanence, $t_{s0} = 0$ and $t_{s1} = 3^{1/6}$. This gives the usual coercivity of remanence $H_{cr}/NM_s = h_{cr}(\infty) = 0.5240$, which agrees with Wohlfarth [1958].

From the Wohlfarth relations, the crossing point of the curves for IRM and DC

demagnetization of SIRM is given by $M_r(\infty, h) = M_r(h)/3$. In this case,

$$t_{s1}^6 = \frac{2 + t_{s0}^6}{1 + 2t_{s0}^6}$$

For $t_{s0} = 0, t_{s1} = 2^{1/6}$ and the field at the crossing point is $h_=^{DC} = 0.5098$.

One aspect of the remanence curves in Figure 2.7 that is unlike measured curves is the sharp takeoff at a field of $0.5NM_s$. In real systems there is some remanence acquisition even in small fields. So far, SD calculations of the switching field that include thermal fluctuations have used a criterion for the energy barrier between minima such as $\Delta E = 25k_BT$ to determine a new switching field [Gaunt, 1968; Joffe, 1969; Chantrell *et al.*, 1985; Walker *et al.*, 1988] so there is still a sharp beginning to IRM acquisition for an ensemble of particles of the same size. In reality, as the field increases the relaxation time increases continuously, so in a given time interval there is an increasing probability of a transition. This spreads out the initial remanence acquisition over smaller fields, and the IRM acquisition depends on how long the sample is exposed to the field. Smaller particles have smaller energy barriers (because the energy barrier is proportional to the volume) so a distribution of particle sizes that extends into the SP range can enhance the small-field acquisition.

The analytical expressions I have derived should be useful for interpreting remanence curves, although as I show below the information one can obtain is limited. The expressions allow us to use DC or AF demagnetization. Most rock magnetists use the latter, but this will often introduce a significant time component because of the many oscillations of the field. For comparison with theory, remanence measurements using short duration DC fields would reduce the time component.

The Effect of Mixing Elongations

Wohlfarth [1958] claimed that a sample of uniaxial SD particles with mixed elongations would have a ratio $H_{cr}/H_c > 1.09$, but he did not demonstrate this. I will show that the ratio is always the same.

Suppose we have a distribution $\rho(N)$ of demagnetizing factors (corresponding to different particle elongations), and for any interval $[N, N+dN]$ the hysteresis behavior is well approximated by the average for a randomly oriented ensemble of particles with demagnetizing factor N.

For a given N, if we consider just the descending branch of the hysteresis curve for $H < 0$, the curve has the form

$$\frac{M}{M_s} = f\left(\frac{H}{NM_s}\right)$$

The function f is single-valued, so it can be inverted to give

$$\frac{H}{M_s} = Nf^{-1}\left(\frac{M}{M_s}\right)$$

Since the coercivity is defined by $M(-H_c) = 0$, $H_c = NM_s f^{-1}(0)$. Similarly, the back-field IRM curve is a single-valued function, and we can write

$$\frac{H}{M_s} = Ng^{-1}\left(\frac{M_r}{M_s}\right)$$

and $H_{cr} = NM_s g^{-1}(0)$.

If we now integrate over all elongations, the ensemble hysteresis curve is

$$\frac{\langle H\rangle}{M_s} = \int N\rho(N) f^{-1}\left(\frac{M}{M_s}\right) dN = \langle N\rangle f^{-1}\left(\frac{M}{M_s}\right)$$

where $\langle N\rangle = \int N\rho(N)dN$; similarly, the IRM curve is

$$\frac{\langle H\rangle}{M_s} = \langle N\rangle g^{-1}\left(\frac{M_r}{M_s}\right)$$

Thus

$$\frac{H_{cr}}{H_c} = \frac{g^{-1}(0)}{f^{-1}(0)} = \frac{H_{cr}}{H_c}\bigg|_{N=1}$$

so H_{cr}/H_c is the same for any mixture of particle elongations. The same argument applies to uniaxial magnetocrystalline anisotropy with varying K_1.

More generally, the main hysteresis loop and IRM curve have a fixed shape that is scaled by the average anisotropy. Surprisingly, we learn no more about uniaxial SD

particles from the entire curve than from a single parameter such as H_{cr}. However, deviations from this curve may provide information about thermal fluctuations, non-SD particles or cubic anisotropy (see below).

2.3.4 SD Particles With Cubic Anisotropy

In a uniaxial SD particle, with energy given by equation 2.25, there are at most two minima that are minima (aside from degenerate cases).[4] If one direction becomes unstable, the magnetization jumps to the other. Particles with cubic anisotropy are more complex. Instead of one easy axis, there are six (for $K_1 > 0$) or eight (for $K_1 < 0$), and there are as many as 26 stationary points. If a given state becomes unstable, it is not obvious which of the other minima the magnetization will jump to. As Johnson and Brown [1961] first pointed out, this makes some parts of the hysteresis curve indeterminate.

We face the same problem in micromagnetic calculations, except that we usually don't even know all the minima. Ideally, we should simulate the dynamic response of the magnetization to a change in the field, but this requires dynamic parameters that are not well known. In practice, we usually run our search algorithm for energy minima and hope it chooses the correct minimum. This is the approach that has been used in modeling particles with cubic anisotropy [Joffe and Heuberger, 1974; Geshev *et al.*, 1990; Geshev and Mikhov, 1992; Walker *et al.*, 1993a,b].

The main hysteresis parameters for SD grains are summarized in Table 2.1. There are minor disagreements in some of the parameters for cubic grains. The susceptibility can be obtained using perturbation theory (Appendix A); the susceptibility of the cubic grains are consistent with an effective uniaxial anisotropy of K_1 for $K_1 > 0$ and $-2K_1/3$ for $K_1 < 0$. For $K_1 < 0$, the values of H_c and H_{cr} are also roughly two thirds those for $K_1 > 0$, but the latter are well under the values for uniaxial anisotropy.

---

[4] The degenerate cases are $N_{11} < N_{22} = N_{33}$ (oblate spheroid) or $N_{11} = N_{22} = N_{33}$ (sphere).

Table 2.1: Some hysteresis parameters for SD particles. The parameter is H_K is $2|K_1|/\mu_0 M_s$ for magnetocrystalline anisotropy and NM_s for shape anisotropy. References: **a** Joffe and Heuberger [1974], Walker *et al.* [1993a] **b** Geshev and Mikhov [1992].

	Uniaxial	Cubic ($K_1 > 0$)	Cubic ($K_1 < 0$)
M_{rs}/M_s	1/2	0.831	0.866
H_c/H_K	0.479	$0.321^{a,b}$	$0.189^a, 0.193^b$
H_{cr}/H_K	0.524	$0.333^a, 0.341^b$	$0.204^{a,b}$
$\chi_0 * 2M_s/H_K$	1/3	1/3	1/2

Geshev and Mikhov [1992] calculated Henkel plots (M_r vs M_r^{DC}) for particles with cubic anisotropy. For both $K_1 > 0$ and $K_1 < 0$, the remanence at the crossing point is above $M_{rs}/2$ (recall that for uniaxial anisotropy it is $M_{rs}/3$). They did not calculate the crossing point for M_r^{AF}, but it will be even higher. Thus the R parameter of Cisowski [1981] is above 0.5. Since R is expected to be below 0.5 for MD particles or interacting SD particles, this parameter may be a useful diagnostic for particles with cubic anisotropy. In particular, it may help determine the origin of remanence in mid-ocean ridge basalts [Gee and Kent, 1995; Tauxe *et al.*, 1996].

2.4 MD Theory

The other widely used model for changes in magnetization is that of domain wall motion. In this section I describe a simple two-domain model of wall motion by Néel [1955] that has been widely used and adapted, especially for theories of TRM. I then describe some of the attempts to construct more realistic models. Many of these models either make assumptions for which the physical explanation is unclear or make predictions that are inconsistent with the two-domain model. Many of these problems can be traced to the internal field approximation. To give an idea of how

the results change when the internal field approximation is not used, I describe a crude model with a force on the domain wall that varies sinusoidally with position in the particle. Finally, I discuss the demagnetizing factor that appears in MD theories and how elongation may affect the magnetic properties.

2.4.1 The Landau-Lifshitz Model

Domain theories are united by some basic assumptions: the magnetization is divided into domains, each of which are uniformly magnetized in an easy direction, and the domains are separated by thin domain walls. In a classic model of a semi-infinite grain with uniaxial anisotropy, Landau and Lifshitz [1935] proposed the structure shown in Figure 2.9a, where most of the magnetization is parallel to the easy axis but there are "closure" domains at the surface. The domain walls at the surface make 45 degree angles with the surface, so $\Delta\mathbf{M}\cdot\hat{\mathbf{n}} = 0$ everywhere and there is no magnetic field (an example of pole reduction - see section 2.1).

The magnetization does not really make a sharp transition between domains. Landau and Lifshitz [1935] derived an equation for the internal structure of the domain wall. If θ is the angle between the magnetization and the easy axis,

$$\cos\theta = -\tanh\left(\frac{x}{w}\right)$$

where $w = \sqrt{A/K_1}$ is a measure of the width of the wall.

Observed domain patterns are often much more complex than the Landau and Lifshitz model; ultimately, much of the complexity is due to the finite size of real bodies. More complex domain theories have been reasonably successful in explaining the observed patterns [Stewart, 1954; Craik and Tebble, 1965].

2.4.2 The Two-Domain Model

It is much more difficult to use domain theories to predict hysteresis properties. The pole-reduction principle (section 2.1) is difficult to apply: instead of the poles $\nabla\cdot\mathbf{M}$

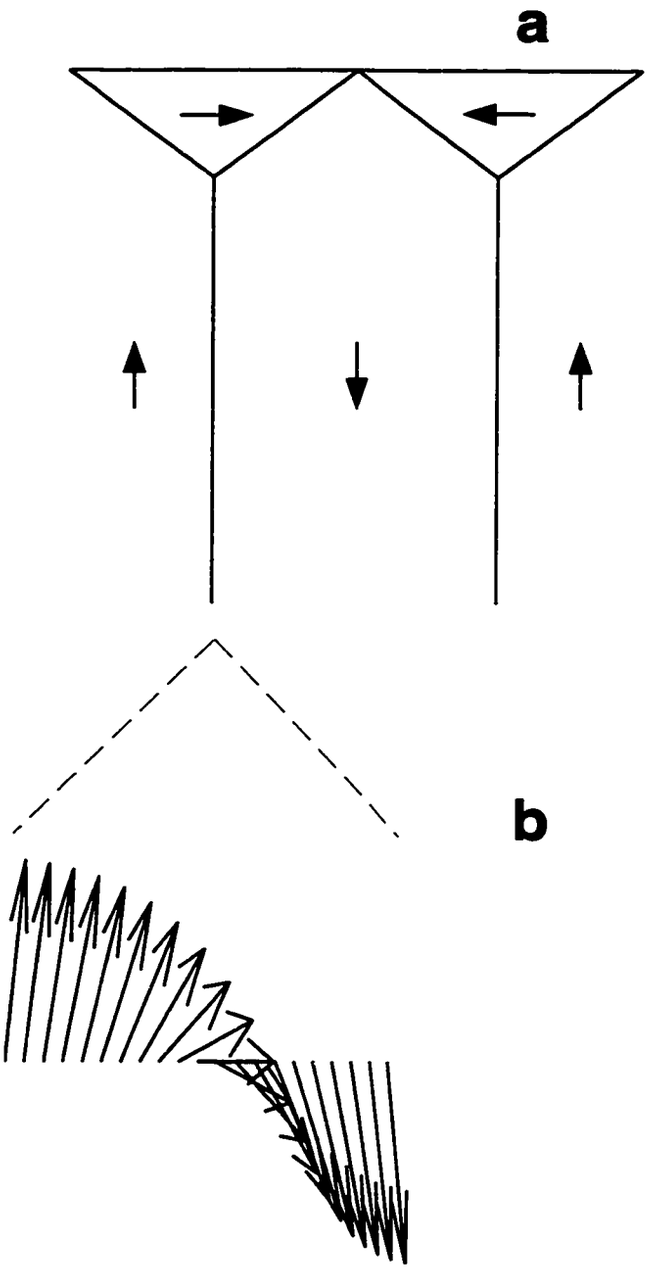

Figure 2.9: The model of Landau and Lifshitz for a particle that is infinite downwards and perpendicular to the page. Directions of magnetization are shown by arrows. (a) The magnetization in each domain is uniform. Lines indicate domain walls. (b) A closer look at the magnetization within a domain wall.

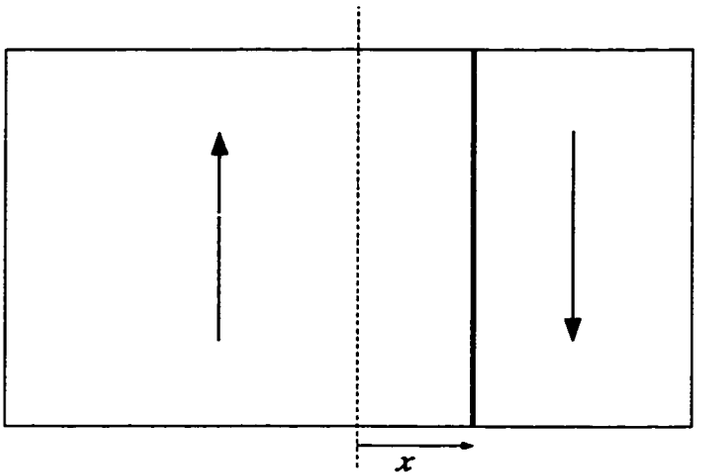

Figure 2.10: The two-domain model. The magnetizations in each domain is in the direction of the arrow. The dotted line indicates the center of the particle.

and $\mathbf{M} \cdot \hat{\mathbf{n}}$ being reduced, they are arranged so as to produce an internal field that opposes the external field. When there is a change in field, the magnetization can respond by rotation within domains or by complex rearrangements of domain walls.

Most MD hysteresis theories assume there are two domains (Figure 2.10). The magnetization in each domain is in the easy direction. The total moment is the sum of the moments of the two domains. If the domain wall is displaced a distance x from the center, the volume-average magnetization is[5]

$$\frac{M}{M_s} = \frac{2x}{L} \tag{2.43}$$

If the magnetic anisotropy in the particle is uniform, the lowest energy position of the wall in zero field is in the middle of the particle, so the remanent magnetization is zero. For nonzero remanence, there must be a non-uniform anisotropy, imposed

[5] Most MD models derive expressions for the total volume-average magnetization M rather than the hysteresis component M_H. If the field is at an angle θ, it is usually assumed the average magnetization does not rotate and $M_H = M \cos\theta$.

on the main anisotropy, which opposes the motion of the domain wall towards the center. The non-uniformity is usually attributed to inverse magnetostriction from the stress fields around defects.

It is also assumed there is a MD demagnetizing factor N such that the demagnetizing energy is $(1/2)\mu_0 N M^2$; this is a reasonably accurate approximation for a lamellar two-domain model, as long as the domain wall is not too close to the edges of the particle.[6]

The energy of the particle is

$$E = -\mu_0 V M H + \frac{\mu_0 V}{2} N M^2 + E_w(M) \tag{2.44}$$

where $E_w(M)$ is the spatially non-uniform part of the wall energy. Strictly speaking, it is a function of the wall position, but since $M \propto x$, it can be expressed as a function of M. Stationary states satisfy $dE/dx = 0$, which is a balance between forces. An equivalent formulation in terms of effective fields is

$$-\frac{1}{\mu_0}\frac{dE}{dM} = H + H_d + H_w = 0 \tag{2.45}$$

where $H_d = -NM$ and $H_w = -(1/\mu_0 V) dE_w/dM$.

A stable state must also satisfy $d^2E/dx^2 > 0$, or

$$\frac{1}{\mu_0}\frac{d^2E}{dM^2} = N + \frac{1}{\mu_0}\frac{d^2E_w}{dM^2} > 0 \tag{2.46}$$

Taking derivatives with respect to H in equation 2.45 gives

$$\frac{dM}{dH} = \left(N + \frac{1}{\mu_0}\frac{d^2E_w}{dM^2}\right)^{-1} > 0$$

The slope of the hysteresis curve is always positive, in agreement with the more general prediction of Brown [1963] (section 2.1.1). As in the SD model (end of

[6] Because the MD models do not work well near saturation, I only show part of each MD hysteresis curve near the origin.

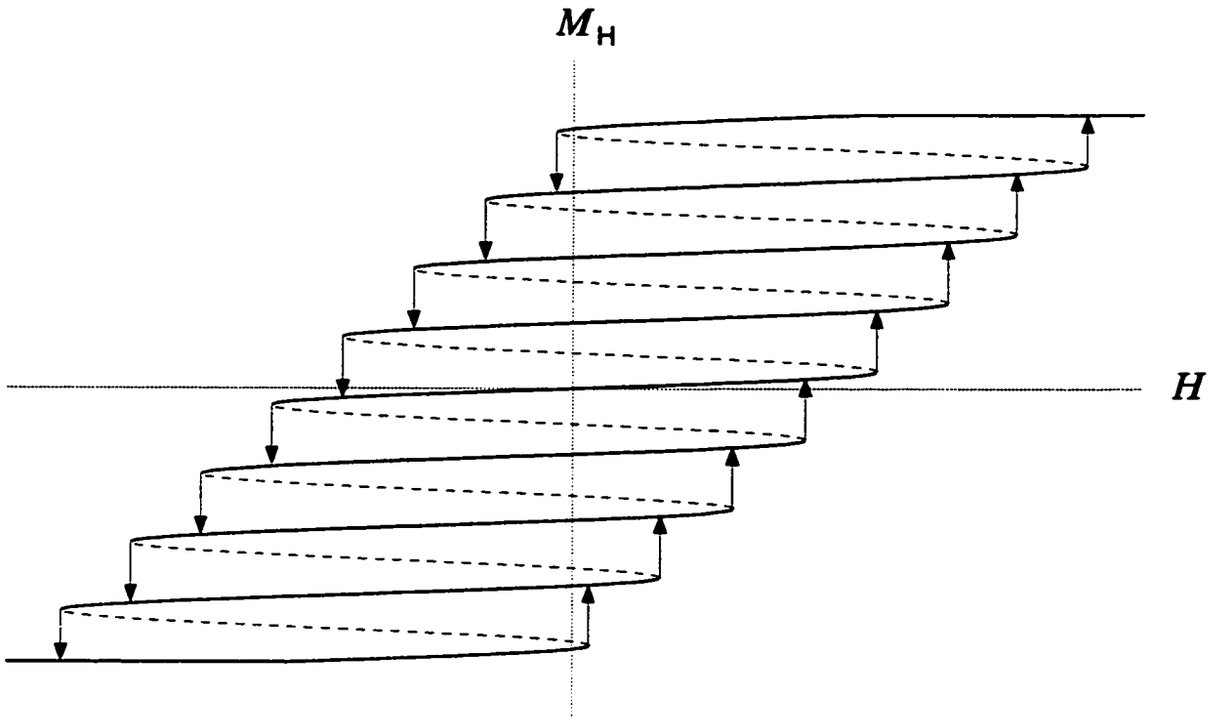

Figure 2.11: A MD hysteresis model with a sinusoidal wall energy. The parts of the curve that correspond to stable states are solid, while unstable states are dotted lines. Arrows indicate irreversible transitions.

subsection 2.3.1), the slope approaches infinity as the field approaches an instability field.

Formulating the equations in terms of the field makes it easier to interpret them in terms of hysteresis. Since equation 2.45 gives H as a function of M, when combined with the stability condition it gives the hysteresis curve directly.

A simple example of a MD model with a sinusoidal wall energy E_w is shown in Figure 2.11. When H reaches a value for which $d^2E/dM^2 = 0$, a jump occurs. As the period $\Delta M/M_s$ of the sinusoid decreases, the jumps get smaller and the model approaches that of Néel [1955] (Figure 2.12).

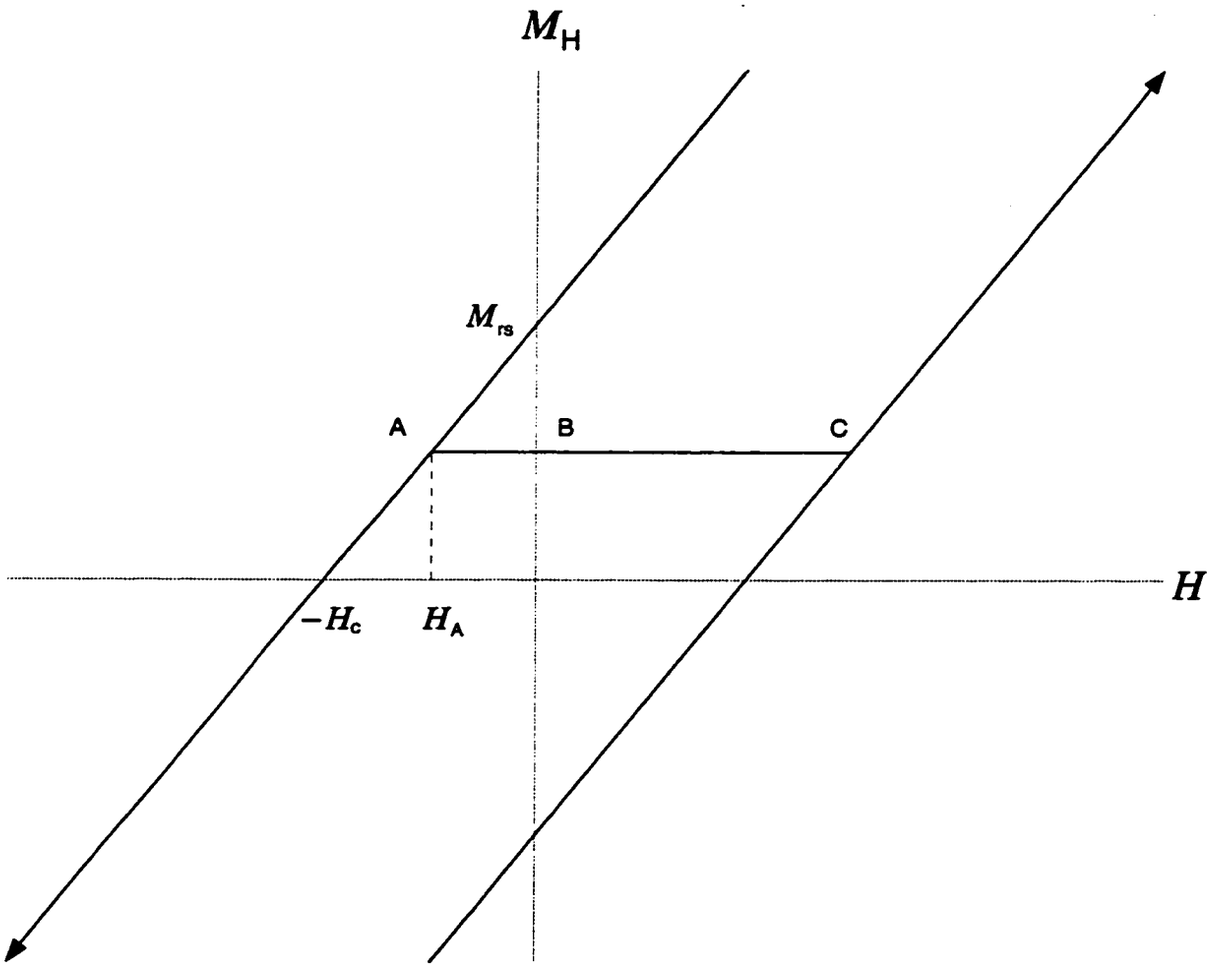

Figure 2.12: Néel's MD hysteresis model with the magnetization plotted as a function of the external field H. The arrows on the ascending and descending branches indicate irreversible change. If the particle is in state A and the field increases, the magnetization does not change until it reaches the point C.

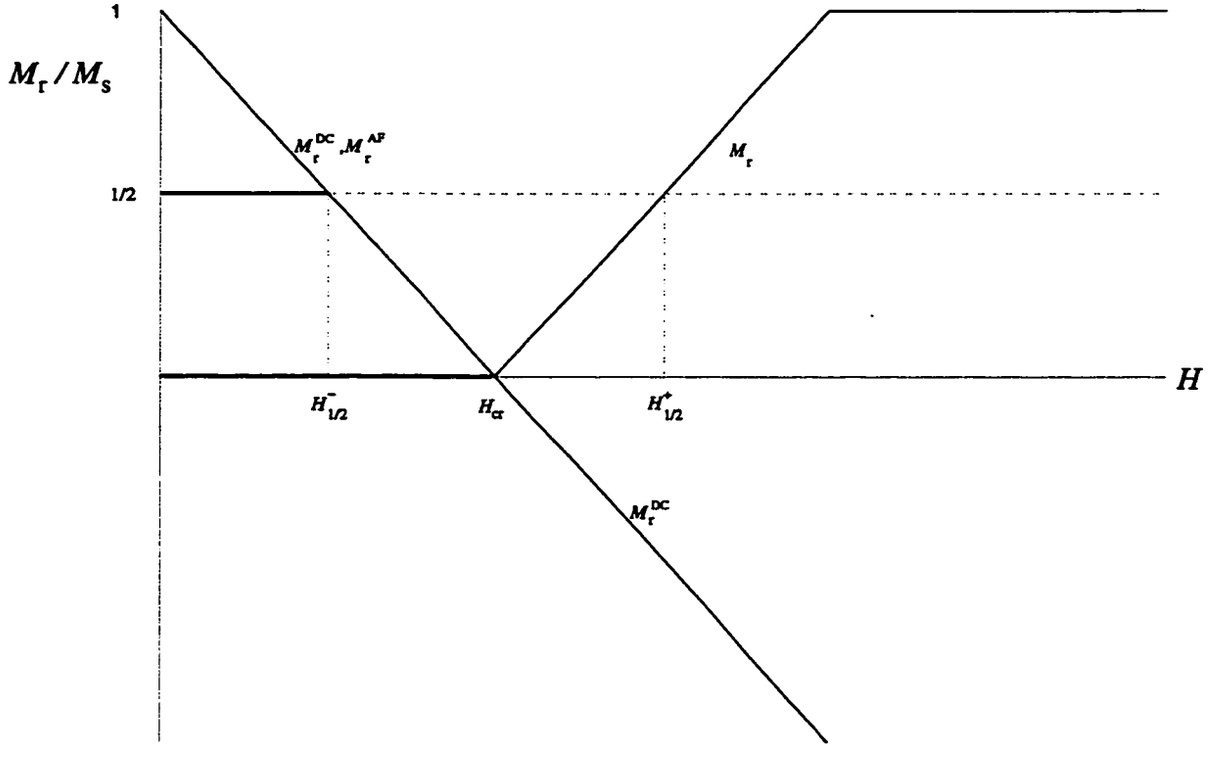

Figure 2.13: The remanence curves for Néel's MD hysteresis model.

2.4.3 Néel's MD Model

In Néel's model, all changes in magnetization are irreversible. $H_{cr} = H_c = NM_{rs}$ and the initial susceptibility is $\chi_0 = 0$. The demagnetized state is at the origin. If the particle is demagnetized and a field H is applied, it does not acquire any remanence until $H > H_c$. If it is in a saturation remanent state, the remanence loss in a DC back field is $\Delta M_r = -H/N$.

The remanence curves are shown in Figure 2.13. This is an extreme example of MD-style remanence curves (compare Figure 2.7). Remanence loss from the SIRM state is the same for DC and AF treatments until $H = H_{cr}$, when the particle is completely demagnetized. Greater DC fields drive the magnetization negative. The R parameter of Cisowski [1981] is zero; $\tilde{H}_{1/2} = H_{cr}/2$ and $H^+_{1/2} = 3H_{cr}/2$.

In Figure 2.12, if the particle is in state B it does not lose any remanence in a negative field until the magnitude of the field is greater than $|H_A|$. Thus the AF or DC demagnetization curve for a low-field remanence is horizontal until it touches the demagnetization curve for SIRM, then it coincides with it. If, as is normally done, the demagnetization curves for saturation remanence and $M_{rs}/2$ are normalized by the initial remanence, the curve for $M_{rs}/2$ lies above the curve for saturation remanence.

Thus, in this model, the lower the acquisition field, the harder the remanence. This is the opposite of what the SD model predicts (subsection 2.3.2), and it will seem counterintuitive to many rock magnetists. The contrast between the SD and MD models suggests an isothermal analogue of the Lowrie-Fuller test (section 1.3), where the stability of a low-field IRM is compared with the stability of SIRM. This has the advantage that IRM is easier to understand than TRM or ARM, and the stability predictions for SD particles are robust because they are based on the Wohlfarth relations.

2.4.4 Other MD Models

The model of Néel [1955] is very simple, and it does not represent many of the properties of real particles - for example, $\chi_0 \neq 0$ and $H_{cr} > H_c$.

There have been numerous attempts to refine the model. All begin by assuming that one can remove the effect of the shape of the particle by looking at the response to an internal field:

$$H_i = H - NM \tag{2.47}$$

The particle is assumed to have an intrinsic susceptibility

$$\chi_i \equiv \frac{dM}{dH_i} \tag{2.48}$$

Combining equations 2.47 and 2.48,

$$\chi_0^{-1} \equiv \frac{dH}{dM} = N + \chi_i^{-1} \tag{2.49}$$

If the intrinsic susceptibility is low ($\chi_i \ll N$) then $\chi_0 \approx \chi_i$. As the intrinsic susceptibility increases, χ_0 approaches $1/N$.

There is also an assumed intrinsic coercivity, but since it is defined by $M = 0$ it is the same as the observed coercivity.

In Néel's theory, $H_c = NM_{rs}$, so the demagnetizing factor can be inferred directly from the hysteresis loop. If the hysteresis loop in Figure 2.12 is shown in internal field coordinates, the sides of the loop are vertical. Some authors argue it is not that simple. Smith and Merrill [1982] assume the sides are not really vertical:

$$S \equiv \left.\frac{dM}{dH_i}\right|_{H_i=-H_c} < \infty$$

so

$$N = \frac{H_c}{M_{rs}} - \frac{1}{S}$$

and N cannot be determined without some assumption about S.

Dunlop [1984] uses equation 2.49 and a heuristic relation first proposed by Kittel [1949]

$$\chi_i H_c \approx \text{constant} \tag{2.50}$$

In such heuristic theories, it is not clear what the physical mechanisms are that give rise to S or Kittel's condition. The demagnetizing factor N is no longer a simple geometrical factor; because of the extra conditions, it depends indirectly on the intrinsic inhomogeneity as well.

Other models calculate the stress fields around defects and use them to derive the hysteresis properties. Such models can be very complex [Trauble, 1969; Xu and Merrill, 1989]. Most of them concentrate on the coercivity, which in the internal field approximation is

$$H_c = \frac{1}{\mu_0 V} \left| \frac{dE_w}{dM} \right|_{max} \tag{2.51}$$

where the integral is over the volume of the particle.

There have been fewer calculations of the susceptibility using defect models. Néel [1955] himself used a "slightly more refined" model for the wall energy to derive hysteresis properties of demagnetized particles in small fields. The effective field $(1/\mu_0)dE_w/dM$ is approximated by a series of random steps with the end points having a Gaussian distribution about a mean of zero. An example of such a distribution is shown in Figure 2.14; it is left to the reader to imagine how this can be reconciled with the sinusoidal model.

The MD Demagnetizing Factor

The magnitude - and applicability - of the demagnetizing factor in MD grains has been the subject of many publications. Néel [1955] assumed that the demagnetizing tensor was roughly the same as in SD particles, and subsequent calculations are consistent with this assumption. One difference that is rarely pointed out, however, is that the demagnetizing factor N that appears in equation 2.44 is not equal to the difference

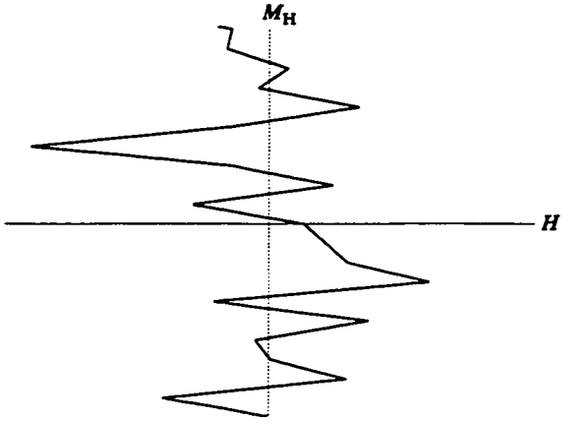

Figure 2.14: An example of a wall pinning model proposed by Néel. The effective field $(1/\mu_0)dE_w/dM$ is a series of steps with the distribution of end points being a Gaussian distribution about a mean.

between components of **N**, as in SD theory: it is equal to the component in the direction of the magnetization. The demagnetizing tensor for a cube is $N_{ij} = \delta_{ij}/2$, so the SD demagnetizing factor is $N = 0$, but the MD demagnetizing factor for the same tensor would be 1/3. However, the MD demagnetizing factor for a two-domain state in a cube is actually 1/6 [Dunlop, 1983a]. [7]

As elongation increases, N decreases for magnetization along the long axis and increases for magnetization along the other two axes. This has some interesting implications for the shape dependence of hysteresis. Let us suppose the long axis is in the z direction. For a field in that direction, $M_{rs} = H_c/N_{33}$ and N_{33} decreases as the aspect ratio increases. The other diagonal components N_{11} and N_{22} decrease as the aspect ratio increases. If H_c does not depend on shape, the saturation remanence

[7] A few models have attempted to estimate the demagnetizing factor for multiple walls [Merrill, 1977; Dunlop, 1983a; Xu and Merrill, 1987, 1990], although the assumptions on the initial wall positions and movements are very restrictive.

is an increasing function of the aspect ratio for a field aligned with the long axis and it is a decreasing function of the aspect ratio for a field aligned with either of the other two axes. Thus there is an increasing anisotropy in the remanence as the aspect ratio increases.

The above conclusion may change if H_c does depend on elongation. As I will show in subsection 2.4.6, the coercivity is affected by the length scale of the pinning field, and a smaller N can enhance the effect. Also, a wall with a greater area intersects more defects; if defects are providing the pinning force, the coercivity may increase or decrease with wall area depending on whether the defects interfere constructively or destructively.

We can at least say, however, that M_{rs}/H_c increases with aspect ratio if the field is parallel to the long axis, and it decreases with aspect ratio if the field is parallel to one of the shorter axes.

The susceptibility χ_0 should also depend on the direction of the field. If the pinning forces are weakly dependent on orientation of the wall, χ_0 should be larger for a field parallel to the long axis because the demagnetizing factor is smaller. By contrast, in SD particles χ_0 is largest parallel to the easy axis.

2.4.5 Critique of the Internal Field Approximation

All MD models use the internal field approximation, where the response to an internal field $H_i = H - NM$ is determined first and then the observed hysteresis properties are derived from a coordinate transformation. It is not obvious that this is an approximation because some of the terms are not defined precisely. For example, in the definition of χ_i (equation 2.48), the field at which it is evaluated is not given - although by analogy to χ_0, one would expect $H_i = 0$. A more precise version of equation 2.49 is

$$\chi_0^{-1} \equiv \left.\frac{dH}{dM}\right|_{H=0} = N + \left.\chi_i^{-1}\right|_{H=0} \tag{2.52}$$

This is only equal to χ_i if $H_i = 0$ when $H = 0$, which implies the remanence is zero.

In the internal field approximation, the field exerts a force $2\mu_0 H_i M_s A$ on the wall (where A is the wall area). The wall moves until the force is balanced by the pinning force dE_w/dx. The wall position changes continuously with increasing H_i as long as dE_w/dx increases monotonically with decreasing x; but if dE_w/dx reaches a maximum, the wall jumps to a new location where dE_w/dx is large enough. A series of such jumps (Barkhausen jumps) may occur before the force on the wall exceeds the maximum pinning force in the particle, and then the magnetization reverses. The coercivity is therefore determined by the maximum pinning force as in equation 2.51. In this model, the coercivity is not affected by the location of the largest pinning force or the spacing of the maxima.

When dE_w/dx is a maximum, $d^2E_w/dx^2 = 0$; equivalently, $d^2E/dM^2 = 0$. This does not agree with the instability criterion based on the total energy (equation 2.46):

$$\frac{1}{\mu_0}\frac{d^2E}{dM^2} = N + \frac{1}{\mu_0}\frac{d^2E_w}{dM^2} = 0$$

The reason for the difference is that the stability criterion in the internal field approximation is based on the assumption that H_i is independent of M. The true independent variable, however, is H, and $H_i = H - NM$.

In Figure 2.15 I illustrate how different the predictions of the internal field approximation can be from those of the correct solution. The correct coercivity is only affected by the forces on the domain wall near the center of the particle.

Implicit in the internal field approximation is the belief that there are "intrinsic" hysteresis properties that are characteristic of a material and can be separated from the effects of shape. The magnetic response to the internal field is often thought of as the response that an infinite magnetic body would have. It is assumed the infinite body, having no surfaces, would have all its demagnetizing factors equal to zero.

In reality, if we try to determine the limit of the demagnetizing tensor N as the particle size approaches infinity, the tensor is conditionally convergent (it depends on

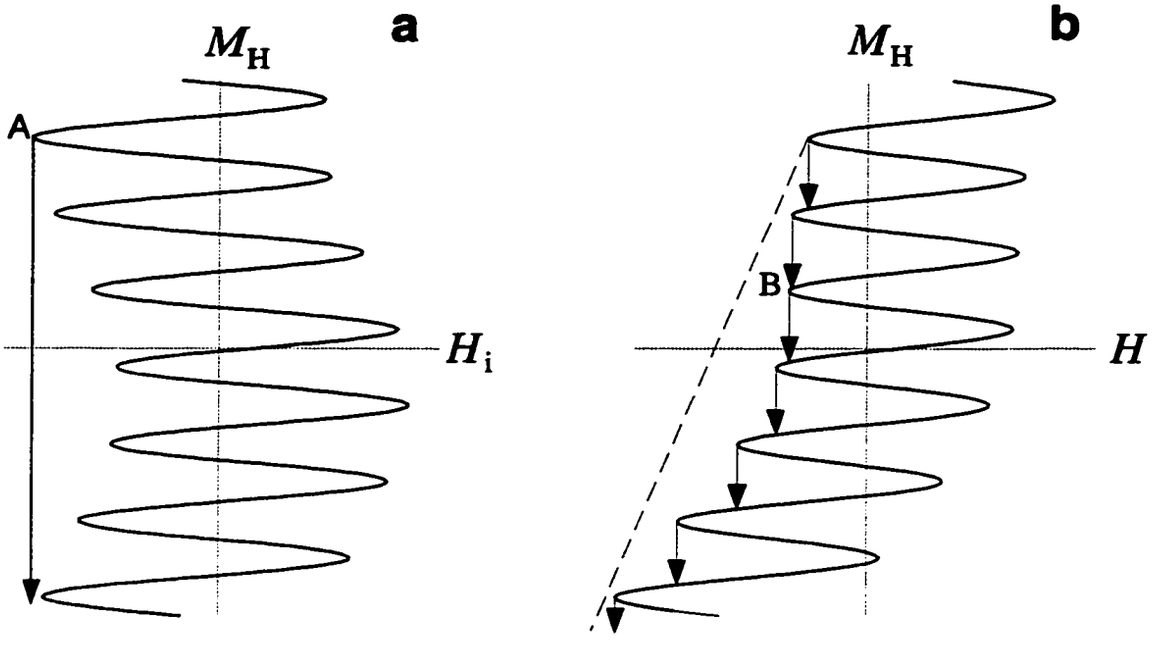

Figure 2.15: Hysteresis predictions for the same wall energy $E_w(M)$ based on (a) the internal field approximation and (b) the correct equations. In the internal field approximation, instability occurs at point A, and this determines the coercivity (to get the observed hysteresis curve, the line with the arrow must be skewed to get a slope of $1/N$). In (b), several jumps occur and the coercivity is determined by the peak at B. The dotted line is the vertical plumb from (a), skewed to the applied field coordinates.

how the dimensions of the particle approach infinity). If the magnetization is uniform and the shape is fixed, then in the limit as the size goes to infinity the demagnetizing tensor is equal to the SD demagnetizing tensor for a finite body of the same shape.

In any case, an infinite body should not have domain walls. When Landau and Lifshitz [1935] derived the structure of a domain wall in an infinite medium, they noted that the lowest energy state for an infinite body should be uniform magnetization: this makes $\nabla \cdot \mathbf{M} = 0$, and the poles $\mathbf{M} \cdot \hat{\mathbf{n}}$ are removed to infinity, so the demagnetizing energy is minimized. They had to constrain the magnetization to be in opposite directions at $x = \pm\infty$. Brown [1962] showed that a one-dimensional domain wall is unstable in an infinite medium. Thus the domain wall owes its very existence to the finite size of real particles.

2.4.6 What Does the Two-Domain Model Really Predict?

The above discussion makes it clear that there is a need for a self-consistent solution for the magnetic properties of a two-domain model. This model assumes the domains are lamellar and the domain wall is thin compared to the particle size. The hysteresis properties predicted by a two-domain model depend on the wall energy, which can be a complex function of position. To predict hysteresis properties for an ensemble, we need to average the response for many particles with defects in random positions. I will not attempt this here. We can get a qualitative idea, however, of how the magnitude and spacing of extrema affect the response by looking again at the sinusoidal model (Figure 2.16). The dashed lines are the tangents to the points where $d^2E_w/dM^2 = 0$, so they represent the hysteresis curve predicted by the internal field approximation. The actual hysteresis curve has a much lower coercivity, and $H_{cr} = H_c$. If the phase of the sinusoid is shifted so point A travels down the dotted line, the coercivity is equal to the field at point A until A reaches $M = 0$. The coercivity and coercivity of remanence are therefore nearly equal.

In the limit of vanishing period $\Delta M/M_s$, the hysteresis curve approaches that

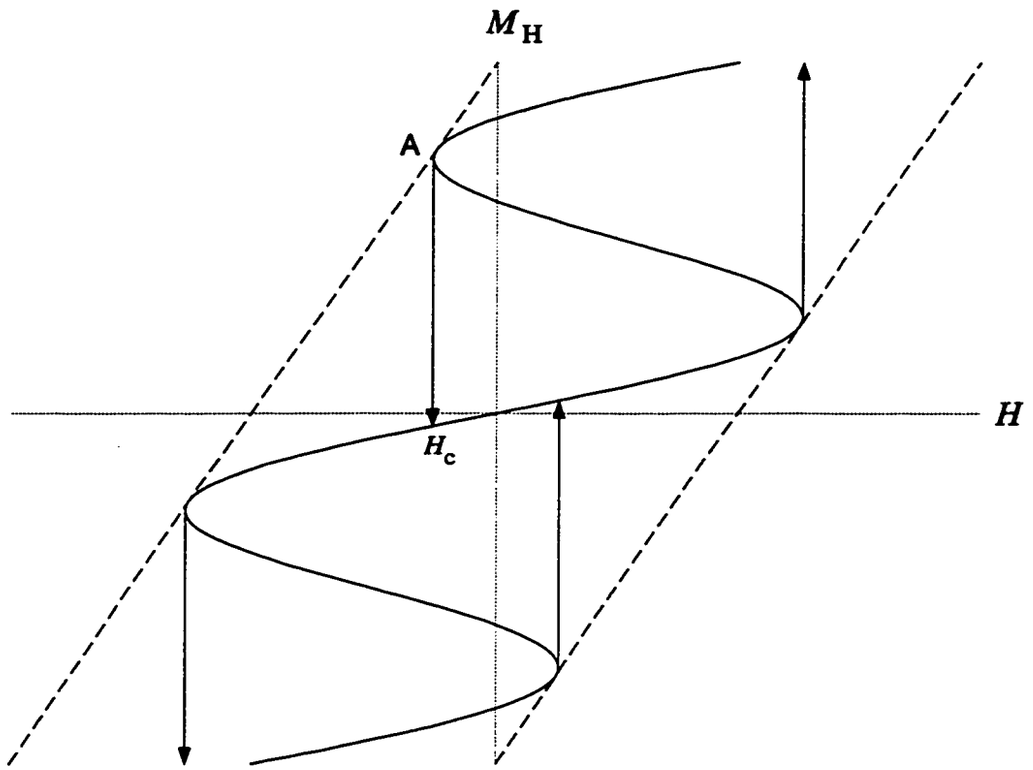

Figure 2.16: The effect of spacing of maxima on hysteresis properties in the two-domain model. The dashed lines represent the hysteresis curve predicted by the internal field approximation. The actual hysteresis curve is shown as the vertical jumps and the reversible sections in between.

predicted by the model of Néel [1955]. As the period increases, the susceptibility increases and the coercivity decreases (a qualitatively similar trend to that predicted by the heuristic relation $\chi_i H_c \approx$ constant of Kittel [1946]).

If the period of the sinusoid gets too large (with the definition of "large" depending on the amplitude of dE_w/dM and the slope $1/N$), the peaks get so far apart that the jumps no longer overlap, and the main hysteresis loop gets split into sub-loops connected by reversible curves. In the limit of infinite period or zero amplitude, the curve is fully reversible and $\chi_0 = 1/N$. Thus the upper limit for χ_0 is the same as it is in the internal field approximation, but it is only attainable if the hysteresis disappears entirely.

If we have an ensemble of particles that are identical except that the phase of $E_w(M)$ has a uniform distribution, the set of hysteresis curves maps onto itself under a translation that preserves $H = NM$; the average hysteresis curve therefore has a slope of $1/N$.

We can expect some of these relationships to remain true for more complex wall energies. In particular, if there is an ensemble of particles that are identical except for the location of defects, and the defects have equal probability of being in any location, the hysteresis curve will have a slope of $1/N$ and therefore $H_c = NM_{rs}$.

If particles with different shapes (and therefore different demagnetizing factors) are mixed together, then far from saturation the combined hysteresis curve is a volume-weighted average of straight lines - so it is also a straight line with slope $1/\langle N \rangle$, where $\langle N \rangle$ is the average demagnetizing factor.

Thus the relation $H_c = NM_{rs}$ appears to be a robust feature of MD models, contrary to the predictions of the heuristic models described in subsection 2.4.4. Similarly, the remanence acquisition curves should be linear, although in general the slope will be less than $1/N$.

2.4.7 The Two-Domain Model and TRM

As I mentioned in Chapter 1, SD particles acquire thermoremanent magnetization (TRM) at the transition from superparamagnetism to hysteresis. As particle size increases, the temperature for this transition approaches the Curie temperature (Chapter 3) and TRM acquisition is dominated by hysteresis. In the MD model of Néel [1955], as the temperature decreases the demagnetizing field H_d and the inhomogeneous field H_w increase. If H_d increases faster than H_w, the wall moves towards the center.

Néel [1955] used the internal field approximation and also assumed that the coercivity had a different temperature dependence than the saturation remanence:

$$H_c(T) \sim M_{rs}(T)^p \tag{2.53}$$

Néel used $p = 2$; Dunlop and Waddington [1975] calculated the thermoremanence $M_{tr}(H)$ and found that

$$M_{tr}(H) \propto H^{1-1/p} \tag{2.54}$$

In the MD model, however, $H_c = NM_{rs}$ and N is a geometrical factor, so p should equal 1. The assumption that $p \neq 1$ is another example of a heuristic model that contradicts the physical model (subsection 2.4.4). Measurements of the hysteresis parameters for sized magnetites show that H_c and M_{rs} do have the same temperature dependence [Heider *et al.*, 1987].

If $p = 1$, equation 2.54 predicts that the TRM does not depend on the inducing field. A correct solution of the MD equation without the internal field approximation will probably recover the field dependence.

In Chapter 1, I proposed that the Thellier and Thellier [1959] method should give the correct paleointensity for SD particles but not for larger particles, while the method of Shaw [1974] may work for larger particles. For the Thellier-Thellier method to work, it must be possible to reverse the process of acquiring TRM by

heating the sample. For a two-domain particle, this would mean that the domain wall should move back out towards the edge of the particle as the temperature increases. This is not what happens. If a two-domain particle is heated in zero field, the only magnetostatic energy term is the demagnetizing energy, and this is a minimum if the wall is in the center of the particle. As the temperature increases, the pinning forces decrease, and the wall moves towards the center. As long as there is some pinning force left to oppose this motion, there will be a remanence. It is hardly surprising, therefore, that in large particles not all of the remanence is demagnetized until the Curie temperature is reached.

2.5 Summary

In this chapter, I extended existing theories for superparamagnetic (SP) and single-domain (SD) particles in order to make more robust interpretations of magnetization curves. For SP particles with no magnetic anisotropy, the magnetization fits the equation $M = \coth a - 1/a$, where $a = \mu_0 M_s^2 HV/k_B T$. Previous authors, using numerical calculations, found a change in the magnetization curve when they gave the particles some magnetic anisotropy. I show that the above equation still applies to an ensemble of particles with any internal anisotropy, as long as there is no bulk anisotropy. A fit to the magnetization curve can determine the odd moments $\langle V^{2k+1} \rangle$ of the volume distribution. The standard deviation cannot be determined because it depends on an even moment.

Using Stoner-Wohlfarth theory, I derived analytical expressions for the acquisition and loss of isothermal remanent magnetization (IRM) in ensembles of SD particles. These expressions apply only to non-interacting SD particles with uniaxial anisotropy. I also showed that the remanence curves and the main hysteresis loop have fixed shapes that are scaled by the average anisotropy. For example, if the anisotropy is pure shape anisotropy, the curves are determined by the volume-average demag-

netizing factor $\langle N \rangle$. No other information on the particles can be inferred from the magnetization curve. However, if there are particles with cubic magnetocrystalline anisotropy, they can be detected by plotting acquisition of IRM against loss of IRM Henkel [1964]. The Wohlfarth [1958] relations predict straight lines for particles with uniaxial anisotropy, and the relations are not affected by bulk anisotropy or thermal fluctuations. Non-interacting SD particles with cubic anisotropy have the opposite curvature on these plots to MD particles or interacting SD particles. The Henkel plot may therefore be a robust tool for identifying the remanence carriers in fine particle systems such as basaltic glasses and some carbonates and soils.

In MD theory, the physical model is a two-domain model. The effect of shape is represented by a dimensionless demagnetizing factor N that depends only on the geometry. Theoreticians have attempted to generalize the two-domain model by adding heuristic assumptions, but the assumptions contradict the initial assumption that N is dependent only on the geometry. In particular, in his MD theory of TRM, Néel [1955] assumes $H_c(T) \sim M_{rs}(T)^p$, where p must be greater than one to get a remanence that increases with the inducing field - but both the assumption about N and measurements of hysteresis parameters require $p = 1$. In addition, all MD models use the internal field approximation, which incorrectly represents the relationship between hysteresis properties and the forces on the domain wall.

I develop a very simple two-domain model and argue that some of the predictions of Néel's MD hysteresis model are robust features of MD models - particularly $H_c = NM_{rs}$. Because the number of defects a domain wall intersects depends on the orientation of the wall, the susceptibility and coercivity H_c probably depend on the direction of the field. Since $M_{rs} = H_c/N$ and N depends on elongation, M_{rs} should also be anisotropic, but the anisotropy depends on the balance between the pinning and demagnetizing forces.

In both SD and MD models, the slope dM_H/dH of the hysteresis curve approaches infinity as the field approaches an instability. This becomes an important criterion

for good micromagnetic results in Chapters 4 – 6.

Chapter 3

SINGLE-DOMAIN CRITICAL SIZES AND NUCLEATION

As I stated in the Introduction, the main purpose of this dissertation is to identify transitions between "SD-like" and "MD-like" hysteresis properties, and examine their relevance to paleomagnetic problems. In this chapter I will look at some critical sizes for SD hysteresis that can already be found in the literature.

The lower bound for the single-domain state is the size L_{sp} at which the transition from superparamagnetism to SD behavior occurs. Strictly speaking, this is the size at which SD remanence first occurs. As the particle size increases, the relative importance of thermal fluctuations decreases and the hysteresis loop approaches that predicted by the Stoner-Wohlfarth theory.

For the transition from SD to non-SD hysteresis, there are at least three definitions of the critical size. To avoid confusion, I give them different names. Most authors in rock magnetism use the global critical size L_0: this is the size below which the lowest energy remanent state is SD.

Two other critical sizes are mostly found in the physics and engineering literature. One, which I call the nucleation critical size L_n, is the upper limit of stability for the SD state (nucleation is the term used in micromagnetics for the initial deviation from uniform magnetization). In particles with $L > L_n$, the remanent state is never SD. In smaller particles, the remanent state may be SD even if some other state has lower energy; Halgedahl and Fuller [1980] argue that remanence in PSD-size particles is dominated by such "metastable" SD states (section 3.1.2).

At the Stoner-Wohlfarth critical size L_{sw}, the first deviation from pure SD hysteresis occurs. For particles with size $L < L_{sw}$, the magnetization is uniform in any

field and it always changes by uniform rotation. It is only below this critical size that the theory of Stoner and Wohlfarth [1947] applies. In larger particles, reversals occur by nucleation (non-uniform rotation), and the coercivity is lower than the SD coercivity.

The critical sizes L_{sw} and L_n are related to the nucleation field H_n, which is the field at which the first non-uniform rotation occurs as the field is reduced from saturation. The definition of the nucleation critical size is equivalent to $H_n(L_n) = 0$, while the Stoner-Wohlfarth critical size is defined by $H_n(L_n) = H_s$, where H_s is the switching field predicted by Stoner-Wohlfarth theory (Chapter 2).

There are some rigorous calculations of critical sizes in the micromagnetic literature, but they can be difficult to interpret. Each author normalizes lengths, fields and magnetizations in a different way, and the term "critical size" is applied indiscriminately to L_0, L_{sw} or L_n. One must look closely at the method to determine which critical size is calculated. Another problem is that the critical size for an ellipsoid is given as a radius or diameter, while the size of a cuboid[1] is usuallythe shortest or longest side. This inconsistency in definition makes it difficult to compare theoretical predictions with each other or with observation. In this dissertation, I define the size of a particle as the cube root of the volume $L = V^{1/3}$. This has the advantage of being appropriate for any shape, it separates shape effects from volume effects, and it makes possible meaningful comparisons between the hysteresis properties of ellipsoids and cuboids (Chapter 5). If I quote a result in the literature, I first convert the length to the cube root of the volume.

In this chapter, I extend published micromagnetic calculations of critical sizes to include magnetocrystalline anisotropy, and I explore their implications for rock magnetism.

---

[1] A cuboid is a rectangular parallelepiped.

3.1 Critical Sizes in Rock Magnetism

3.1.1 The Global Critical Size

Calculations of the global critical size go back a long way in rock magnetism (for example, Stacey [1963]), but I begin with the paper by Butler and Banerjee [1975]. Their Figure 7, showing the dependence of critical size on elongation, is reproduced in many of the recent textbooks on paleomagnetism [Butler, 1992; Thompson and Oldfield, 1986; Opdyke and Channell, 1996] and biomagnetism [Kirschvink and Walker, 1985].

In a model of a cuboid particle, Butler and Banerjee calculate the energy of a two-domain state with variable domain wall width. The energy density of this state decreases as the size increases, while the energy density of the SD state remains constant. The point where the energies cross is the global critical size L_0.

The calculations of Butler and Banerjee are not self-consistent. For the magnetocrystalline and exhange energy, they use an expression for a Bloch wall in an infinite medium [Lilley, 1950], while for the demagnetizing energy they approximate the wall by a region with magnetization perpendicular to the magnetization in each domain [Amar, 1958].

As Brown [1945] pointed out, one of the problems with domain theory is that its predictions depend on the ingenuity of the theorist. There is always the possibility that there is some lower energy state that has not been considered. Butler and Banerjee also try to estimate the energy of a circular, or "curling" spin configuration (Figure 3.1a). They conclude that this state will always have a higher energy than the two-domain state. A curling state does look inappropriate for a square particle, but three-dimensional micromagnetic models [Schabes and Bertram, 1988; Williams and Dunlop, 1989] find the lowest energy state is often a "vortex" state which looks quite similar to the curling state. Perhaps Butler and Banerjee would have refected the two-domain state if they had estimated the energy of a closure domain state

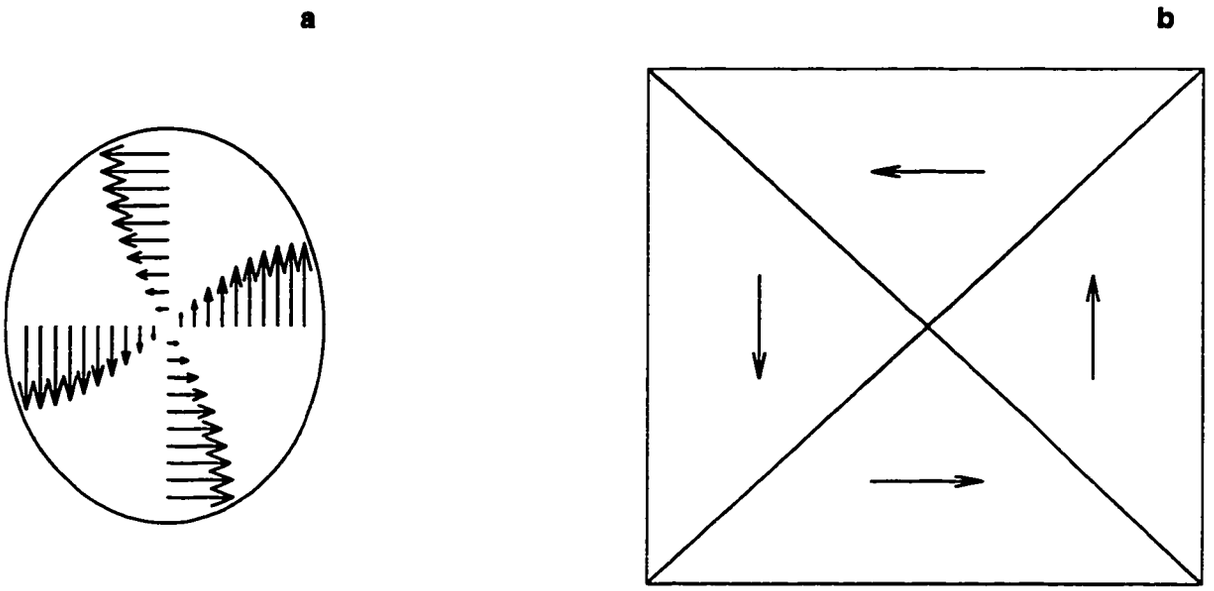

Figure 3.1: (a) A curling state, after the equation for the infinite cylinder [Brown, 1963, equation 5-37]. Each arrow indicates the direction and magnitude of the magnetization within the plane; the total vector has unit magnitude. (b) A closure domain state, after Kittel [1946]

(Figure 3.1b); this state has zero demagnetizing field, so the demagnetizing energy is much lower than that of the two-domain state.

Some one-dimensional micromagnetic models [Moon and Merrill, 1984; Enkin and Dunlop, 1987; Newell *et al.*, 1990] are at least self-consistent, although they cannot represent the curling mode. Fabian *et al.* [1996] use a three-dimensional micromagnetic model to calculate the global critical size as a function of elongation for magnetite.

Most of the theoretical work has focussed on the global critical size L_0, but I will show in this chapter that L_0 has little relevance to hysteresis properties. The critical sizes L_{sw} and L_n are the important ones.

3.1.2 Local Energy Minima

Before 1978, rock magnetists assumed that above the global critical size L_0, the SD state became unstable and jumped to the new lowest energy state, usually assumed to be the two-domain state. It was difficult to explain the observed size dependence of remanence using a two-domain model, although there were numerous attempts [Stacey, 1963; Stacey and Banerjee, 1974; Dunlop, 1977]. However, as Brown [1962] pointed out much earlier, the magnetization does not have to be in the lowest energy state - indeed, if it always were, there would be no hysteresis.

Levi and Merrill [1978] were the first rock magnetists to recognize that the SD state could remain stable for $L > L_0$ because an energy barrier could separate it from lower energy states and prevent nucleation. Halgedahl and Fuller [1980] found evidence for inhibition of nucleation in $x = 0.6$ titanomagnetites (TM60) by looking at Bitter patterns on particles with saturation remanence. Some particles did not have domain walls even though much smaller particles did. Halgedahl and Fuller [1983] showed that depending on the history of the applied field, a given particle could have different numbers of domains; for example, new walls could nucleate in back fields and remain when the field was removed. Even identical thermal or AF treatments of a particle could give rise to very different numbers of domains [Halgedahl, 1991].

Theoretically, materials with large magnetocrystalline anisotropy should never develop domain walls, yet very large particles almost invariably do. The experimental evidence suggests that defects can cause nucleation, particularly near surfaces. Large particles have a lot of defects, so they almost always nucleate walls before the field is reduced to zero. Smaller particles have fewer defects on average, so they are more likely to have a saturation remanent state that is SD.

Halgedahl and Fuller [1983] distinguish between two kinds of nucleation. "True" nucleation is the initial departure from uniform magnetization, so it can only occur if the particle is saturated to begin with. In some particles, a domain wall seems to

be trapped at the surface and requires a surprisingly large field to remove. When the field decreases, there is a critical field where the wall jumps to the middle of the particle: this is false nucleation.

If the particle is really saturated to begin with, the nucleation field should have the same magnitude in both directions and the wall should appear in the same place (ultimately, this is due to the time-reversal symmetry of Maxwell's equations). When a wall is trapped at the surface, it is not always visible and the magnetization can be indistinguishable from saturation, but we can sometimes infer its presence from an asymmetry in the wall movement.

Moon and Merrill [1984] introduced the term "local energy minimum (LEM)" for a domain state which remains stable even though it does not have the lowest energy. Using a one-dimensional model of magnetite, Moon and Merrill [1985] calculated the size range for stability as a function of the number of domains. One-dimensional calculations are highly constrained, however, and they cannot represent nucleation as it occurs in real particles.

3.2 Rigorous Micromagnetic Calculations

Although critical sizes calculated using three-dimensional numerical micromagnetic models are an improvement over domain calculations, they also have problems. An accurate numerical solution of the micromagnetic equations is difficult and consumes a lot of CPU time. The result of a micromagnetic simulation depends on the initial guess, and we cannot be sure we have found all the solutions - or even the lowest energy solution (Chapter 4). In particles of most shapes the magnetization is never uniform in equilibrium, so even the definition of the SD state is ambiguous (Chapter 5). Finally, it is difficult to demonstrate that a state has become unstable (Chapter 6).

The ellipsoid is the only known shape for which the demagnetizing field is uniform when the magnetization is uniform [Morrish, 1966, section 1.5]. This makes it possible

for a state of uniform magnetization to be stable, and it has been proved rigorously that it is stable in a large enough field [Shtrikman and Treves, 1963].

Theorists have managed to determine analytical conditions for the stability of the SD state in ellipsoids of rotation. For the limiting cases of the sphere and the infinite cylinder, they have calculated the nucleation fields for all possible modes of nucleation; for the general cylinder of rotation, they have explored a broad class of modes (the curling modes) that are the nucleation modes in the sphere and cylinder except for a very small size range in the cylinder. They have also calculated a lower bound on the global critical size L_0 by placing rigorous bounds on the energy of any non-uniform state and comparing the bounds with the energy of a SD state.

Thus the calculations for ellipsoids have some advantages that numerical models cannot have: they are not subject to numerical inaccuracies and they involve an exhaustive exploration of possible solutions. The calculations below should be the baseline for any numerical calculations, and in later chapters I will be comparing my numerical results with them.

The published analytical calculations are for zero magnetocrystalline anisotropy. I extend them to include magnetocrystalline anisotropy, and I show the modified equations have some important consequences for rock magnetism.

3.2.1 The Nucleation Field

To prove a state is stable, one must show that any variation $\delta\mathbf{M}(\mathbf{r})$ of the magnetization will increase the energy. In general, this is extremely difficult to do. To prove a state is unstable, it is enough to find one variation that reduces the energy. In the ellipsoid, uniform magnetization is stable if the applied field is large enough. As the field decreases to zero and changes to the opposite direction, the SD state eventually becomes unstable. If the mode of instability is non-uniform, the instability field is called the nucleation field.

The nucleation field is determined by linearizing the micromagnetic equations as

follows [Brown, 1963]. First, a reference state of uniform magnetization is chosen which is stable in a large field. Solutions have only been obtained for the simplest configuration where the moment, the field, the long axis of the particle and the magnetocrystalline anisotropy are all aligned.

Suppose the applied field is in the z direction. The energy is then expanded to second order in the transverse components α and β, using $\alpha^2 + \beta^2 + \gamma^2 = 1$ to eliminate γ. With a variational calculation, one obtains eigenvalue equations [Brown, 1963, eqns. 5-18, 5-19]

$$-2\nabla^2\alpha + (2\kappa_{11} - \lambda)\,\alpha + 2\kappa_{12}\beta + M_s\frac{\partial U}{\partial x} = 0 \tag{3.1}$$

$$-2\nabla^2\beta + 2\kappa_{12}\alpha + (2\kappa_{22} - \lambda)\,\beta + M_s\frac{\partial U}{\partial y} = 0 \tag{3.2}$$

where U is the magnetic potential due to the deviations α and β, and the coefficients κ_{ij} are the coefficients of α^2, β^2 and $\alpha\beta$ obtained by eliminating γ from the expression for the magnetocrystalline energy. If λ_0 is the smallest eigenvalue for the above equations (with appropriate boundary conditions), the instability field is $H = -\lambda_0/\mu_0 M_s$.

For the sphere [Aharoni, 1959] and the infinite cylinder [Aharoni and Shtrikman, 1958], the entire spectrum of eigenfunctions has been explored and the nucleation field rigorously determined. There are only three instability modes; the main two are uniform rotation or a curling mode, which in cylindrical coordinates (z, ρ, ϕ) is [Brown, 1963, equation 5-33]

$$\delta\hat{m}_\phi = \delta\hat{m}_\phi(\rho), \quad \delta\hat{m}_\rho = 0 \tag{3.3}$$

A third mode, the buckling mode, occurs in a narrow size range in infinite cylinders.

For prolate ellipsoids of rotation, Aharoni [1959] calculated the instability fields for uniform rotation and generalized curling modes (where the magnetization depends on z as well as ρ). If the demagnetizing factors are N_a for the long axis and $N_b \geq N_a$ for the short axis, then the nucleation field for the curling mode is

$$\frac{H_n}{M_s} = N_a - \frac{kL_{ex}^2}{L^2} \tag{3.4}$$

The dimensionless parameter k is 22.5 for a sphere and decreases monotonically to 17.6 as the elongation increases to infinity. It is possible that there is a larger nucleation field corresponding to the buckling mode for some range of aspect ratios and particle sizes. Aharoni [1986] showed that uniform rotation and curling are the only instability modes for aspect ratios up to 4.6, so the buckling mode cannot be ruled out for more elonated particles - but this mode is not very important in the infinite cylinder, so it is probably safe to ignore it.[2]

Aharoni [1959] neglected magnetocrystalline anisotropy. For a few simple cases, the solutions are easily modified. In equations 3.1 and 3.2, if $\kappa_{12} = 0$ and $\kappa_{11} = \kappa_{22} \equiv \kappa$, then we can solve for λ with $\kappa = 0$ and then replace it by $\lambda' = \lambda + 2\kappa$ to include the effect of magnetocrystalline anisotropy. If H_n is the nucleation field for zero magnetocrystalline anisotropy, then $H_n - 2\kappa/\mu_0 M_s$ is the nucleation field with nonzero magnetocrystalline anisotropy.

To determine κ_{ij}, as I mentioned above, the magnetocrystalline energy must be expanded in terms of the coordinates perpendicular to the SD moment; κ_{11} is then the coefficient for α^2, κ_{22} for β^2, and κ_{12} for $\alpha\beta$. There are some simple cases where this approach can be applied (see Appendix A):

1. Uniaxial anisotropy with $K_1 > 0$ and the [001] easy axis in the z direction: $\kappa = K_1$.

2. Cubic anisotropy with $K_1 > 0$ and the [001] easy axis in the z direction: $\kappa = K_1$.

3. Cubic anisotropy with $K_1 < 0$ and the [111] easy axis in the z direction: $\kappa = -2K_1/3$.

4. Cubic anisotropy with $K_1 < 0$ and the [001] hard axis in the z direction: $\kappa = K_1$.

---

[2] Aharoni [1966] also showed that uniform rotation and curling are the only instability modes for oblate spheroids of rotation.

The fourth case is different from the others because the [001] direction is not the easy axis, so it will not be the direction of remanence unless there is a stress or shape anisotropy in the [001] direction that is larger than $|K_1|$.

With magnetocrystalline anisotropy added, the equation for the nucleation field is given by

$$\frac{H_n}{M_s} = N_a - \frac{kL_{ex}^2}{L^2} - \frac{2\kappa}{\mu_0 M_s^2} \tag{3.5}$$

From Stoner-Wohfarth theory, the critical field for rotation is

$$\frac{H_r}{M_s} = (N_a - N_b) - \frac{2\kappa}{\mu_0 M_s^2} \tag{3.6}$$

The magnetocrystalline anisotropy enters in the equations for H_n and H_r in the same way; this is to be expected, since uniform rotation is also a solution of equations 3.1 and 3.2.

If $H_r > H_n$, the magnetization is uniform in any field and it can only change by rotation. At the Stoner-Wohlfarth critical size, $H_n = H_r$, so

$$L_{sw} = \left(\frac{k}{N_b}\right)^{1/2} L_{ex} \tag{3.7}$$

The nucleation critical size is obtained from equation 3.5 by setting $H_n = 0$:

$$L_n = \left(\frac{k}{N_a}\right)^{1/2} \left(1 - \frac{2\kappa}{\mu_0 M_s^2 N_a}\right)^{-1/2} L_{ex} \tag{3.8}$$

Again, k is 22.5 for a sphere and 17.6 for an infinite cylinder.

3.2.2 Rigorous Bounds on the Global Critical Size

The first rigorous bounds on the global critical size were calculated by Brown [1968] for a perfect spherical crystal with uniaxial magnetocrystalline anisotropy.

Since one can rarely calculate rigorous bounds for the critical size, it is worth describing Brown's approach. The most difficult parts of the micromagnetic equations

are the constraint $\alpha^2 + \beta^2 + \gamma^2 = 1$ and the calculation of the demagnetizing energy. Brown relaxes the former condition, requiring instead that

$$\frac{1}{V}\int \left(\alpha^2 + \beta^2 + \gamma^2\right) dV = 1 \tag{3.9}$$

where the integral is over the volume of the particle. This increases the set of possible states, so if the SD state has the lowest energy in this set, it also has the lowest energy among solutions to the micromagnetic boundary value problem. Brown also shows that a lower bound on the magnetostatic energy is the energy of a uniformly magnetized particle with the same total moment. These approximations reduce Brown's equations to a differential equation, and the lowest energy solution is easily identified. The critical size for this calculation is therefore a lower bound on the global critical size. Aharoni [1988] extends this lower limit to prolate ellipsoids of rotation :

$$L_0 \geq L_0^{<} \equiv \left(\frac{k}{N_a}\right)^{1/2} L_{ex} \tag{3.10}$$

For small κ, Brown calculates the energy for a particular nucleation mode. The nucleation critical size in equation 3.5 provides a better lower bound because it is the most favorable nucleation mode:

$$L_0 \leq L_n \tag{3.11}$$

Since L_n diverges as $\kappa/\mu_0 M_s^2$ approaches N_a, L_n is not a useful upper bound for high-anisotropy materials. It is difficult to obtain good constraints. For a sphere, Brown [1968] calculates an upper limit for the energy of a two-domain state, and obtains an upper bound on the global critical size:

$$L_0 \leq 13.80 \left(\frac{k}{N_a}\right)^{1/2} \left(1 + \frac{\pi}{2}\frac{\kappa}{\mu_0 M_s^2}\right)^{1/2} L_{ex} \tag{3.12}$$

This leaves an uncertainty of an order of magnitude or more for L_{sw}, and no one has calculated a rigorous upper bound for other shapes.

For a prolate ellipsoid of rotation with elongation $q = a/b > 1$, the demagnetizing factors are [Chikazumi, 1964, pg. 21]

$$\begin{aligned} N_a &= \frac{1}{q^2-1}\left[\frac{q}{\sqrt{q^2-1}}\ln(\sqrt{q^2-1}+q)-1\right] \\ N_b &= \frac{1}{2}(1-N_a) \end{aligned} \tag{3.13}$$

For $q = 1$, $N_a = N_b = 1/3$.

3.3 A Reassessment of Critical Sizes in Rock Magnetism

The critical size calculations described above are a great improvement over previous calculations, for a few reasons. First, they are rigorous. They are for a specific shape - the ellipsoid of rotation - but I will show in Chapter 5 that they can be extended to more general shapes. I will be exploring some extensions in chapter 5.

Secondly, the expressions for the critical sizes are very simple. The only parameter that is difficult to calculate is k in equation 3.5 for the nucleation field: the calculations by Aharoni [1959] involve expansions of prolate spheroidal functions. However, it is the square root $k^{1/2}$ that appears in the expressions for the critical sizes, and the upper and lower bounds on $k^{1/2}$ only differ by 10%. For most calculations I use $k = 20$ so $k^{1/2}$ is close to its mean value.

The ease of calculation is important because the magnetic parameters are generally not well constrained. They are reasonably well known for magnetite, but in the rest of the titanomagnetite series ($Fe_{3-x}Ti_xO_4, 0 \leq x \leq 1$) there is considerable uncertainty because the parameters are sensitive to differences in stoichiometry [O'Reilly, 1984]. Indeed, the exact composition of a titanomagnetite is often uncertain because there is inconsistency between different methods of determining the oxidation parameter z and there tend to be small scale chemical inhomogeneities [Moskowitz, 1987]. Often, theorists are tempted to understate the uncertainty because it is too laborious to repeat numerical calculations with different parameters; but with the simple

expressions that I have developed in this chapter, it is easy to assess the effect on the critical sizes of changing parameters.

I will give a short review of each constant for two substances of particular importance: magnetite and TM60 ($Fe_{2.4}Ti_{0.6}O_4$).

Curie temperature For magnetite, $T_c \approx 580°C$. For TM60, the range of Curie temperatures is $(150 - 220)°C$ for a range of oxidation parameters $z = 0 - 0.1$ [O'Reilly, 1984].

Saturation magnetization For magnetite, $M_s = 4.8 \times 10^5 Am^{-1}$. I use a range of $(1 - 1.5) \times 10^5 Am^{-1}$ for TM60 [O'Reilly, 1984].

Exchange constant In principle, A can be determined from inelastic neutron scattering and other methods, but for ferrimagnets the interpretation of the measurements is complex and the values of A do not always agree well. Moskowitz and Halgedahl [1987] and Heider and Williams [1988] both analyze the literature and obtain $A = 1.3 \times 10^{-11} Jm^{-1}$; this value is twice that used by Butler and Banerjee [1975] because of a correction to the model for the interactions between sublattices. Moskowitz and Halgedahl [1987] point out that the uncertainty in A could still be 50%.

For titanomagnetites other than magnetite, A can only be estimated indirectly with assumptions about the dependence of A on composition and temperature [Moskowitz and Halgedahl, 1987]. Fortunately, A appears inside a square root in the expressions for the critical sizes. I will take a conservative approach and use a range $A = (10^{-12} - 10^{-11}) Jm^{-1}$. It is reasonable to assume the coupling is weaker than in magnetite because M_s and the Curie temperature are both smaller.

Magnetocrystalline anisotropy constant For magnetite, $K_1 = -1.1 \times 10^4 Jm^{-3}$.

As titanium content increases, there is a general trend from negative to positive K_1, but the dependence of K_1 on x is complex and there is considerable scatter in the measurements. Somewhere between $x = 0.56$ and $x = 0.6$ this constant changes sign. Moskowitz and Halgedahl [1987] estimate $K_1 = 4000\text{Jm}^{-3}$ for TM60 by interpolating the measurements of Syono [1965], while Sahu and Moskowitz [1995] measure $K_1 = 2000\text{Jm}^{-3}$ for TM61.

So far I have ignored magnetostriction, but it becomes important as titanium content increases. In SD particles, the effect of magnetostriction is similar to that of magnetocrystalline anisotropy. One can easily take it into account by using a "zero-stress" constant K_1' instead of the "zero-strain" constant K_1. Fortunately, most methods for measuring anisotropy actually measure K_1' [Ye *et al.*, 1994].

If the magnetization is non-uniform, magnetocrystalline anisotropy and magnetostriction are decoupled and it is much more difficult to determine the effect of magnetostriction. At the nucleation field, however, the expressions for H_n and L_n are probably still accurate if we replace K_1 by K_1'.

Magnetostriction constants For magnetite, $\lambda_{100} = -19 \times 10^{-6}$ and $\lambda_{111} = 78 \times 10^{-6}$ [Fletcher and O'Reilly, 1974]. For TM61, $\lambda_{100} = 140 \times 10^{-6}$ and $\lambda_{111} = 95 \times 10^{-6}$ [Sahu and Moskowitz, 1995].

3.3.1 The Stoner-Wohlfarth Critical Size and Isothermal Hysteresis

The Stoner-Wohlfarth critical size does not depend on magnetocrystalline anisotropy, and it is only weakly dependent on elongation: as the shape changes from a sphere to an infinite cylinder, L_{sw} increases by only 40%. The other critical sizes are strongly dependent on elongation, so only L_{sw} can be stated as a single number for a material.

A particle with $L < L_{sw}$ is truly single-domain. If it has uniaxial anisotropy,

its hysteresis properties are given by Stoner-Wohlfarth theory (although the effect of thermal fluctuations can be important). The hysteresis parameters M_{rs}/M_s, H_c and H_{cr} have their maximum values, and the R-parameter of Cisowski [1981] is 0.5.

The critical size L_{sw} is also, in effect, a lower bound for non-uniform remanent states. In principle, one could calculate lower limits for non-uniform states in the same way as the upper limits on the SD state, but in practice it is far more difficult. If there are non-uniform states in particles with $L < L_{sw}$, however, there is no way of getting to them in a hysteresis cycle (see Chapter 6).

For $L > L_{sw}$, the hysteresis curves begin to deviate from the predictions of Stoner-Wohlfarth theory. As particle size increases, the nucleation field increases and we can expect to see changes in the coercivity while H_n is still negative. Levi and Merrill [1978] measured the hysteresis properties of highly elongated acicular magnetite particles synthesized by Toda Industries; M_{rs}/M_s was $0.44-0.45$ (nearly equal to the SD value), but the coercivity was less than one sixth of the SD coercivity ($H_c \approx 0.5\mu_0 M_s$). Halgedahl [1995] measured hysteresis curves for single platelets of hematite which spanned more than a decade in length; H_c decreased as $L^{-0.6}$ while M_{rs}/M_s remained near the SD value over the entire size range.

3.3.2 Critical Sizes and Metastable SD States

The arguments for the importance of metastable SD states has mainly come from experimentalists who base their arguments on domain observations of high-Ti titanomagnetites and pyrrhotite [Halgedahl and Fuller, 1980, 1983; Metcalf and Fuller, 1987, 1988; Halgedahl, 1991]. These results appear to disagree with micromagnetic models of magnetite [Williams and Dunlop, 1989; Newell *et al.*, 1993b] which consistently obtain global critical sizes below 0.1μm and predict the remanence will decrease rapidly above this size. The theorists cast doubt on the interpretation of Bitter patterns [Williams and Dunlop, 1989; Williams *et al.*, 1992; Newell *et al.*, 1993b] or proposed that some important effect such as inverse magnetostriction from an ap-

plied stress was missing from the theoretical model. In this section I will show that we can reconcile theory and experiment if we take into account the dependence of the critical sizes on composition.

For this discussion I will need the critical size L_{sp} for the transition from superparamagnetic to SD. The critical volume V_s satisfies the blocking criterion for a given temperature T:

$$V_s = \frac{k_B T}{\Delta e} \ln\left(\frac{\tau_s}{\tau_0}\right) \tag{3.14}$$

where k_B is the Boltzmann constant, τ_s is the time scale of interest, τ_0 is a characteristic relaxation time, and Δe is the difference in energy density between the minimum and the saddle point or maximum separating the minima. The critical size is $L_{sp} = V_s^{1/3}$.

The critical size is not very sensitive to the choices of τ_0 and τ_s because they appear in the logarithm. I will use $\tau_0 = 10^{-9}$ seconds and $\tau_s = 1\text{year} \approx \pi \times 10^7 \text{seconds}$.

In deriving an expression for the energy barrier, Butler and Banerjee [1975] consider cubic particles and elongated particles as two disjoint cases. For $K_1 < 0$ and the [111] easy axis aligned with the long axis of the particle, the saddle point between the [111] and $[\bar{1}\bar{1}\bar{1}]$ directions is the $[1\bar{1}0]$ direction, which coincides with the direction of maximum magnetostatic energy. We can simply add the two energy barriers to get

$$\Delta e = \frac{\mu_0}{2}\left(N_b - N_a\right) M_s^2 + \frac{|K_1|}{12} \tag{3.15}$$

For $K_1 > 0$ with the [001] easy axis aligned with the long axis, the saddle points between easy axes are $< 111 >$ directions, which do not coincide with the magnetostatic barrier. The above expression is still an upper bound for Δe; it can be used to give a lower bound on L_{sp} which approaches the correct barrier for equant or highly elongated particles.

In Figure 3.2, I show the dependence of the room temperature critical sizes on elongation for magnetite and TM60. The lengths are well defined for magnetite, but there is a considerable range in some of the parameters that go into the critical

sizes for TM60. The exchange length $L_{ex} = (A/\mu_0 M_s^2)^{1/2}$ for TM60 may be between 0.006μm (the same as for magnetite) and 0.028μm. In Figure 3.2, I use the larger L_{ex} to put a strong limit on the SD size range. For magnetite, $\kappa = -2K_1/3$ and $2\kappa/\mu_0 M_s^2 = 0.06$; for TM60, $\kappa = K_1$ and $0.14 \leq 2\kappa/\mu_0 M_s^2 \leq 0.64$.

Figure 3.2 illustrates the advantages of using $V^{1/3}$ instead of the long axis for the particle size. So defined, the critical sizes L_{sp} and L_{sw} have a weak dependence on elongation. In Figure 7 of Butler and Banerjee [1975], the superparamagnetic threshold length decreases then increases to infinity as $q \to \infty$ - but this increase is in $q^{2/3}$, the ratio between the long axis and $V^{1/3}$. Another advantage of using $V^{1/3}$ is that its relationship to the volume, and therefore the total moment, does not depend on elongation.

In both magnetite and TM60, the Stoner-Wohlfarth critical size decreases slightly as $q \to \infty$; thus in both substances, the size range for purely SD hysteresis is fairly narrow and weakly dependent on elongation. The global critical size, on the other hand, is a steeply increasing function of $1/q$, as it is in earlier studies.

The biggest difference between the two materials is in the upper bound for stability of the SD state. For magnetite, L_n has an asymptote at $q \approx 5$, but until q is very close to 5 there is very little difference between L_n and $L_0^<$ (the lower bound on L_0). The stability range can be much larger for TM60: for an equant particle, L_n/L_0 can be from 1.3 to infinity, and even for the smallest estimate of the anisotropy $L_n \to \infty$ at an elongation of 2.4.

L_n can be increased by adding a uniform stress, although the effect depends on the direction of the principal stress components. We can get some idea of the range of response by considering cases 3 and 4 in section 3.2.1. Surprisingly, if there is a uniaxial tension or compression in the [111] direction, the inverse magnetostriction energy (equation 2.8) is constant and contributes nothing to the anisotropy. If there is a uniaxial compression $\sigma < 0$ in the [100] direction, the anisotropy is equivalent to a uniaxial magnetocrystalline anisotropy of $-(3/2)\lambda_{100}\sigma$ (which is positive because

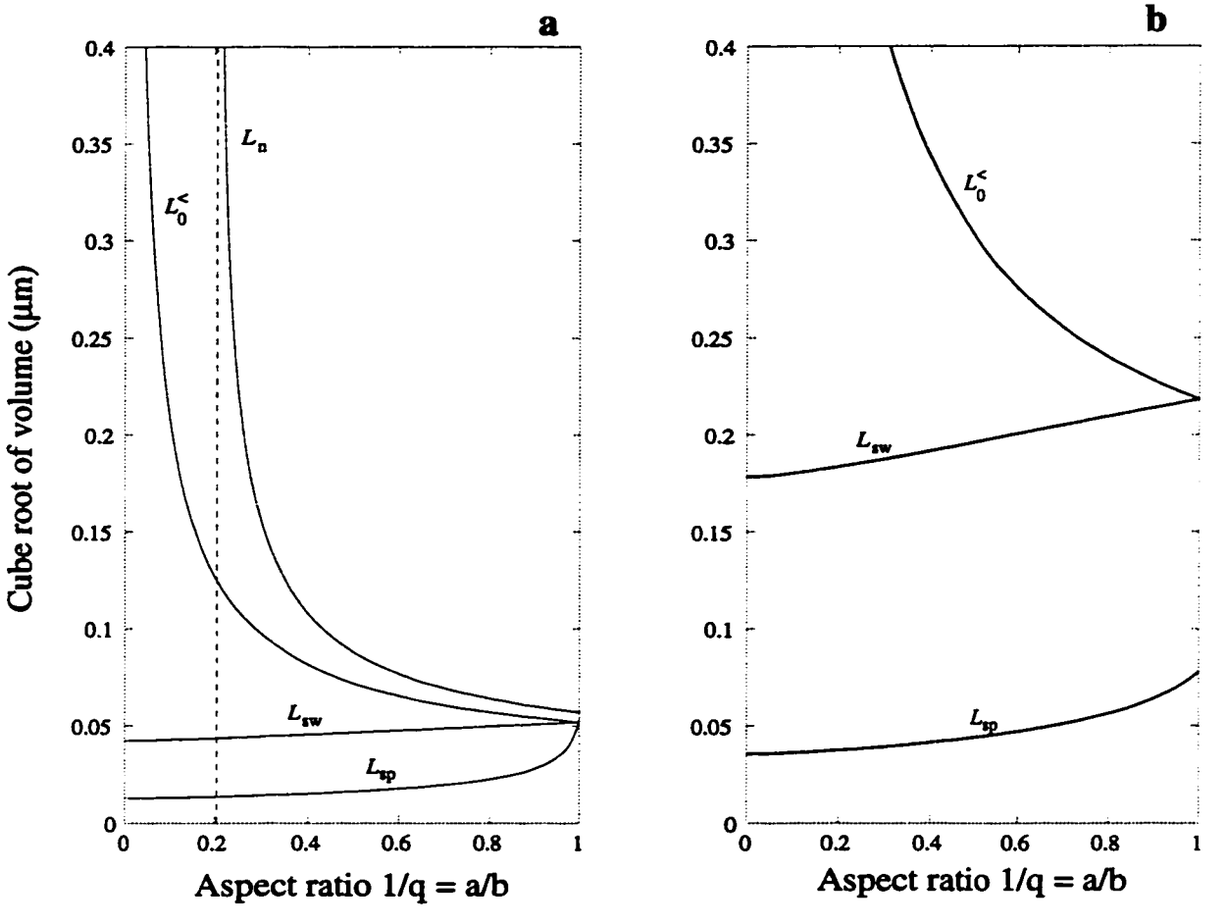

Figure 3.2: Critical sizes as a function of elongation for (a) magnetite (b) TM60. $L_0^<$ is the lower bound to the global critical size. For TM60, L_{sp}, L_{sw}, and $L_0^<$ are calculated with the parameters chosen to maximize them ($A = 10^{-11}\mathrm{Jm}^{-1}$, $M_s = 10^5\mathrm{Am}^{-1}$, and $K_1 = 4000\mathrm{Jm}^{-3}$). For most values of the constants, L_n is well above a micron. For magnetite, the asymptote for L_n are shown as a dotted line.

$\lambda_{100} < 0$). This is added to the magnetocrystalline anisotropy $\kappa = K_1$. In TM60, $K_1 > 0$ and the magnetostriction constants are large, so the combined anisotropy can be considerable. In magnetite the [100] axis is a hard axis and $\kappa = K_1 < 0$, so the two anisotropies are in opposition. For a remanence in the [100] direction to be stable, $K_1 - (3/2)\lambda_{100}\sigma$ must be positive, and this requires a stress of 440MPa. Clearly, stress does little to increase the SD stability range in magnetite.

Thus nucleation theory is consistent with the metastable SD states that Halgedahl and Fuller [1980, 1983] observe in large TM60 particles. Where nucleation occurs for $L < L_n$, it may be induced by imperfections. In addition, the bounds shown in Figure 3.2 are for the most favorable orientation of the easy axes; an unfavorable orientation can reduce the nucleation critical size considerably. Finally, the probability of a SD remanent state will depend on the type of remanence.

In magnetite, there is no mechanism (aside from elongation) that will allow SD states in magnetite particles larger than 0.1μm. Enormous stresses would be needed to increase the SD range significantly. It is worth noting, however, that as x increases from zero, K_1 initially becomes increasingly negative, reaching a minimum of $-2.5 \times 10^4 \mathrm{Jm}^{-3}$ at $x \approx 0.1$ [Syono, 1965], while M_s decreases roughly as $M_s(x = 0)(1 - 1.125x)$ [O'Reilly, 1984]. Thus for TM10, $\kappa \approx 0.07$. This does not increase the SD size range much for equant particles, but the asymptote for L_n moves to $q = 2.3$. SD states could occur in anomalously large magnetite particles if the magnetite is non-stoichiometric.

Some observations seem to contradict this theory: Boyd *et al.* [1984] see apparently SD states in magnetite particles $30 - 40\mu$m in size - far larger than the critical sizes for magnetite. These observations have not been reproduced in other magnetites, however. Even in submicron magnetites down to about 0.5μm [Smith, 1980; Geiß*et al.*, 1996], no SD states have been observed. The samples of Boyd *et al.* [1984] come from a granodiorite in the Tatoosh complex, and magnetites in felsic plutonics are generally nearly pure magnetite [Frost and Lindsey, 1991, page 437]; but natu-

ral samples are inherently complex. A re-examination of these samples would be a valuable contribution to rock magnetism.

Thus the apparent disagreement between theory and experiment over metastable SD states may be just a difference in the properties of magnetite and high-Ti titanomagnetites because of the sensitivity of L_n to magnetocrystalline anisotropy.

3.4 Summary

I have derived rigorous expressions for three SD-PSD critical sizes: the Stoner-Wohlfarth critical size L_{sw}, the global critical size L_0 and the nucleation critical size L_n. The expressions are based on micromagnetic critical size calculations by Aharoni [1959, 1988] which I have extended to include the effect of magnetocrystalline anisotropy.

The Stoner-Wohlfarth critical size L_{sw} is the upper limit for which hysteresis is fully SD, with a dependence of magnetization on field that is predicted by Stoner-Wohlfarth theory. For $L > L_{sw}$, we can expect the hysteresis parameters (especially H_c) to change. This critical size is nearly independent of elongation and magnetocrystalline anisotropy.

The nucleation critical size L_n is the upper stability limit for a SD remanent state, and it is strongly dependent on elongation and magnetocrystalline anisotropy. With most plausible estimates of M_s, A and K_1 for TM60, L_n is well above a micron and can even be infinite, in agreement with the observations of Halgedahl and Fuller [1980, 1983]. For magnetite, L_n can be large in very elongated particles ($q > 5$), but for equant particles the upper limit for SD remanence is well under 0.1μm. Even a stress of 400MPa has little or no effect on the range. Thus the apparent disagreement between theory and observation can be resolved if we take into account the dependence of the critical sizes on composition.

Chapter 4

THE NUMERICAL MODEL

Since the first three-dimensional numerical micromagnetic models [Fredkin and Koehler, 1987; Schabes and Bertram, 1988; Williams and Dunlop, 1989], several groups in rock magnetism and the magnetic recording industry have developed codes. In 1996, group at the National Institute of Standards and Technology invited researchers to calculate a hysteresis loop for a specific particle size, shape and composition and a specific field direction. So far, there have been seven anonymous submissions.[1]. Some of the hysteresis curves look smooth, while others have several jumps. The coercivities and remanences differ by as much as two orders of magnitude.

Much of the effort in developing codes has gone into optimizing the calculation of the demagnetizing energy, which is very time consuming because of the non-local interactions [Fredkin and Koehler, 1990; Ramstöck *et al.*, 1994]. The most popular method is to use fast Fourier transforms [Mansuripur and Giles, 1988; Yuan and Bertram, 1992]. This allows users to run models with larger grid sizes. The demagnetizing energy should be more accurate if the resolution is finer, but no one knows how accurate they are because there are no analytical solutions. The calculation of the demagnetizing energy is a problem in quadrature, and a difficult one because the integrand has a third order singularity (equation 2.5). The usual approach to this problem is to replace the continuous function $\mathbf{M}(\mathbf{r})$ by a stepwise constant function (Section 4.2). A quadrature method of this sort, essentially a lowest order Simpson method, does not converge quickly even for much more well behaved one-dimensional

[1] http://cobalt.nist.gov/mumag/prob1/prob1report.html

quadrature problems [Acton, 1990], so it is unlikely to be an efficient method for calculating the demagnetizing energy. However, the expression for the energy calculation is exact for uniform magnetization, and near the SD size range it should be reasonably accurate. For most of my simulations, I use a grid with $5 \times 5 \times 5$ points and stay near the SD size range.

The methods that have been tried for solving the micromagnetic equations include iterative methods [Aharoni and Jakubovics, 1986], dynamic methods [Schabes and Bertram, 1988], energy minimization using the conjugate gradient method [Williams and Dunlop, 1989] and energy minimization using simulated annealing [Fukuma and Dunlop, 1997]. There is no guarantee that any of these methods can reliably distinguish a stationary point from a minimum. Around a stationary solution, the energy surface in configuration space is flat (the first derivatives of the energy are zero), and it can be difficult to find a search direction that reduces the energy. This problem may get worse as the grid size increases. In this chapter I develop methods to identify and eliminate the unstable solutions.

4.1 Solving the Micromagnetic Equations

I have extended the algorithm described in Newell *et al.* [1993a,b] to three dimensions and reformulated the energy in a more elegant way, which I have since discovered is very similar to that of Berkov *et al.* [1993]. If we define

$$\mathbf{h} \equiv \mathbf{H}/M_s \tag{4.1}$$

$$\mathbf{h}_d \equiv \mathbf{H}_d/M_s \tag{4.2}$$

$$\mathbf{h}_{ex} \equiv \frac{2A}{\mu_0 M_s}\nabla^2\hat{\mathbf{m}} \tag{4.3}$$

$$\mathbf{h}_a \equiv \frac{K_1}{\mu_0 M_s}\frac{\partial g_a}{\partial \hat{\mathbf{m}}} \tag{4.4}$$

then the free energy can be written in a dimensionless form [Berkov *et al.*, 1993]

$$\frac{G}{\mu_0 M_s^2 V} = -\frac{1}{2V}\int \mathbf{m}(\mathbf{r}) \cdot [2\mathbf{h}(\mathbf{r}) + \mathbf{h}_d(\mathbf{r}) + \mathbf{h}_{ex}(\mathbf{r}) + \eta\mathbf{h}_a(\mathbf{r})]\, dV \tag{4.5}$$

where $\eta = 2$ for uniaxial anisotropy and $\eta = 4$ for cubic anisotropy.

If Cartesian coordinates are used, Lagrangian multipliers must be added for the constraint $\hat{\mathbf{m}} \cdot \hat{\mathbf{m}} = 1$. I have used polar coordinates θ, ϕ such that $\alpha = \cos\phi \sin\theta, \beta = \sin\phi \sin\theta, \gamma = \cos\theta$.

The gradient of the energy is needed for the optimization algorithm. It can be expressed very simply as

$$\frac{1}{\mu_0 M_s^2 V} \frac{\partial G}{\partial \theta} = -\mathbf{h}_{\text{eff}} \cdot \frac{\partial \hat{\mathbf{m}}}{\partial \theta} \tag{4.6}$$

$$\frac{1}{\mu_0 M_s^2 V} \frac{\partial G}{\partial \phi} = -\mathbf{h}_{\text{eff}} \cdot \frac{\partial \hat{\mathbf{m}}}{\partial \phi} \tag{4.7}$$

where $\mathbf{h}_{\text{eff}} = \mathbf{h} + \mathbf{h}_{\text{d}} + \mathbf{h}_{\text{ex}} + \mathbf{h}_{\text{a}}$.

4.2 Numerical Implementation

The model has $N \times M \times L$ grid points in the x, y and z directions, with indices (i, j, k). If the size of the particle is $X \times Y \times Z$, each grid point represents the magnetization at the middle of a cell with volume $\Delta V = \Delta x \times \Delta y \times \Delta z = X/N \times Y/M \times Z/L$. As described above, I represent each magnetization vector by angles $(\theta_{ijk}, \phi_{ijk})$, but I still express the energy in terms of the direction cosines:

$$\begin{aligned} \alpha_{ijk} &= \cos\phi_{ijk} \sin\theta_{ijk} \\ \beta_{ijk} &= \sin\phi_{ijk} \sin\theta_{ijk} \\ \gamma_{ijk} &= \cos\theta_{ijk} \end{aligned}$$

The dimensionless energy is

$$\mathrm{G} = -\sum_{ijk} g_{ijk} \Delta V \tag{4.8}$$

where

$$g_{ijk} = \frac{1}{2} \mathbf{m}_{ijk} \cdot [2(\mathbf{h})_{ijk} + (\mathbf{h}_d)_{ijk} + (\mathbf{h}_{ex})_{ijk}] \tag{4.9}$$

The exchange field is discretized using a three-point formula:

$$\frac{\partial \alpha_{ijk}}{\partial x} = \frac{\alpha_{i+1jk} - 2\alpha_{ijk} + \alpha_{i-1jk}}{(\Delta x)^2} \tag{4.10}$$

At the boundary, not all these terms exist (e.g. for $i = 1$, there is no α_{0jk}); but since $\partial \mathbf{m}/\partial n = 0$ (equation 2.10, a reasonable approach is to pretend that there is a mirror at the boundary (e.g. for $i = 1$, replace α_{i-1jk} by α_{i+1jk}).

The demagnetizing field can be written [Newell *et al.*, 1993a]

$$(\mathbf{h}_d)_{ijk} = -\sum_{i'j'k'} \mathsf{N}_{ijk}^{i'j'k'} \cdot \mathbf{m}_{ijk} \tag{4.11}$$

Each tensor $\mathsf{N}_{ijk}^{i'j'k'}$ depends only on the shape of each cell and the relative positions $(i' - i, j' - j, k' - k)$; since these remain fixed, it need only be calculated once, at the beginning of the simulation.

To search for energy minima, I used the conjugate gradient method [Powell, 1977], which only requires the gradient of the energy for selecting search directions.

4.3 Strategic Considerations

4.3.1 The Problem of the Initial Guess

Regardless of the algorithm for finding a solution, one must provide an initial guess for the magnetic structure. The micromagnetic problem is nonlinear and there are often many minima, only one of which can be obtained at a time. Clearly, the solution will depend on the initial guess. One of the challenges of micromagnetics is to come up with an intelligent way of sampling the configuration space to find all the minima - or at least the minima corresponding to states that are likely to occur in real particles.

Theorists have used various strategies to find micromagnetic minima. Williams and Dunlop [1989, 1990] began with randomly oriented magnetization vectors in one octant of the particle; they obtained the magnetization in other octants by requiring that the magnetization was symmetric or antisymmetric with respect to the first

octant. This strategy was used in part to save CPU time, but they were also hoping that by trying all the symmetries, they would find all the possible minima.

Xu *et al.* [1994] used initial guesses that were mostly inspired by domain theory (uniform magnetization and lamellar two- and three-domain states), although a curling state was another initial guess. Fabian *et al.* [1996] used uniform magnetization and a curling state as initial guesses.

In the above papers, the authors tried to cover configuration space with a few widely spaced initial guesses, hoping the minimization algorithm is robust enough to go from the initial guess to a low energy solution that is often very different from the initial guess. Algorithms like the conjugate gradient method assume that the initial guess is close enough to the solution that the energy can be approximated by a quadratic expansion in the model variables about the minimum, and a bad guess can lead to a bad solution.

The simulated annealing algorithm [Press *et al.*, 1992] is more robust than the conjugate gradient method because it attempts to find the lowest energy state (as opposed to a local energy minimum). Fukuma and Dunlop [1997] applied it to the same initial guesses as Xu *et al.* [1994], and their results confirm the shortcomings of the conjugate gradient method. They obtain states with much lower energies than Xu *et al.* [1994].

I use a different approach: I model an isothermal process, such as hysteresis beginning with saturation. In a large enough applied field, we can be reasonably sure that there is only one solution - nearly uniform magnetization with the moment in the direction of the applied field. This makes the choice of initial guess easy. After I obtain the solution for the saturating field, I use it as an initial guess for a minimum energy search in a slightly smaller field. The solution for that field is used as the initial guess for the next smaller field, and so on.

For more information on the size dependence of remanent states, I simulate a different isothermal process, that of grain growth in zero field [Newell *et al.*, 1993b].

This process is interesting in itself, and it also provides another independent source of remanent states for comparison with those from hysteresis simulations. Many of the same considerations apply to grain growth and hysteresis simulations: for example, there are vertical jumps in the grain growth curve, and new curves can be obtained by reversing the direction of change in size.

4.3.2 Hysteresis Curves

An example of a hysteresis loop is shown in Figure 4.1. Most of the curve is continuous; at each step, the initial guess is close to the solution, so the conjugate gradient method works well. I can also check that the smooth parts of the curve are reversible, and they satisfy the general thermodynamic condition $dM_{\mathrm{H}}/dH > 0$ [Brown, 1963].

Another consistency check is based on a symmetry of Maxwell's equations [Jackson, 1975]. The equations are invariant under time reversal, but $\mathbf{H}$ and $\mathbf{M}$ both change sign under time reversal. Thus the hysteresis curve should be the same if it is inverted ($\mathbf{M} \rightarrow -\mathbf{M}, \mathbf{H} \rightarrow -\mathbf{H}$). When I calculate the hysteresis curve, I only calculate each branch for one direction of change of the field (aside from reversibility checks) and then I include the inverse curve on the plot. As we see in Figure 4.1, the curves do connect with each other.

There are two vertical jumps in the curve. At the jump, the energy surface around the minimum is flat, since both the first derivatives and the Jacobian are zero at an instability. There is no guarantee that the conjugate gradient method will choose the right direction to search for the minimum - and there is generally more than one choice for the minimum. After each jump, the magnetization state has changed considerably, so the initial guess is not close to the solution. Usually, however, the correct minimum should be closest to the instability, so it is most likely to be chosen.

Vertical jumps are common in micromagnetic solutions and real hysteresis curves. When I began this work, I wondered what would happen if I reversed the direction of change of the field after a jump. I tried it, and obtained a first order reversal curve

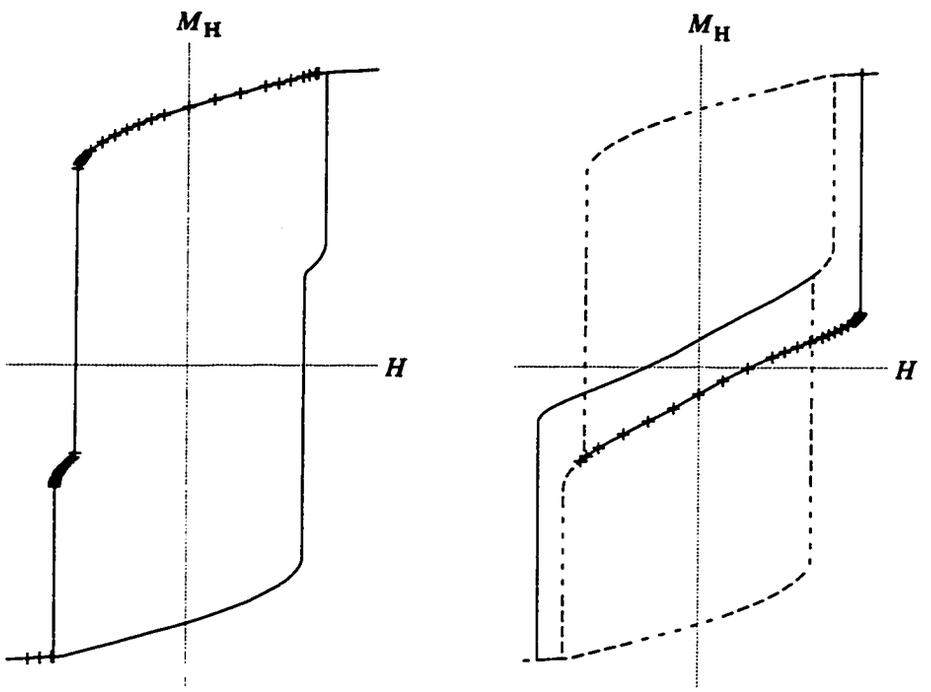

Figure 4.1: A hysteresis loop for a particle with $X = 1.5Y = 1.4Z$ and volume $(0.084\mu\text{m})^3$ in a field with direction $(8, 1, 4)$. The calculated points are shown by the crosses: note the increased density near jumps. The other half of the hysteresis curve is obtained by the inversion $\mathbf{M} \to -\mathbf{M}, \mathbf{H} \to -\mathbf{H}$ (see text). On the right is the first iteration: the main curve, descending field. On the left is the second iteration: the reversal curve.

(Figure 4.1). Surprisingly, no one has done this before with a micromagnetic model.

In addition to adding some interesting complexities to the magnetic hysteresis, reverse curves are a rich source of remanent states. In this example, the saturation remanent state is a curling state with moment along the long axis. The remanent state on the first order reversal curve is another curling state, but with moment along the shortest axis. Typically, with a hysteresis simulation for one field direction, I obtain two or three distinct remanent states. With hysteresis simulations for two or three field directions, I obtain all the remanent states I am going to obtain, and there is more than one example of each remanent state.

The redundancy of the remanent states is advantageous. In a micromagnetic simulation, there is no objective criterion for terminating the search for the minimum energy state, and no way of estimating the precision of the moment or the energy. With two or more independent solutions for the same state, however, I can compare the moments and energies. In subsequent chapters, I often check all the solutions for a given particle size by comparing the moments and repeating the minimization until they agree to a given accuracy. This comes at a cost: I often have to run the program several times, and for a given number of significant figures in the moment, I typically need agreement in the energy to twice as many significant figures. In one case, to get five significant figures in the moment, I needed thirteen significant figures in the energy!

These comparisons only indicate the precision of the results, not the accuracy - but they do reassure us that the solutions are reproducible.

4.3.3 Identifying Unstable Solutions

As I discussed in Chapter 2, the slope dM_H/dH should approach infinity just before the jump. This can be seen in all the curves in Figure 4.1. Unfortunately, a very fine spacing of points is often necessary to show the curvature. For example, the hysteresis curve for $L = 0.076\mu$m in Figure 6.3 required repeated refinement of the

initial curve. On the first pass with a field decreasing from positive saturation, I got a sequence of SD states and a jump to negative saturation just beyond $H = -0.04M_s$, but there was no curvature indicating an approach to an instability. I started at a lower magnitude field and tried smaller steps, and obtained a jump before $-0.04M_s$. This suggested that the state at $-0.04M_s$ was not really stable.

After repeating this process a few times, I obtained the curve shown in Figure 4.2a. There was still no approach to an instability, but now there was a small jump to an intermediate state with some curl. Starting with the intermediate state, I added positive increments to the field and obtained a curve that met the upper curve at $-0.01M_s$. Continuing the curve downwards in very small steps, I finally obtained a smooth approach to an instability (Figure 4.2b). The resolution I needed to see this jump was $0.0001M_s$!

As the upper and lower curves converge, so do the curling and SD states. Since at the meeting point the curling state is obtained by a small perturbation from the SD state, and the curling state has lower energy, the SD state must be unstable. I frequently encounter this situation, where nucleation has occurred and yet I still obtain the SD state at more negative fields.

There are two good reasons for thinking the SD state is unstable beyond the nucleation field. First, I often get an apparently stable solution at one field, and then get instability at a more positive field. Secondly, the SD state does not approach an instability smoothly. Since for a $5 \times 5 \times 5$ grid there are 250 variables in the energy minimization, it is hardly surprising if the minimum-seeking algorithm cannot always find the instability mode.

In this dissertation, I refine the hysteresis curves using the above procedure of pruning unstable branches; this often simplifies the hysteresis considerably. At the same time, it is easy to identify transitions such as nucleation when an unstable branch meets a stable one. Unfortunately, this is quite time consuming, and it has limited the number of good hysteresis curves I could obtain. I also developed this

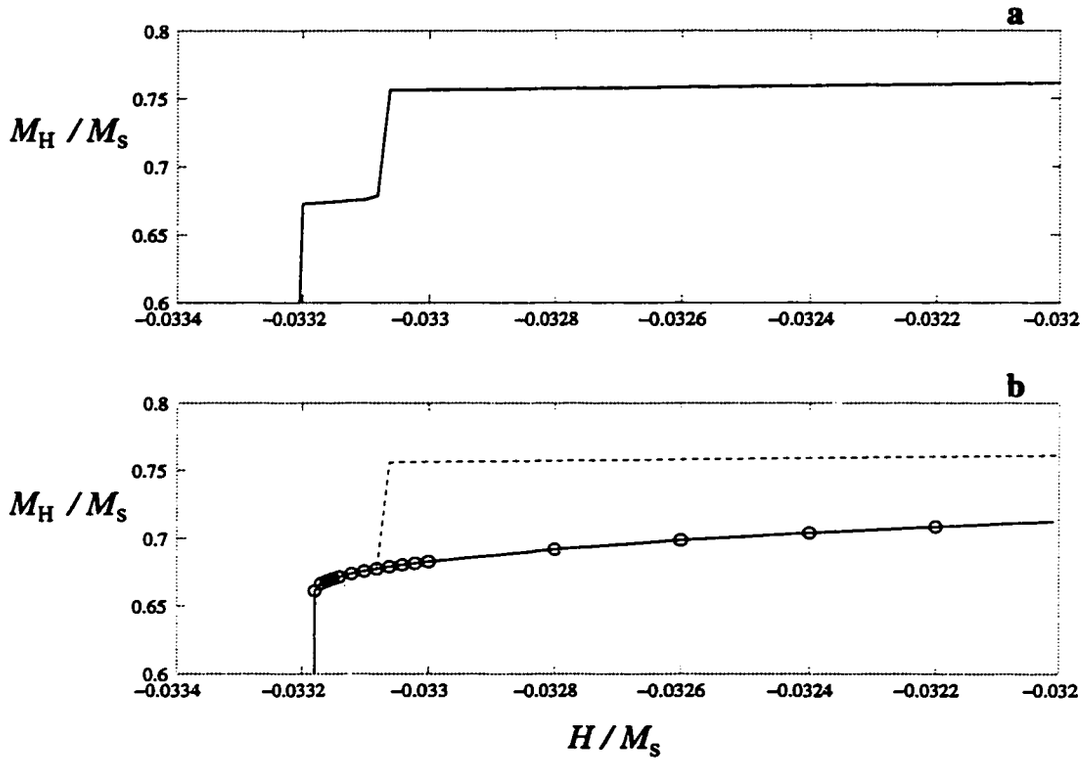

Figure 4.2: An example of the procedure for identifying the true instability field. (a) After a process described in the text, a curve with a jump from an SD state to a curling state is obtained. (b) The curve for the curling state is extended to more positive fields, and a step size of $0.0001 M_s$ is used for more negative fields to get a smooth approach to the jump.

method long after I had already done a lot of simulations; unfortunately, most of those simulations now appear untrustworthy.

4.4 *Comparison with Fukuma and Dunlop*

Using the simulated annealing method, Fukuma and Dunlop [1997] obtained states with much lower energy than those found by Xu *et al.* [1994] using the conjugate gradient method with the same initial guesses. There were two pairs of solutions: two curling states which are different only in the corners, and two three-domain states (again, with minor differences). The curling states have significantly lower energies than the three-domain states.

A good test of my method is to try it on the same problem - a two-dimensional model of a one micron cube with magnetocrystalline easy axes oriented as in Fukuma and Dunlop [1997]. To save CPU time, I used a 25×25 grid (theirs was 50×50). I calculated hysteresis curves for two field directions, $\mathbf{H} \parallel (7,4,1)$ and $\mathbf{H} \parallel (1,7,4)$; the directions were chosen so as not to coincide with any easy axis or symmetry axis of the cube. Since my goal was only to find remanent states, I did not refine the hysteresis curves using the approach described in the previous section, so they are not shown.

For $\mathbf{H} \parallel (7,4,1)$, the saturation remanent state is a curling state that looks like Figure 4e of Fukuma and Dunlop [1997]. Both states have the magnetization perpendicular to the xy plane in the center and all four corners, and the magnetization in each corner is in the same direction as in the center. The volume-average magnetization for both states is $\overline{M} = 0.012 M_s$. The energy of my state is $0.055 E_{SD}$, where $E_{SD} = \mu_0 M_s^2 V/6$; their state has energy $0.053 E_{SD}$. The energy difference is small enough that it is probably due to the difference in the grid size; for comparison, the energy of the curling state in Xu *et al.* [1994] is $0.062 E_{SD}$.

After cycling through a reverse field $\mathbf{H} = -0.05 M_s$, I get a new remanent state.

This is also a curling state, but two corners have magnetization in the opposite direction to that in the center. This is the same as the state shown in Figure 4a of Fukuma and Dunlop [1997], and both states have $\overline{M} = 0.001 M_s$. The energy of my state is $0.055 E_{SD}$, while theirs is $0.052 E_{SD}$.

Thus in one hysteresis cycle, I obtain the two lowest energy states that Fukuma and Dunlop [1997] obtained using the simulated annealing method. Clearly, my method solves the problem of choosing a good initial guess for the conjugate gradient method.

In addition to finding the remanent states, I obtain information about the hysteresis properties of the particle - including how a given hysteresis state may be obtained. Fukuma and Dunlop [1997] claimed a three-domain state was the saturation remanent state, but their reasoning was indirect, whereas I got my saturation remanent state directly from a hysteresis simulation. When I use a field in the $(1, 7, 4)$ direction, much closer to the easy axis, I still do not get a three-domain state. Instead, I get a third curling state, this time with three corners magnetized in the same direction as the center (Figure 4.3). The energy is $0.055 E_{SD}$ again, and the volume-average magnetization is $0.011 M_s$.

The differences in the corners between the curling states may be an artifact of the discretization. The state in Figure 4.3 is very similar to the closure domain state in Figure 3.1. In the latter figure, the demagnetizing energy is equal to zero because $\mathbf{M} \cdot \hat{\mathbf{n}} = 0$ on all surfaces and domain boundaries. In the micromagnetic model, the cube is divided into rectangular prisms that cross the diagonals of the particle, so the magnetization cannot change across the diagonals. In the corners, the magnetization cannot be parallel to all surfaces. With a triangular discretization, the remanent state might be even closer to a closure domain state.

As a method for finding remanent states, my hysteresis method is even more discriminating than previous methods using an initial guess in zero field. Of course, one could try using the simulated annealing method to calculate a hysteresis loop,

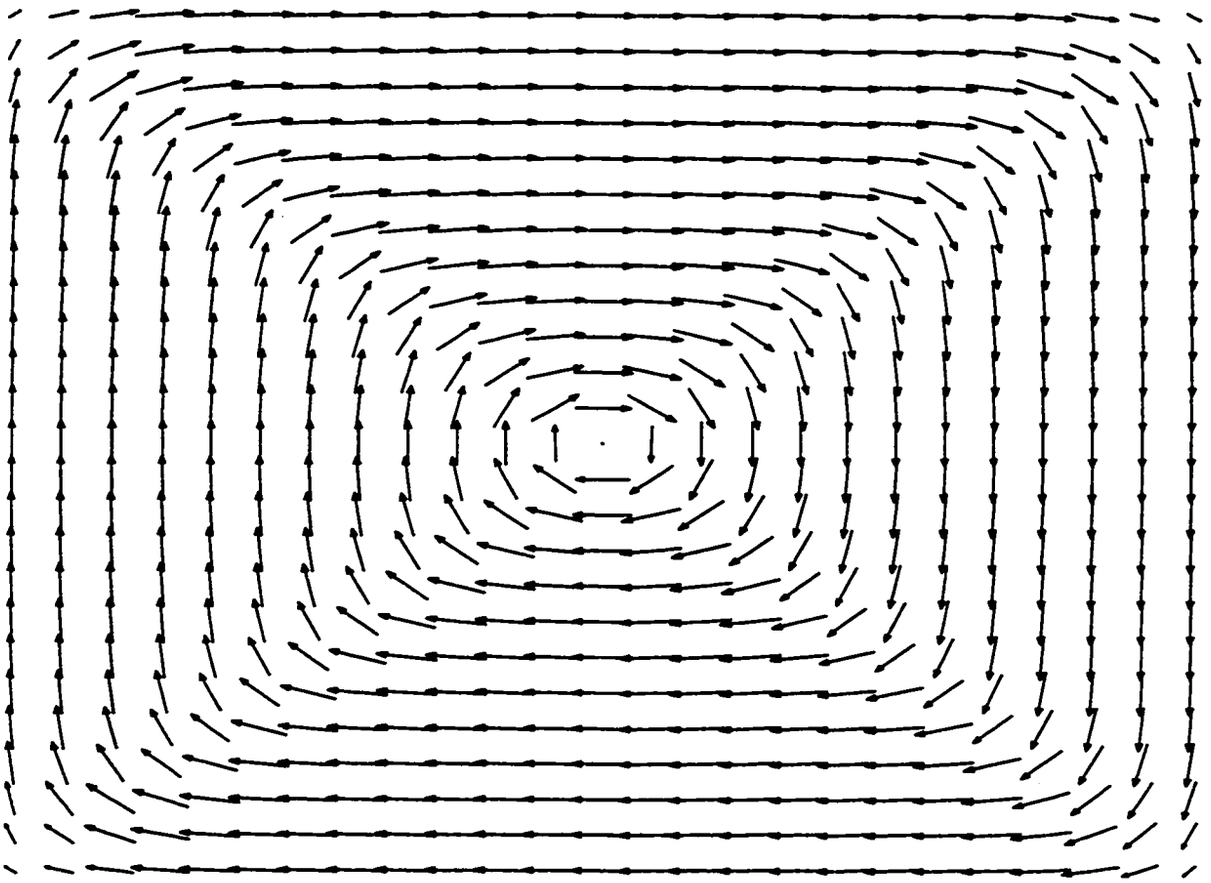

Figure 4.3: The remanent state for the two-dimensional model of a one micron cube in a field parallel to $(1, 7, 4)$. The arrows indicate the magnitude and direction of the component of magnetization in the plane. In the lower left corner, the magnetization points down, while in the other four corners it points up.

but it is much less efficient than the conjugate gradient method because it searches a larger region in configuration space in an attempt to find the global energy minimum. Worse, if the simulated annealing method were perfect, it would always find the global energy minimum and there would no hysteresis. Fukuma and Dunlop [1997] get a different remanent state for each initial guess, so the algorithm is clearly not perfect, but it is still quite likely that the method would jump to the lowest energy state prematurely and miss part of the hysteresis loop.

4.5 Controversy Over the Number of Domains

The controversy over the size range for stability of the SD state (Chapter 3) is part of a broader question about the number of domains as a function of particle size. Models with lamellar domains [Moon and Merrill, 1985] and one-dimensional micromagnetic models [Enkin and Dunlop, 1987; Newell *et al.*, 1990] predicted many more domains than were actually observed [Worm *et al.*, 1991].

There have been many attempts to explain the discrepancy. One was based on the concept of local energy minima: the domain states with lower numbers of domains happened to be inaccessible in ordinary hysteresis processes. Unfortunately, many of the domain states that are commonly seen in particles above a micron in size were predicted to be unstable in one-dimensional models. Some authors cast doubt on the Bitter pattern images: either some walls were not meeting the viewing plane [Heider and Hoffmann, 1992] - or, if they were, they were not always imaged by the Bitter technique [Williams *et al.*, 1992; Newell *et al.*, 1993b]. Ye and Merrill [1995] tried including a macroscopic stress in a quasi-two-dimensional model, but they decided it would not have much effect on the domain structure of magnetite.

One theory predicted fewer domains than were observed, but it seemed to attract little attention. Worm *et al.* [1991] calculated the energy of a two-domain state with closure domains and compared it with the energy of lamellar domain states; they

concluded this should be the lowest energy state for all sizes above the global critical size!

With the two-dimensional models of Xu *et al.* [1994] and Fukuma and Dunlop [1997], theory and observation for magnetite seemed to have converged. When the initial guess was a lamellar domain structure, closure domains appeared spontaneously there were far fewer domains than in one-dimensional models. The two-dimensional models obtained curling states that were very similar to the closure-domain structure predicted by Worm *et al.* [1991], and they were the lowest energy states. Thus to explain the greater number of domains in real particles, Fukuma and Dunlop [1997] had to invoke the concept of local energy minima (section 3.1.2). They predicted the three-domain state would be the saturation remanent state.

Now my results close the LEM loophole. Not only do the curling states have the lowest energy, but they are the only kind of remanent state I obtain. So now the question is why are *more* domains seen than the theory predicts. The closure domain structure is very effective in reducing the magnetostatic energy (because of the pole reduction principle); adding more domains increases the total area of the domain walls (and hence the domain wall energy) without reducing the magnetostatic energy.

Worm *et al.* [1991] suggested that magnetostriction might increase the number of domains (an idea that was first considered by Lifshitz [1944]). If there are no surface tractions on a body, a uniform magnetization causes the body to deform uniformly in the direction of the magnetization. If adjacent domains are magnetized perpendicular to each other (as with closure domains), the strains are incompatible and stresses appear in the crystal. Increasing the number of domains may decrease the energy by decreasing the volume of the closure domains.

Unfortunately, it is very difficult to solve the boundary value problem for magnetostriction and the existing calculations only provide upper bounds for the magnetostriction energy that are probably well above the true energy, so we don't know whether increasing the number of domains will really reduce the energy.

Before worrying about the number of domains, we should answer the zero-order question: when do closure domains occur? If domain states with closure domains are the lowest energy states for magnetite, why are they often not seen?

One possibility is that many particles are under stress. Magnetite particles synthesized by the glass ceramic method [Worm *et al.*, 1991; Geiß*et al.*, 1996; Pokhil and Moskowitz, 1997] tend to have curved domain walls and lack closure domains. The magnetite particles in glass ceramics share welded boundaries with a silicate matrix which is believed to have a significantly higher coefficient of thermal expansion than magnetite [Worm *et al.*, 1991]. The particles are synthesized at 900°C, and as they cool a considerable compressive stress can develop. Indeed, some of the structures observed by Pokhil and Moskowitz [1997] (especially their Figure 11) look like the branching structures that are characteristic of a large uniaxial anisotropy [Lifshitz, 1944]. However, it is not clear what would give rise to a large uniaxial anisotropy: as we saw in Chapter 3, a prodigious stress would be required to produce a large anisotropy.

Another possibility is that in many studies, the crystallographic orientation of the surface is not known [Özdemir *et al.*, 1995]. It is well known that there can be enormous differences in the surface domain pattern depending on the orientation of the surface; it is often supposed that these patterns mask a much simpler pattern below that is the "true" domain structure, but we don't really know. If any orientation for magnetite reflects the internal domain structure for magnetite, it is likely to be the (100) plane because it contains two of the $< 111 >$ easy directions. Textbook examples of closure domains were seen in a set of studies where the crystallographic orientation of the viewing plane was carefully controlled [Özdemir and Dunlop, 1993; Özdemir *et al.*, 1995].

Even when the orientation is known, most domain observation techniques can only be used on flat, highly polished surfaces, and the polishing stresses the surface. Two exceptions are Lorentz force microscopy [Smith, 1980] and the dried colloid SEM

method [Soffel *et al.*, 1990]. It is probably significant that in the papers that use this technique, the two-domain state with closure domains is common.

Thus before we try adding magnetostriction to domain models, we should probably explore the effect of changing the orientation with respect to the surface of the magnetocrystalline easy axes, and see whether this can inhibit closure domains.

4.6 Summary

I have developed an approach to solving micromagnetic problems that uses a combination of field-based hysteresis simulation and grain growth simulation to get reliable results. I show that stable solutions should lie on a hysteresis curve with a slope dM_H/dH that approaches infinity near an instability. Back continuation of such curves to the nucleation field is a powerful method for eliminating unstable solutions.

I use a hysteresis method to find the remanent states for a two-dimensional model of magnetite. The remanent states are consistently as low or low as those obtained for the same configuration by previous methods. My results reinforce the closure domain paradox of Worm *et al.* [1991]: the two-domain state with closure domains appears to have the lowest energy of all remanent states, and it is the only kind of remanent state I obtain in hysteresis simulations. In real particles, many more domains can be seen. Since the closure domains appear to be the reason there are so few domains, future theoretical work should focus on the conditions for formation of closure domains.

Chapter 5

NUCLEATION IN MAGNETICALLY ISOTROPIC CUBOIDS

Before computers were fast enough for theorists to solve two- or three-dimensional micromagnetic equations numerically, there was a gap between domain theory and nucleation theory. In MD models, magnetization changed by motion of domain walls, but there was no mechanism for the walls to enter the particle. In nucleation theory, the curling mode was a perturbation that led to instability of uniform magnetization, but it was not clear what happened after nucleation occurred. Most theorists assumed the instability caused a domain wall to appear or the moment of the particle reversed. Some even assumed that the moment reversed in internal field coordinates, so there was a hysteresis curve with slope $1/N$.

One of the most common solutions of three-dimensional numerical models looks like a curling mode [Fredkin and Koehler, 1987; Schabes and Bertram, 1988; Williams and Dunlop, 1989]. For a cube, Schabes and Bertram [1988] obtained a state like that in Figure 5.1. They described it as a "type of generalized curling," but because of the association of the curling mode with instability they called it a vortex state. This name has been adopted by most researchers in magnetics.

Schabes and Bertram [1988] did not call their solution a curling state because the curling mode is a mode of instability, and it has often been assumed that when uniform magnetization becomes unstable, there is a sudden reversal of the magnetization (this is true for the infinite cylinder [Aharoni and Shtrikman, 1958]).

The term instability has two meanings. One is a discontinuity such as the jump

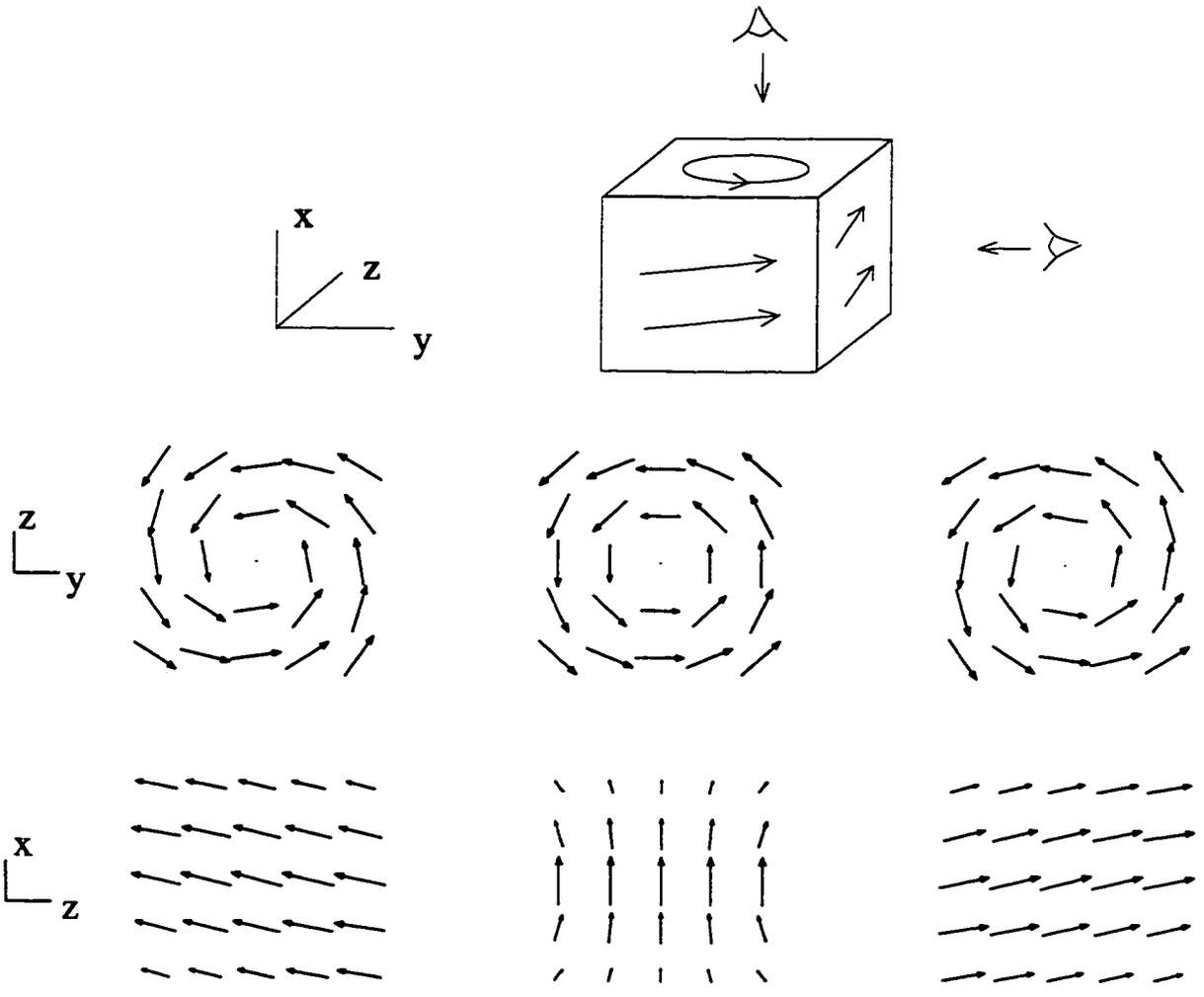

Figure 5.1: The curling state: magnetization vectors for a particle with $L = 12.4L_{ex}$ (0.084μm in magnetite). At the top is a schematic. The middle three plots show the magnetization as seen looking down from the x direction (the direction of the moment). The bottom three plots show the magnetization as seen from the y or z direction. Going from left to right, the cross-sections are the back, middle and top of the particle as seen by the eyes in the top diagram. The vectors show the component of magnetization in the plane; where they are small, the perpendicular component is large.

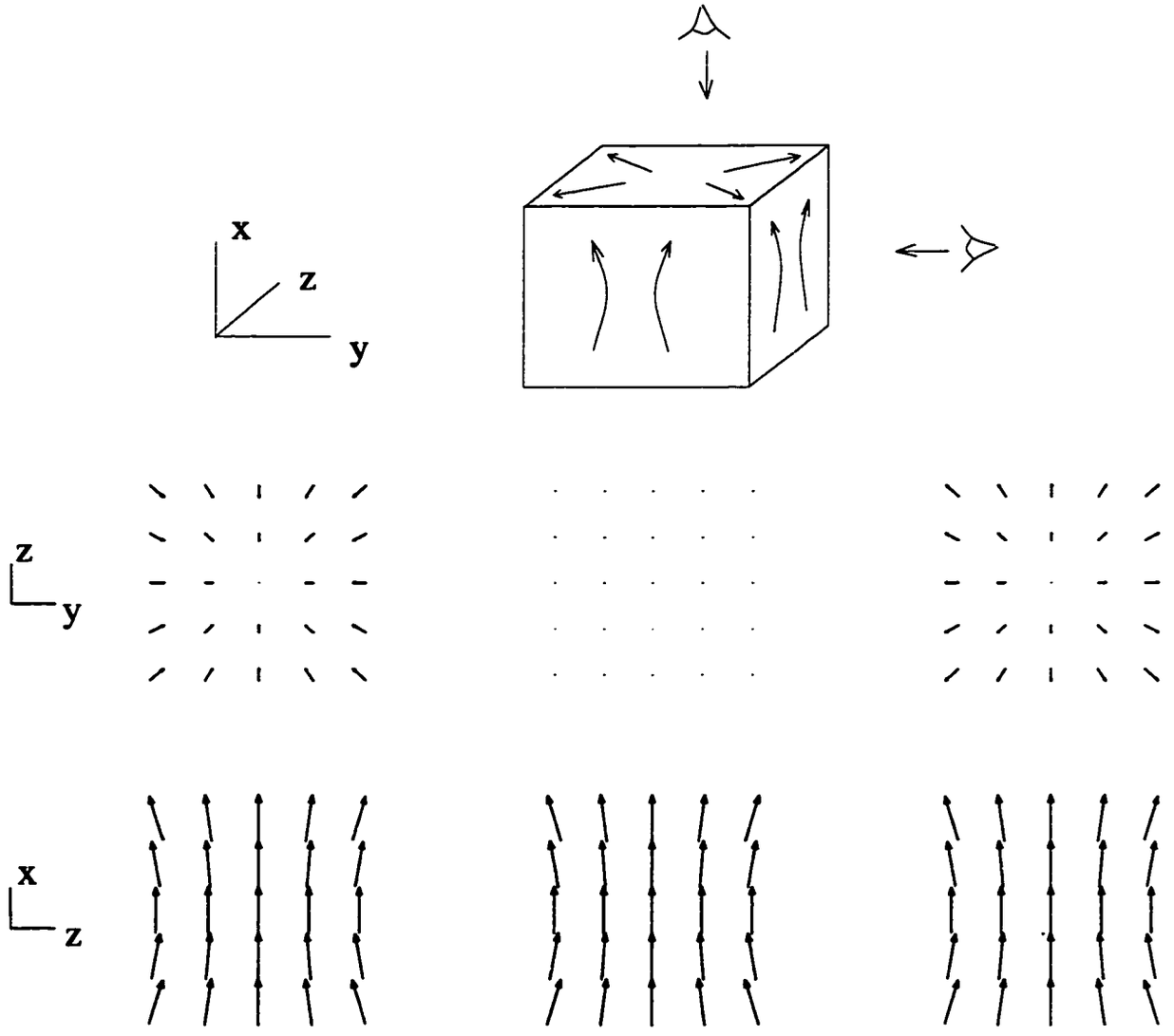

Figure 5.2: The flower state: magnetization vectors for a cube with $L = 9.03L_{ex}$ (0.061μm in magnetite). Same conventions as in Figure 5.1.

that occurs at the switching field (Figure 2.3). Above the switching field, the magnetization (and the corresponding local energy minimum) changes continuously with the field. At the switching field, the minimum disappears entirely and the magnetization must jump to a new minimum. In the other sense, a precisely defined state becomes unstable, but there is not necessarily a jump. For example, a uniformly magnetized state with its moment in a particular direction is destabilized by a field in some other direction. However, this may just lead to a small rotation of the moment, as in SD theory.

Often nucleation appears to be the latter kind of instability. In micromagnetic models of ellipsoids, the curling perturbation is added to uniform magnetization to form a curling *state* [Fredkin and Koehler, 1988, 1989; Aharoni and Jakubovics, 1990]. This state evolves continuously away from uniform magnetization.

In a cube, the magnetization is non-uniform even in the SD size range (Figure 5.2). Schabes and Bertram [1988] called this state the flower state, because of the way the magnetization vectors open outwards at the ends. The magnetization is nearly uniform, but there is a small transverse component which is inward at the bottom (the end where $\mathbf{M} \cdot \hat{\mathbf{n}} < 0$, $\hat{\mathbf{n}}$ being the outward normal to the surface) and outward at the top. As the field increases, the magnetization in the flower state approaches uniform magnetization, but it never becomes perfectly uniform. Nevertheless, it is sufficiently close to uniform that it might be considered uniform magnetization with a perturbation added.

Models of the approach to saturation in ferromagnets often invoke local deviating forces exerted by non-uniformities in the crystal. If the deviating forces are local and small, it is possible to treat them with linear perturbation theory Brown [1940]. If the flower state can also be considered a perturbation of uniform magnetization, with the deviating forces coming from the normal component of magnetization at the surface (subsection 5.1.2), we would expect the mode of nucleation to be similar to that in ellipsoids. We would also expect that nucleation theory could be adapted to

cubes.

In this chapter, I show that the flower state plays the same role as the SD state in ellipsoids, and the theory for nucleation in ellipsoids can be adapted to cuboids.

5.1 The SD (Flower) State in the Cube

5.1.1 The Demagnetizing Field and the Flower State

Since the difference between the sphere and the cube is in the demagnetizing field, I begin with a description of this field. In a cube with magnetization that is uniform and perpendicular to two surfaces, the only magnetic poles ($\mathbf{M}\cdot\mathbf{n}$) are surface charges $+M_s$ on one surface and $-M_s$ on the other. The equations for the demagnetizing field are then identical to the more familiar equations for an electric field between capacitor plates [Dunlop *et al.*, 1990].

In an ellipsoid of rotation, if the field is along the symmetry axis of the particle, the demagnetizing field is parallel to the moment, and instability can only occur when the sign of the total field $\mathbf{H} + \mathbf{H}_d$ changes in some region of the particle. In the cube, there is also a perpendicular, or transverse, component. Because of this component, there is a non-uniform torque $\mu_0\mathbf{M} \times \mathbf{H}_d$ on the magnetization. Since there is nothing to balance this torque, uniform magnetization is not stable in any applied field. Instead, there is a flower state as in Figure 5.2.

The magnetization in the flower state curves the opposite way to the demagnetizing field in Figure 5.3. It is instructive to look for a reason. In an equilibrium state, Brown's equation (2.9) implies the magnetization must be parallel to the total effective field, which in the isotropic cube is the sum of an exchange field and the demagnetizing field. If there is a non-uniform perturbation in the magnetization, the exchange field increases in opposition to it.

I tried creating an "anti-flower" state by changing the sign of the transverse component of the magnetization in the flower state. The magnetization and effective

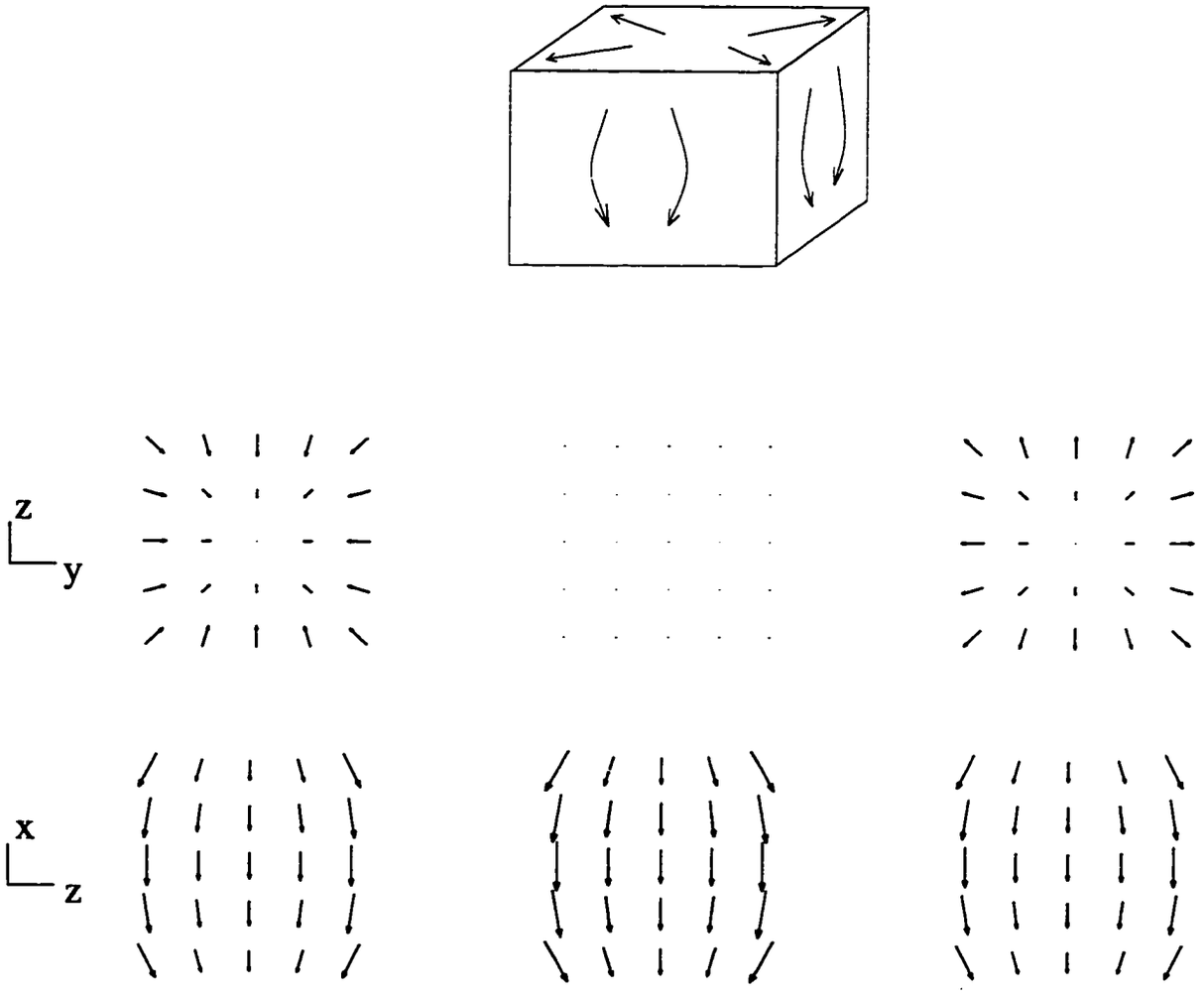

Figure 5.3: The demagnetizing field for uniform magnetization. The demagnetizing field has the opposite sign to the magnetization. Same conventions as in Figure 5.2.

field are nearly parallel, indicating a possible solution to Brown's equation - yet the energy of the anti-flower state is much higher than that of the flower state, and the anti-flower state is unstable.

The flower state has lower energy than the anti-flower state because the magnetic poles are the same or smaller everywhere in the particle. Consider the top half of the particle, going from the middle to the $+\hat{\mathbf{x}}$ face: the x component of the magnetization decreases because it rotates away from this face, so $dM_x/dx < 0$. The magnitude of the pole $|\nabla \cdot \mathbf{M}|$ is therefore reduced if both dM_y/dy and dM_z/dz are negative. In the lower half of the particle, $dM_x/dx > 0$, so $|\nabla \cdot \mathbf{M}|$ is reduced if the other two derivatives are positive. This is consistent with the flower pattern, and the opposite of the anti-flower pattern. Since the anti-flower state appears to be stationary, it may be a saddle point or maximum.

For the flower state, the demagnetizing field still curves inward, as it does for uniform magnetization, but its magnitude is much smaller in the corners than the demagnetizing field.

5.1.2 Approach to Saturation

When we say the magnetization is saturated, we imply that it has reached its maximum value. In real particles, the magnetization continues to increase as the field increases, although dM_H/dH decreases. Even in simple theoretical models, the magnetization approaches saturation asymptotically.

For an isotropic ensemble of Stoner-Wohlfarth particles, the magnetization in the approach to saturation is well approximated by [O'Reilly, 1984, page 73]

$$M_s = M_H \left(1 - \frac{b}{H^2}\right) \tag{5.1}$$

where $b = N^2 M_s^2/15$ for shape anisotropy. For cubic anisotropy with $K_1 > 0$, $b = (8/105)K_1^2/\mu_0^2 M_s^2$.

In large particles, defects and inclusions add other terms to the expansion. Inclusions give rise to a $-1/H$ term [Néel, 1948]; concentrations of defects add $H^{-n/2}$ terms, with $n = 1, 2, 3$ for point, line and plane concentrations of random deviating forces [Brown, 1940].

It seems reasonable to think of the demagnetizing field of the cube as a deviating force concentrated near the poles $\mathbf{M} \cdot \hat{\mathbf{n}}$ at the surface of the particle. I tried fitting the approach to saturation for the cube to the above power laws; it agreed well with an $H^{-1.5}$ law (Figure 5.4), the same as for the equation of Brown [1940] for plane concentrations of random deviating forces. His assumptions are very different from the conditions of my simulations, but the law is consistent with deviating forces that are concentrated at the surface.

5.2 Nucleation in the Cube

5.2.1 Particle Size Dependence of the Nucleation Field

In the cube, the demagnetizing field could promote or discourage nucleation: the transverse fields in the corners could destabilize the SD state by forcing the magnetization to rotate, or the antiparallel demagnetizing field in the center could be smaller, thus making the SD state more stable. In Figure 5.5, I plot the nucleation field as a function of particle size for the isotropic cube and sphere. The demagnetizing field for the sphere is predicted by equation 3.5:

$$\frac{H_n}{M_s} = N_a - \frac{kL_{ex}^2}{L^2}$$

with $N_a = 1/3$ and $k = 22.5$. The nucleation fields obtained by the numerical model of Aharoni and Jakubovics [1990] (circles) agree well with this equation. The nucleation fields for the cube are also a good fit to this equation if N_a is replaced by an effective demagnetizing factor $N_a = 0.26$.[1]

[1] This result also shows that it is appropriate to compare particles of different shapes by their volume. This is not obvious. Since the curling pattern is two-dimensional, H_n could be determined

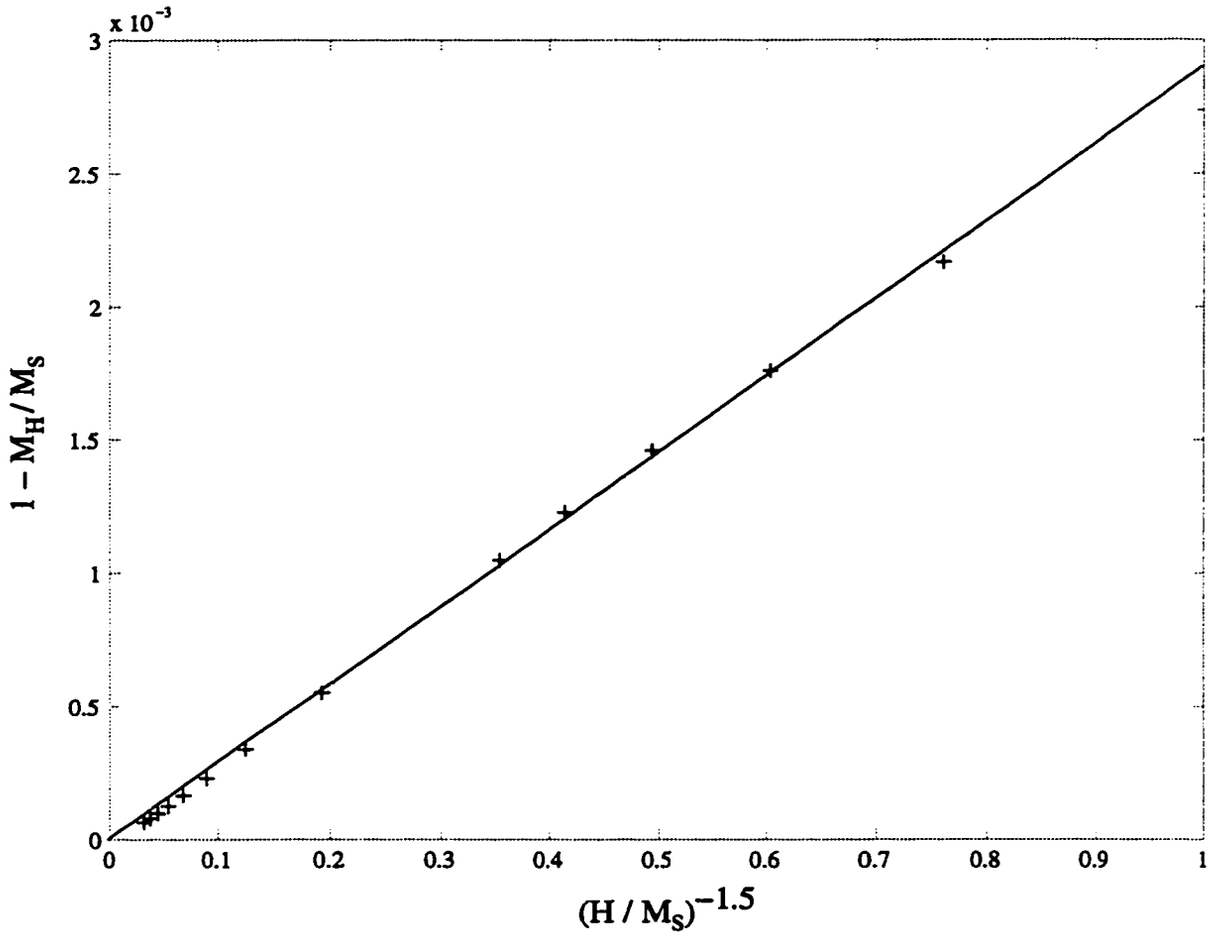

Figure 5.4: The approach to saturation for a particle with $L = 9.03L_{ex}$ (0.061μm in magnetite). The solid line is $1 - M_H/M_s = 0.0029(H/M_s)^{-1.5}$.

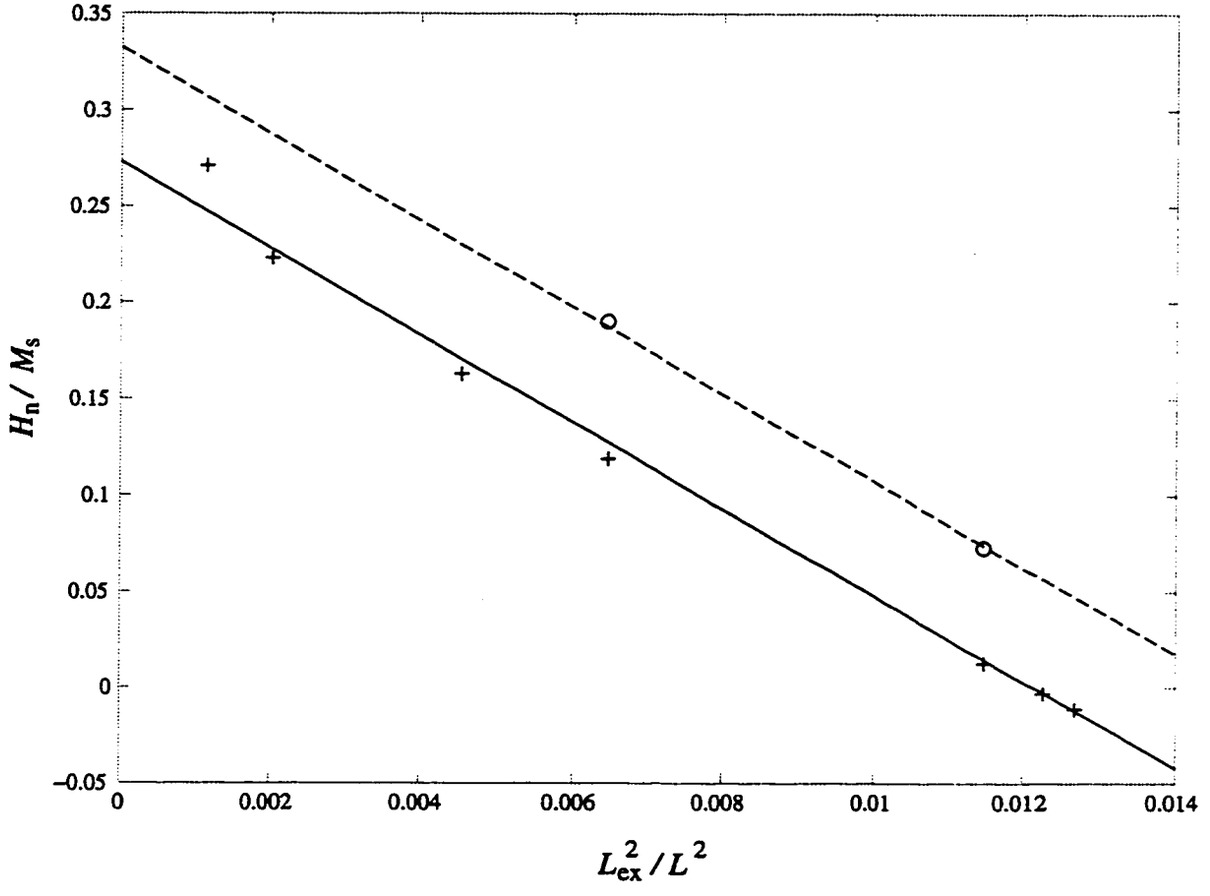

Figure 5.5: A plot of nucleation field as a function of particle size for an isotropic cube. The dotted line is the theoretical nucleation field for a sphere of equivalent volume, and the two circles are the nucleation fields obtained by Aharoni and Jakubovics [1990]. The crosses are my nucleation fields for the cube; the solid line is the best fitting line with slope $k = -22.5$, the theoretical slope for the sphere.

Since the nucleation field is smaller in the cube than in the sphere, it is probably determined primarily by the antiparallel component. The effective demagnetizing field of $0.26M_s$ at the nucleation point is well below the maximum antiparallel component ($0.50M_s$) and well above the minimum component ($0.18M_s$ for $L = 9.03L_{ex}$ and $0.20M_s$ for $L = 12.4L_{ex}$) - but it is fairly close to the volume average ($0.30M_s$).

This implies that conditions for nucleation are not local - hardly surprising given the non-local magnetostatic interactions and the small size of the particle. Indeed, the term "nucleation" is misleading: it implies a change that starts locally (from a nucleus) and spreads. Instead, the curling perturbation occurs throughout the particle and increases outwards from the center.

5.2.2 Dependence of the Nucleation Field on Grid Size

We must be careful how we interpret the result for the nucleation field, because it depends on the accuracy of the demagnetizing field. In the numerical model, the demagnetizing field at a grid point is the average over the volume element around the grid point [Newell *et al.*, 1993a]. Since the demagnetizing field depends on position, the volume average depends on the shape and size of the volume element.

In Figure 5.6, I plot the extrema for the antiparallel and transverse components of the demagnetizing field for uniform magnetization. For a grid size of one, the transverse field is zero and the maximum and minimum parallel fields are equal to the average field $M_s/3$. As the grid size increases, the maximum and minimum parallel fields initially diverge quickly and then are nearly independent of grid size. The transverse component, by contrast, increases rapidly with grid size.

Fortunately, the demagnetizing field does not seem to depend significantly on the transverse field. In Figure 5.7, the nucleation field is shown as a function of grid size.

---

by the cross-sectional area perpendicular to the moment. If so, the nucleation fields for the cube and sphere would have the same slope if the square root of the area was used for the length; in Figure 5.5, the slopes would be different by a factor of about 1.2.

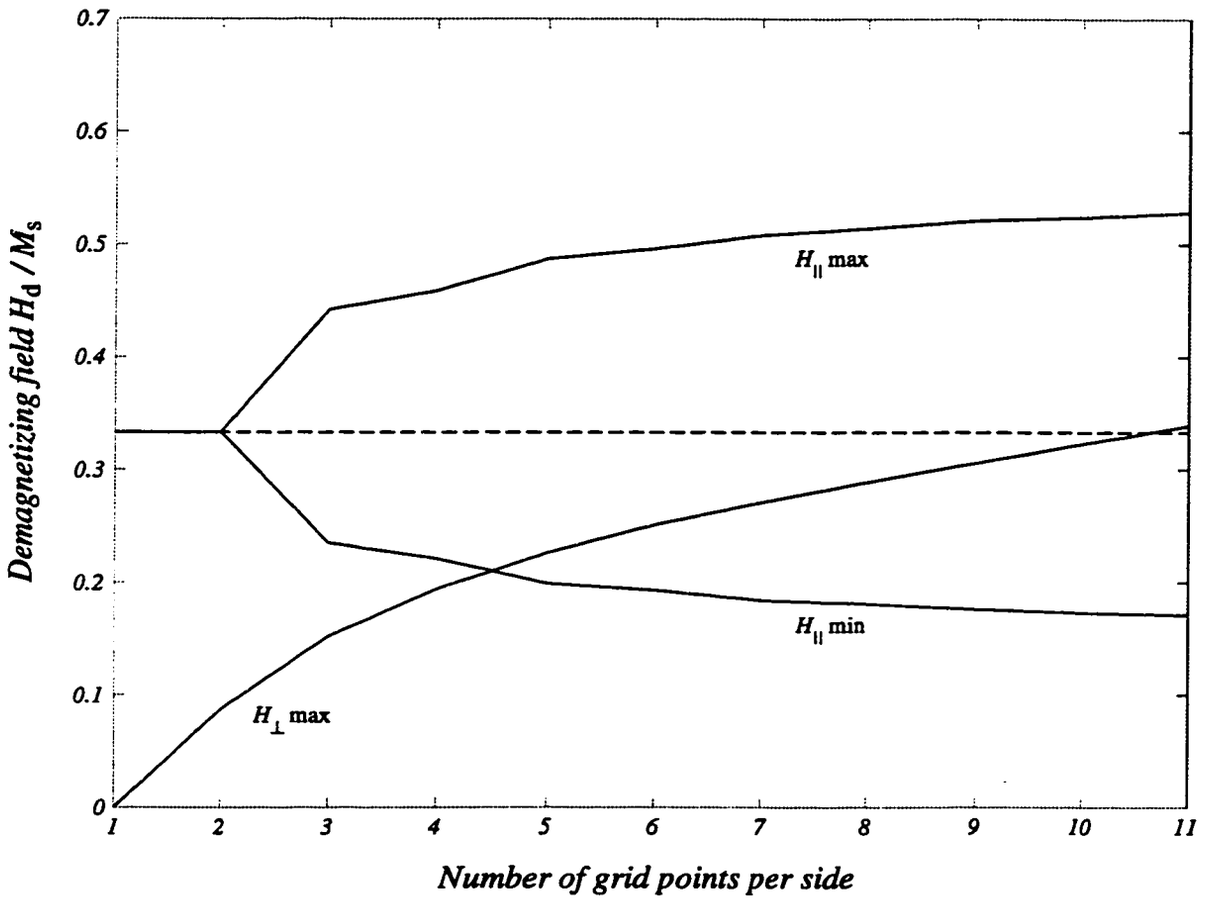

Figure 5.6: The extrema of the demagnetizing field for a uniformly magnetized cube, as a function of grid size. For reference the volume-average field, $M_s/3$ is shown as a dotted line.

For a grid size of three or more, the nucleation field does not change significantly, and it is best predicted by the mean demagnetizing field.

5.2.3 Brown's Paradox

It has long been known that nucleation typically occurs much more easily in real particles than the theory for perfect crystals predicts. For an ellipsoidal particle with non-uniform intrinsic anisotropy, Brown [1945] derived a rigorous bound on the nucleation field:

$$\frac{H_n}{M_s} \leq -\frac{2\kappa_{min}}{\mu_0 M_s^2} \tag{5.2}$$

where κ_{min} is the minimum magnetocrystalline anisotropy in the crystal. This has the same form as equation 3.5 in the limit $L \to \infty$ with $N_a = 0$ (for infinite elongation). In experiments on iron whiskers [Bozorth, 1951, page 561], the nucleation field was much larger than this upper limit: to resolve the discrepancy, κ_{min} would have to be a factor of 5000 smaller than the predicted coercivity. This discrepancy is called Brown's paradox.

Imperfections, for example dislocations or cavities, can reduce the local value of κ by inverse magnetostriction, or they destabilize the magnetization by exerting transverse forces on it. However, no one has been able to demonstrate theoretically that such local deviations are enough to resolve Brown's paradox. The forces required are sufficiently large that the linear approximation breaks down [Brown, 1959].

Shtrikman and Treves [1960] predicted the field at edges and corners could cause nucleation, and proposed that it might be a solution to Brown's paradox. The continuous demagnetizing field approaches infinity near the edges of the cube. Clearly, numerical models cannot determine the effect of this on the magnetization. It is possible, however, that at a moderate grid size there might be a qualitative change in the magnetic behavior the transverse field gets bigger.

Hartmann [1987] measured the hysteresis curve for single-crystal iron whiskers be-

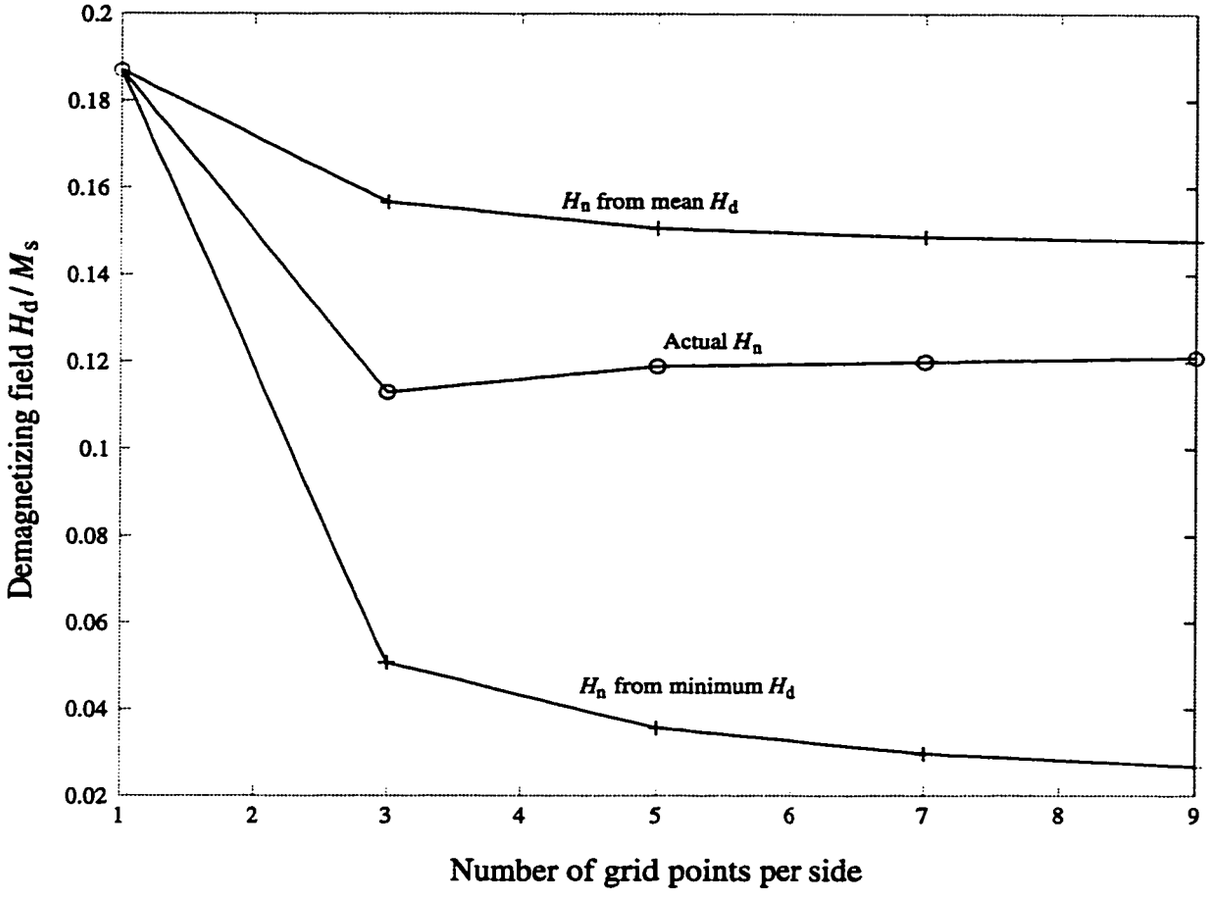

Figure 5.7: The nucleation field for a 0.084 micron cube as a function of grid size. For comparison, I include nucleation fields predicted using the mean demagnetizing field and the minimum parallel demagnetizing field in equation 3.5

fore and after polishing the corners. When a crystal had sharp corners, the hysteresis curve was very narrow; after polishing, it was a nearly rectangular loop with a coercivity very close to the theoretical nucleation field. Thus sharp corners can increase the nucleation field considerably. This particular solution to Brown's paradox may not be common in nature, however. Aharoni [1989] estimates that if the corners are smoothed by as little as the radius of an atom, the demagnetizing field only reaches about $1.5M_s$. Hartmann examined his crystals with an electron microscope and found they were "bounded by perfect sharp corners," so his result may be consistent with this estimate, but most particles may be better represented by rounded edges and corners.

Thus micromagnetic models with their present resolution probably do a reasonably good job of representing nucleation in real particles.

5.2.4 Field Not Aligned With a Symmetry Axis

All the above work is for a field that is aligned with a fourfold symmetry axis of the cube. In Figure 5.8, I show an example of nucleation for a field in a direction that breaks the symmetry. The vectors are the difference by vector subtraction between the states before and after nucleation. As is true for a field aligned with the symmetry axis, nucleation is associated with the appearance of curl, but the curl is centered around an axis that is roughly in the same direction as the field.

5.3 SD States and Nucleation in a Triaxial Cuboid

In this section, I model the magnetic behavior of a triaxial cuboid - a particle with rectangular faces and three unequal sides. The ratios of the sides are $X = 1.4Y = 1.5Z$, so the X axis is the long axis, the Y axis is the intermediate axis, and the Z axis is the short axis.

I use a combination of hysteresis and grain growth simulations to find the remanent

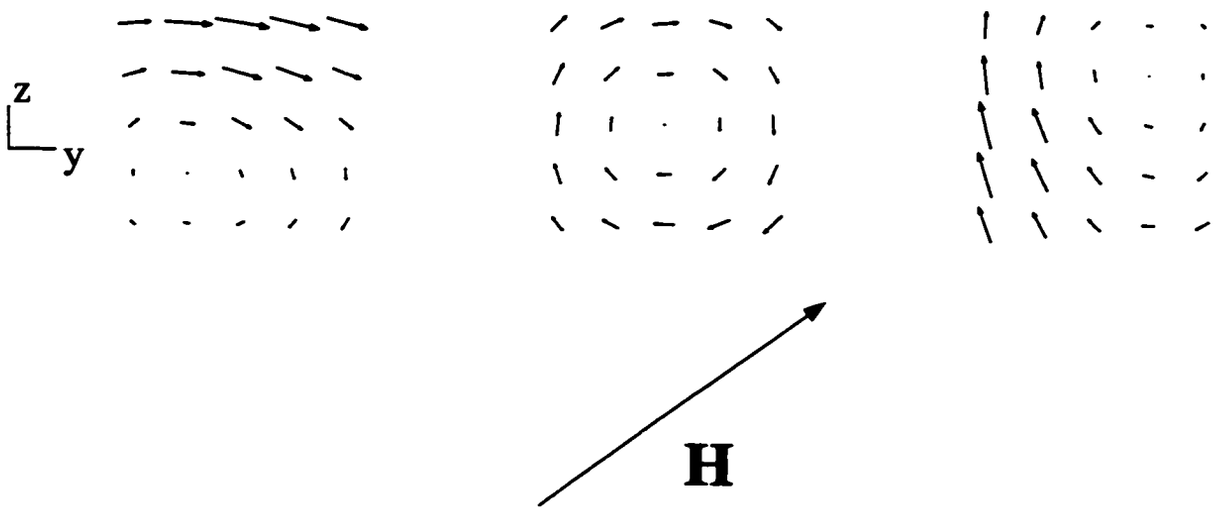

Figure 5.8: The difference between magnetization vectors before and after nucleation. The view is from the x direction, and the vector shows the direction of the field in the $y-z$ plane. There is a curl centered around the direction of the field. The same conventions are used as in Figure 5.1.

states for the triaxial cuboid as a function of size up to 0.15μm. I restrict myself to this size range because the grid size I am using is not large enough to represent the small-scale changes of magnetization in larger particles. As I will show, the size range near the SD critical sizes is worth a careful exploration because the magnetic properties are changing rapidly.

As I mentioned in Chapter 4, I checked the remanent states at a few particle sizes (0.09, 0.11, 0.13 and 0.15μm) by comparing the moments derived from hysteresis curves with those from grain growth simulations. Each component of the normalized volume-average magnetization, if given in the form $x.xxxx$, was reproducible to four decimal places.

5.3.1 Remanent states and Nucleation Sizes

In zero field, an ellipsoidal ferromagnet in the SD size range has two energy minima for magnetization aligned with the long axis; the intermediate and short axes correspond to saddle points and maxima (Figure 2.1). The cuboid also has a flower state with moment along the intermediate axis (but not the short axis). I obtained the intermediate-axis state by the other method I described in Chapter 4: simulation of changes in particle size. In 0.09μm particles, curling states occur with moment along the intermediate and short axis. By decreasing the size, I obtained a sequence of states for the intermediate axis that turned into flower states. The short-axis curling state becomes unstable at 0.067μm.

In a plot of magnetization against particle size, the nucleation critical size L_n can be identified by a sudden change in the slope dM_H/dH. In Figure 5.9, I show the magnetization as a function of particle size in the region where the nucleations occur.

An example of a long-axis remanent state just above nucleation is shown in Figure 5.10. At nucleation, the magnetization does not change suddenly; a small amount of curl is added to a flower state. As particle size increases, the component in the x direction decreases and the state looks increasingly like a pure curling state.

Above the nucleation size, I continue to get the flower state. As I showed in Chapter 4, this state is unstable, so I represent it in Figure 5.10 by dotted lines. When the long-axis flower state becomes *numerically* unstable, it turns into the state shown in Figure 5.11. This looks similar to that in Figure 5.10, but the curls at the top and bottom of the particle are in opposite directions. It appears that the corresponding M vs L curve should continue back to join the curve for the flower state, but the state becomes unstable before they join (Figure 5.9). The state also becomes unstable at 0.094μm.

Schabes [1991] observed a similar state in models of hematite particles with a large aspect ratio; he called it a $+-$ vortex state. As with the curling state, this state

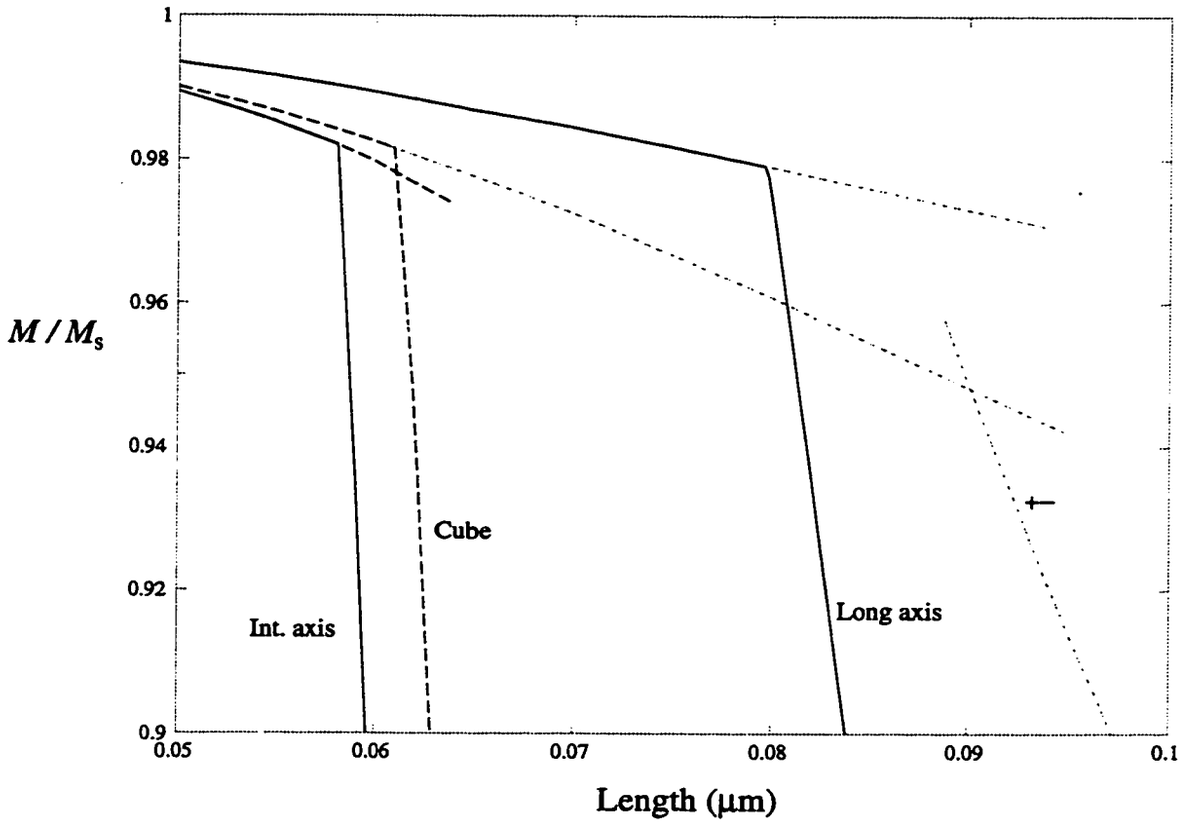

Figure 5.9: Volume-average magnetizations of the remanent states in the region where nucleation occurs. The solid lines are for the triaxial cuboid; for comparison, the magnetization for the cube is shown as a dashed line. Where nucleation occurs, there is a sharp bend in the magnetization; the continuation of the flower state is shown as a dotted line because it is probably not stable. Also shown with the +− label is the +− vortex (second order curl) state: this state is probably also not stable.

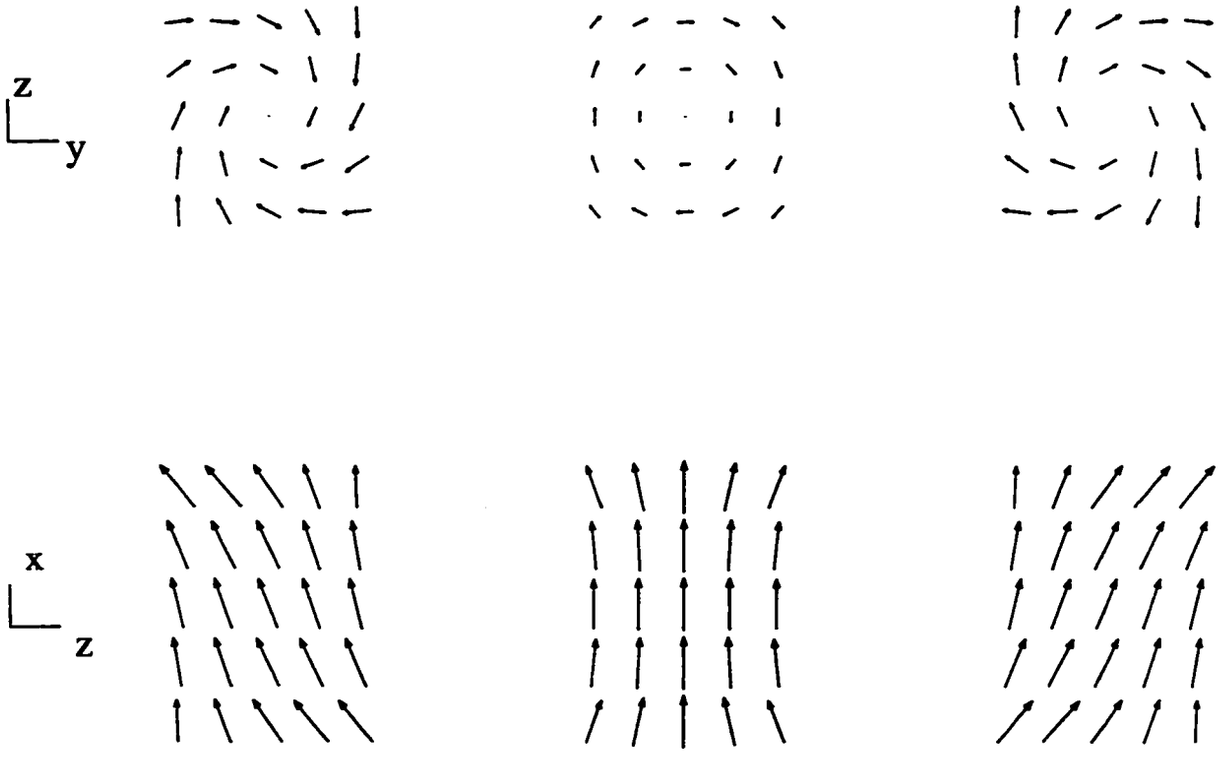

Figure 5.10: A magnetic state for $L = 0.084\mu$m, just above the nucleation size. The state is a flower state with some curl added.

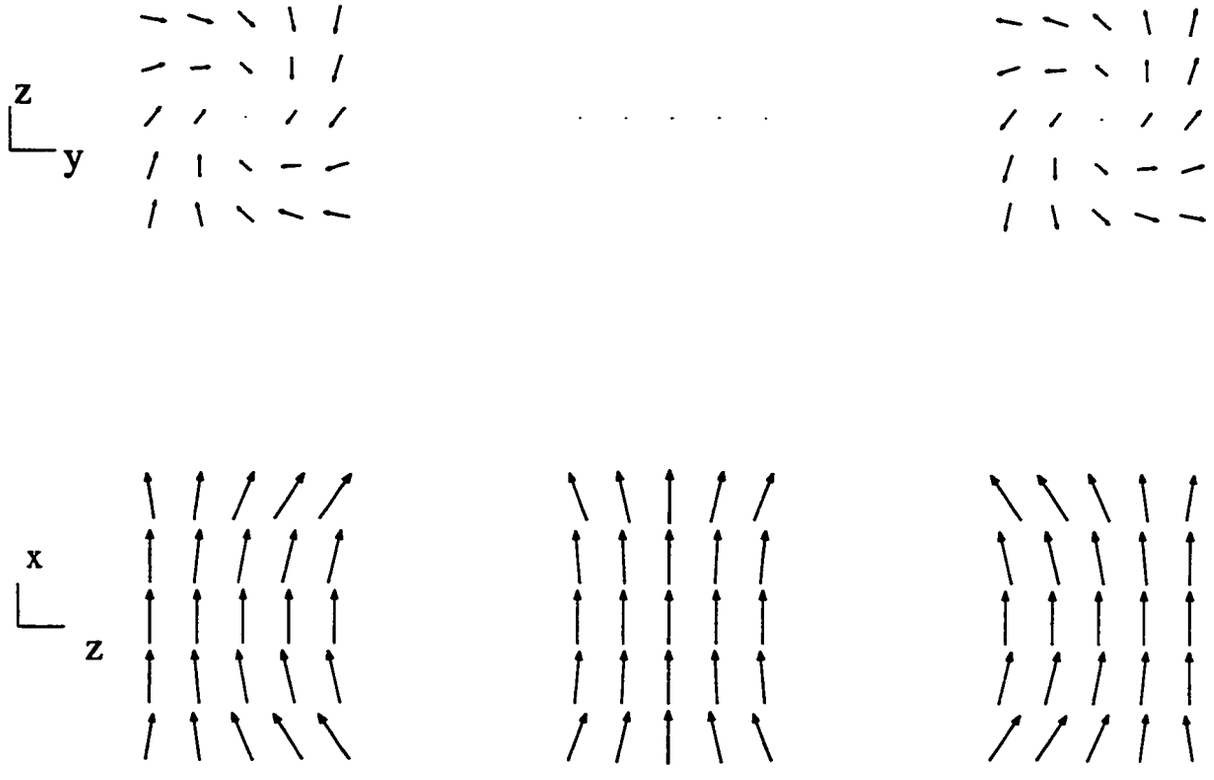

Figure 5.11: A magnetic state for $L = 0.09\mu$m: a flower state with second order curl added.

has a precedent in nucleation theory. The curling mode described in equation 3.3 is just one of a set of modes that in general depend on the vertical coordinate as well: in cylindrical coordinates [Brown, 1963],

$$\delta\hat{m}_\phi = \delta\hat{m}_\phi(\rho, z), \quad \delta\hat{m}_\rho = 0 \tag{5.3}$$

In my coordinates, z is replaced by x. If we take the vector difference between the magnetization vectors of the state in Figure 5.11 and those of the pure flower state (Figure 5.12), the result is a perturbation mode that is well described by equation 5.3. The x dependence is such that $\mathbf{M} \parallel \pm\hat{\mathbf{x}}$ at the surface, thus reducing the surface poles.

In the nucleation theory for ellipsoids (Chapter 3), the higher order nucleation modes never occur because the lowest order mode destabilizes the SD state before they can occur. This is true for the cuboid as well, and I have not obtained this state in the field-based hysteresis simulations. Thus the state is probably unstable.[2]

5.4 Nucleation and Curling

Since the magnetization is never uniform in a cube, there cannot be nucleation in the strict sense of a change from uniform to non-uniform magnetization. If we could not generalize the concept of nucleation, it would have little relevance to real particles. Fortunately, as I showed in Section 5.3, there is a well defined nucleation field where a sharp change in the slope dM_H/dH occurs. If the change in magnetization is continuous, there is a topological change in the magnetization. Above the nucleation field, the flower state has zero curl; below it, there is a combination of curl and flower state. Similarly, in ellipsoids after nucleation, there is a combination of uniform magnetization and a curling perturbation.

Schabes and Bertram [1988] made this statement quantitative by defining a helicity Λ that is proportional to a line integral of the magnetization along an oriented

[2] The short-axis curling state also appears suddenly at 0.067μm, but it then has the lowest energy of all states and it appears in field-based hysteresis simulations, so it is undoubtedly stable.

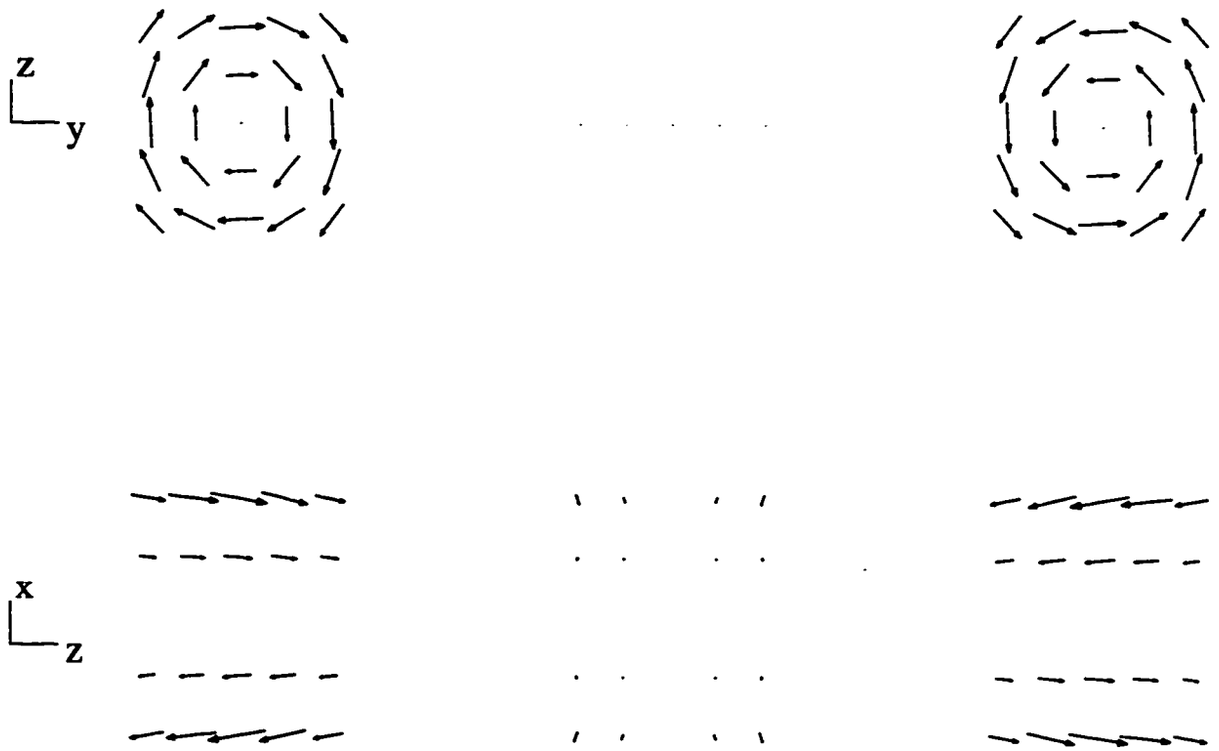

Figure 5.12: The difference between the magnetic state in Figure 5.11 and the pure flower state for the same particle size.

closed curve C:

$$\Lambda \propto \oint_C \mathbf{M} \cdot d\mathbf{l} \tag{5.4}$$

They showed that Λ is zero for the flower state and nonzero for the curling state.

We can express the above integral in another form using Stokes' theorem:

$$\oint_C \mathbf{M} \cdot d\mathbf{l} = \oint_S \nabla \times \mathbf{M} \cdot d\mathbf{a}$$

where S is any surface bounded by the curve C and within the volume where $\mathbf{M}$ is continuous.

The curl $\nabla \times \mathbf{M}$ is zero throughout the particle in the flower state and nonzero after nucleation. We can also say, in analogy to fluid mechanics, that the magnetization has vorticity.[3] It probably also has helicity, although helicity is usually defined as $\mathbf{M} \cdot (\nabla \times \mathbf{M})$ [Merrill *et al.*, 1996].

Thus curling and vortex are appropriate names for the state after nucleation has occurred. I prefer curling because of its continuity with earlier micromagnetic theory.

5.5 Transitions in Remanent States

As I described in Chapter 5, the long-axis and intermediate-axis curling states nucleate at 0.058 and 0.08 microns, while the short-axis curling state first appears at 0.067μm. Near 0.11μm, further transitions occur in the magnetic states. These transitions are associated with changes in the curl. I will begin the discussion of transitions with the z axis (short axis) curling state. Up to $L = 0.112\mu$m, this state is a combination of a flower component and some curl. As the particle size increases, the component of magnetization in the z direction decreases, but otherwise the state looks the same. The state at 0.112μm is shown in Figure 5.13.

Just above $L = 0.112\mu$m, the moment starts to rotate towards the x axis (Figure 5.14), and there appears to be a slight curl around the x axis. This curl probably

[3] $\nabla \times \mathbf{M}$ is also called an effective current density [Jackson, 1975, equation 5.79].

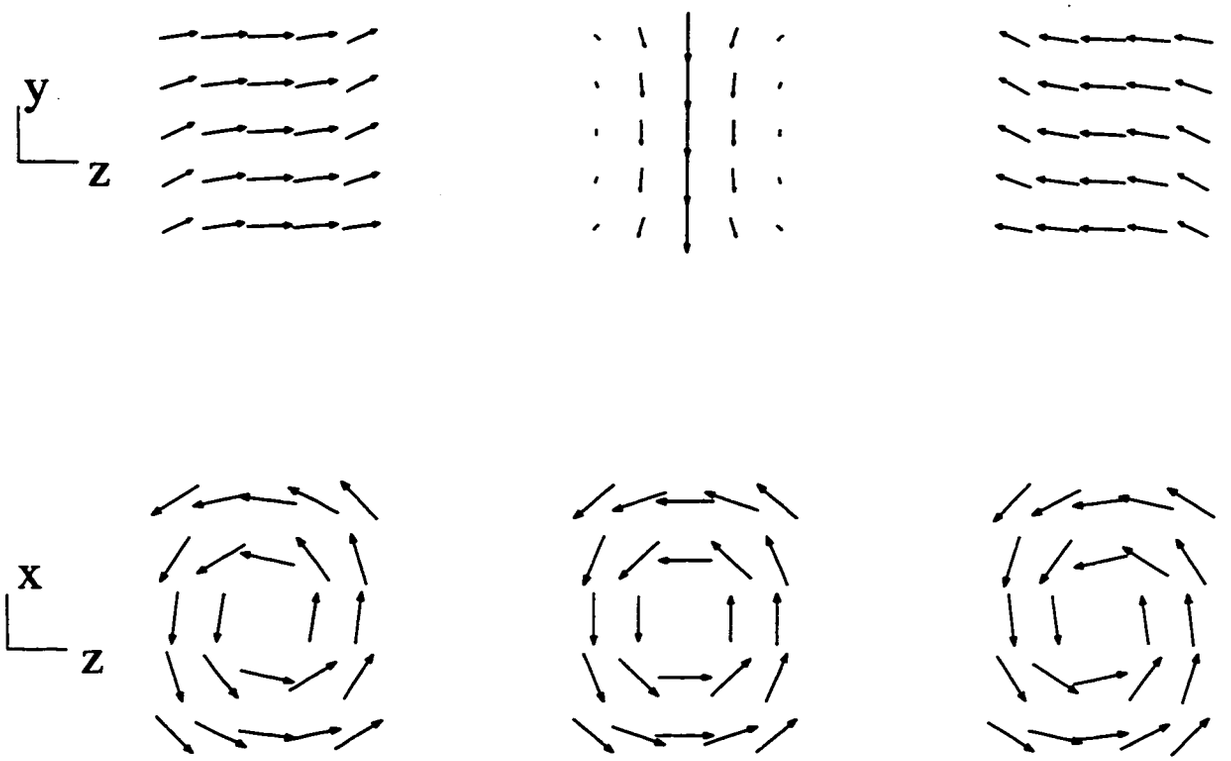

Figure 5.13: The intermediate axis curling state at 0.112μm, just before a transition occurs. The moment is in the z direction and there is only nonzero curl about the z axis.

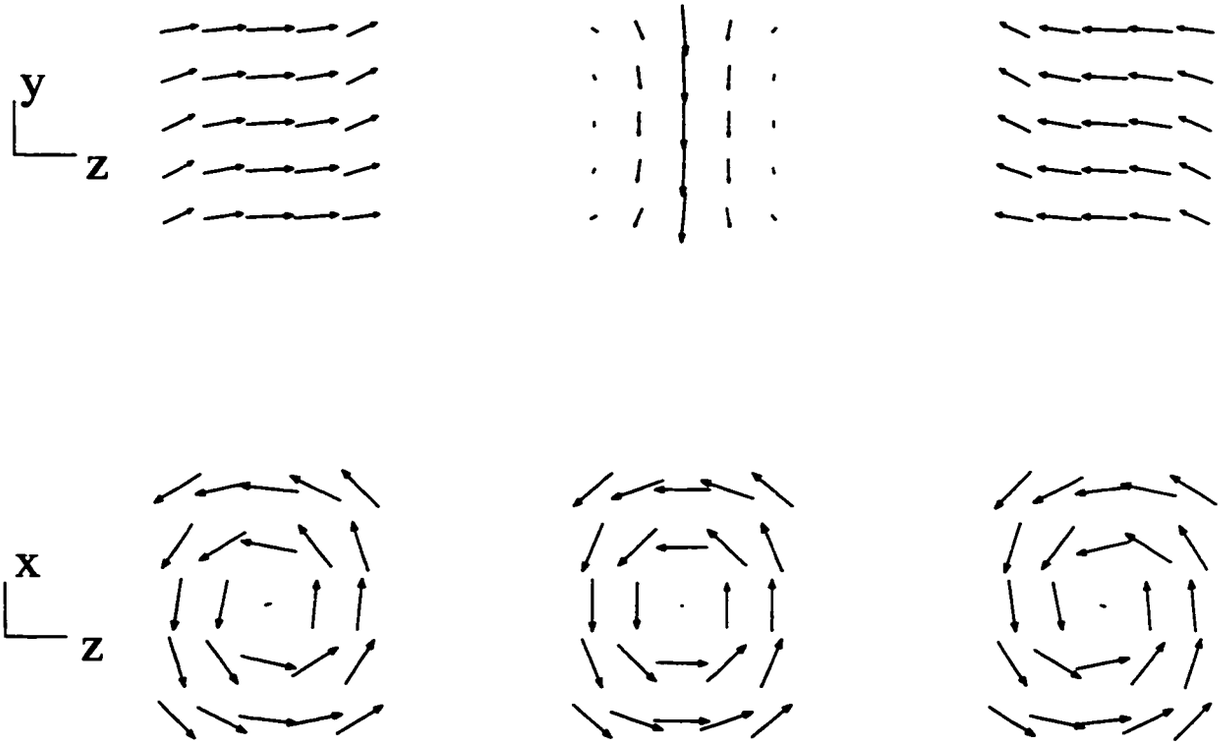

Figure 5.14: The intermediate axis curling state at 0.113μm, just after the transition occurs. The moment now has an x component, and there is also some curl about the x axis.

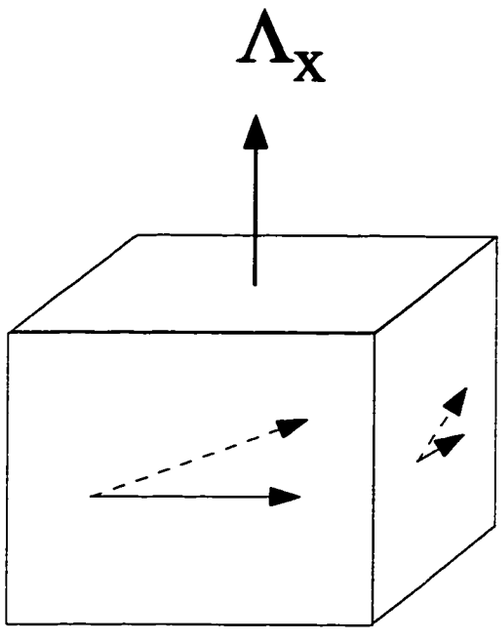

Figure 5.15: An illustration of the calculation of the x component of the normalized curl parameter $\mathbf{\Lambda}$. The y components of $\mathbf{M}$ in the xy planes and the z components of $\mathbf{M}$ in the xz planes are added in a right-handed screw sense.

reduces the energy by reducing the surface poles on the $\pm\hat{\mathbf{y}}$ surfaces.

To investigate topological changes in the magnetization, I generalize the Λ parameter of Schabes and Bertram [1988] to a vector quantity $\mathbf{\Lambda}$. For a direction $\hat{\mathbf{x}}_i$, I choose circuits $\mathbf{l}(x_i) \perp \hat{\mathbf{x}}_i$ around the outside of the particle (with a right-handed screw sense), and I average the component of $\mathbf{M}$ along $\mathbf{l}_i$:

$$\Lambda_i = \int dx_i \oint \mathbf{M} \cdot d\mathbf{l}(x_i) \Big/ \int dx_i \oint dl(x_i) \tag{5.5}$$

An example for the component of $\mathbf{\Lambda}$ in the x direction is shown in Figure 5.15. The components of $\mathbf{\Lambda}$ can be thought of as normalized volume-average curls about each axis; the normalization is such that the maximum possible value is 1.

In Figure 5.16, I show the components of the volume-average magnetization and of the curl parameter $\mathbf{\Lambda}$ as a function of particle size. In Figure 5.16a and c, the z

components are shown. At the nucleation point $L = 0.058\mu$m, a curl develops about the z axis. The volume average curl is roughly constant at 0.055, but as particle size increases the curl becomes more localized around the central z axis. In Figure 5.16b and d, I show the x components. Both have a vertical takeoff just above $L = 0.112\mu$m.

The intermediate-axis curling state (Figure 5.17) has a similar behavior with particle size, except that it begins by nucleating at 0.058μm. The curl about the y axis takes off vertically and rapidly reaches a plateau at about 0.65, higher than the value for the short-axis state. At 0.11μm, an x component appears in both the magnetization and the curl.

There is also a transition for the long-axis curling state at $L = 0.11\mu$m, but it is strikingly different in two ways (Figure 5.18). First, there is a discontinuous change in the main component of magnetization and curl (Figure 5.18a,c). Secondly, the new component along the short axis starts large and decreases (note, however, that the curve starts out vertical, as do the curves for the other nucleations).

Together, Figures 5.16, 5.17 and 5.18 indicate that there are transitions in all the remanent states at $L = 0.11\mu$m. These transitions reduce the symmetry of the states, and this has the result of removing some of the constraints on the direction of the moment. Instead of being in a fixed direction, the moment of each state is confined to a plane: the xz plane for the short-axis curling state, the yz plane for the intermediate-axis curling state, and the xz plane for the long-axis curling state. This is an indication that the shape of the particle is having a decreasing effect on the magnetization.

5.6 Nucleation and Bifurcations

When a curl is added, the sense of the curl is chosen arbitrarily. In Figure 5.1, for example, the curl is right-handed (the moment being upwards out of the page). It could equally well be left-handed, with the same moment; the energy would be the

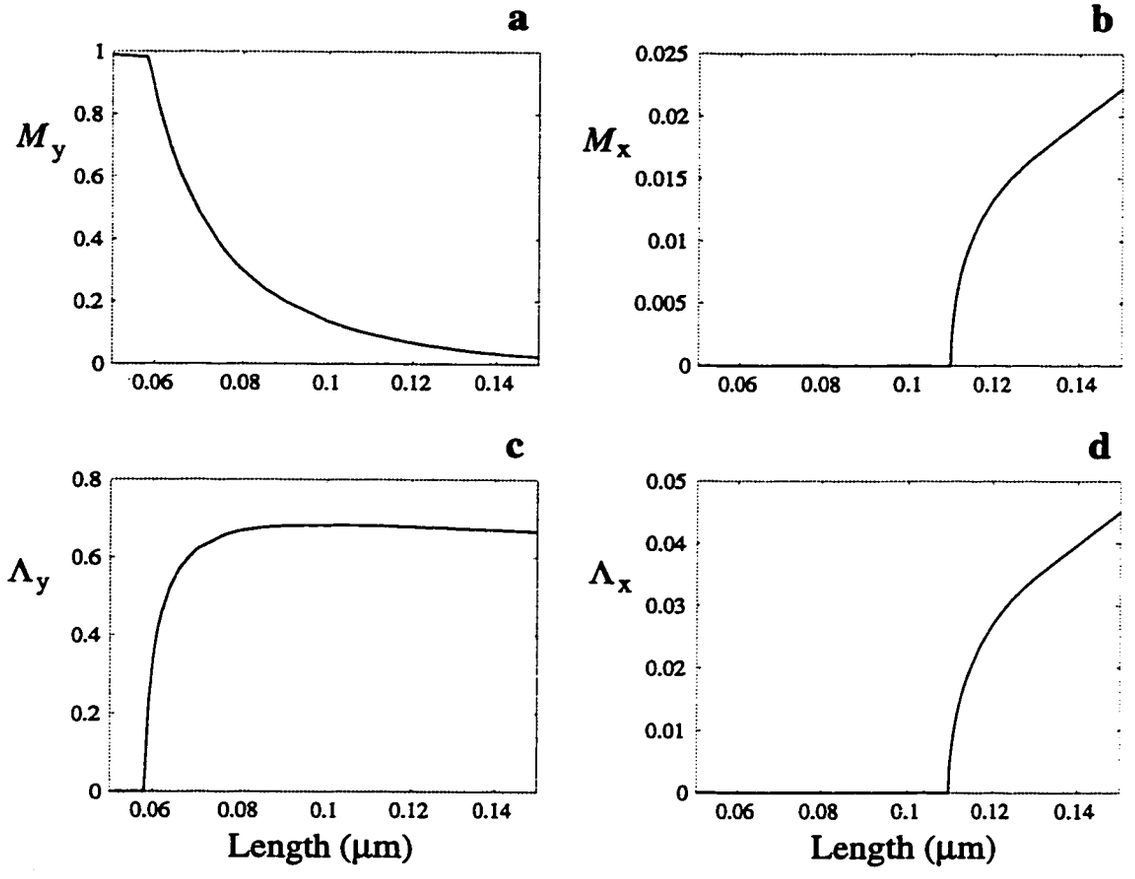

Figure 5.16: Components of normalized volume-average magnetization $\mathbf{M}/M_s$ and normalized volume-average curl $\mathbf{\Lambda}$ for the intermediate-axis curling state. The curling state nucleates at $L = 0.058\mu$m, as indicated by a vertical takeoff for the curl around the intermediate axis (figure c). At $L = 0.11\mu$m, an x component is added to the magnetization and the curl. Again, there is a vertical takeoff.

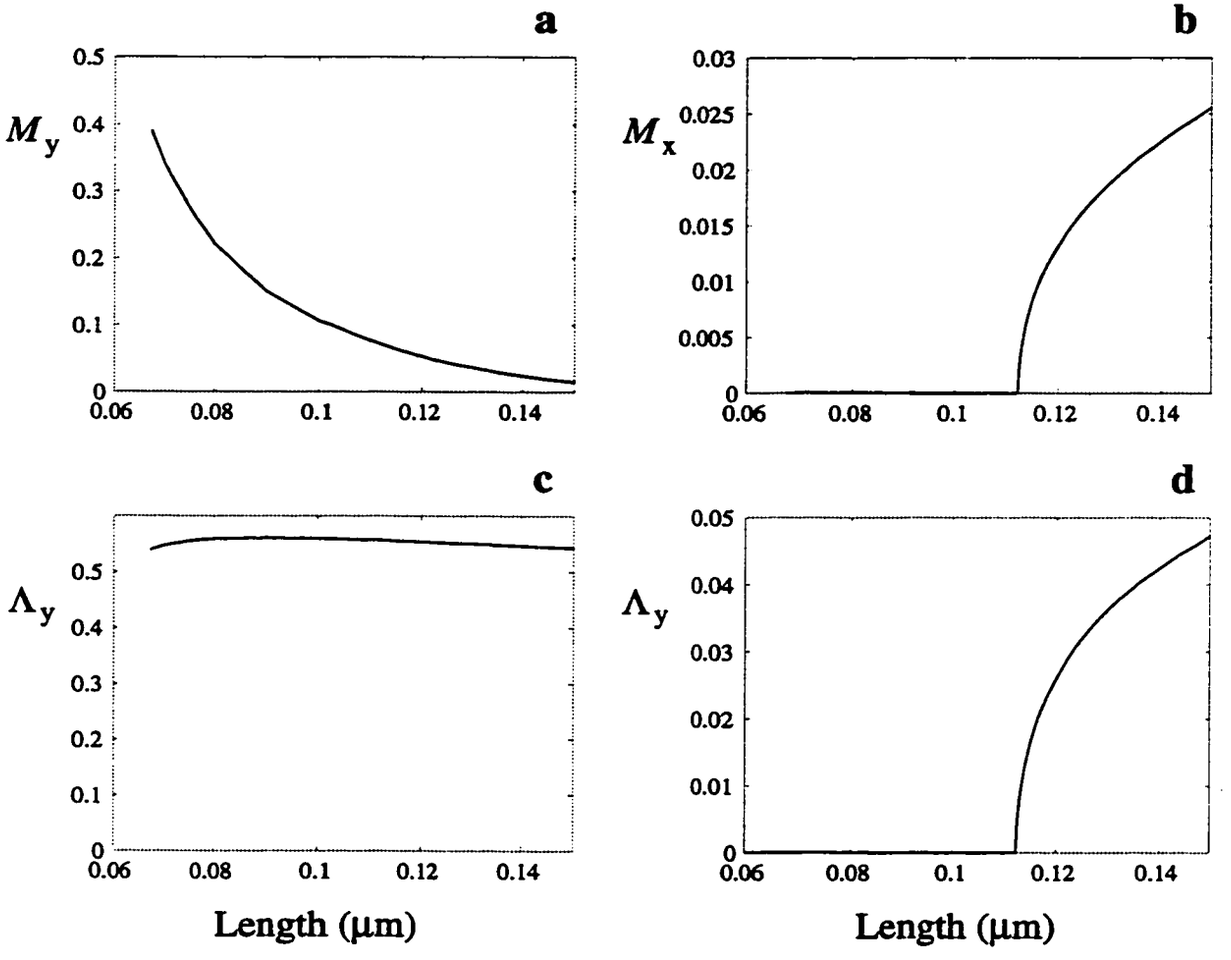

Figure 5.17: Components of normalized volume-average magnetization $\mathbf{M}/M_s$ and normalized volume-average curl $\mathbf{\Lambda}$ for the short-axis curling state. The curling state appears suddenly at 0.067μm and long-axis components of magnetization and curl appear at 0.11μm.

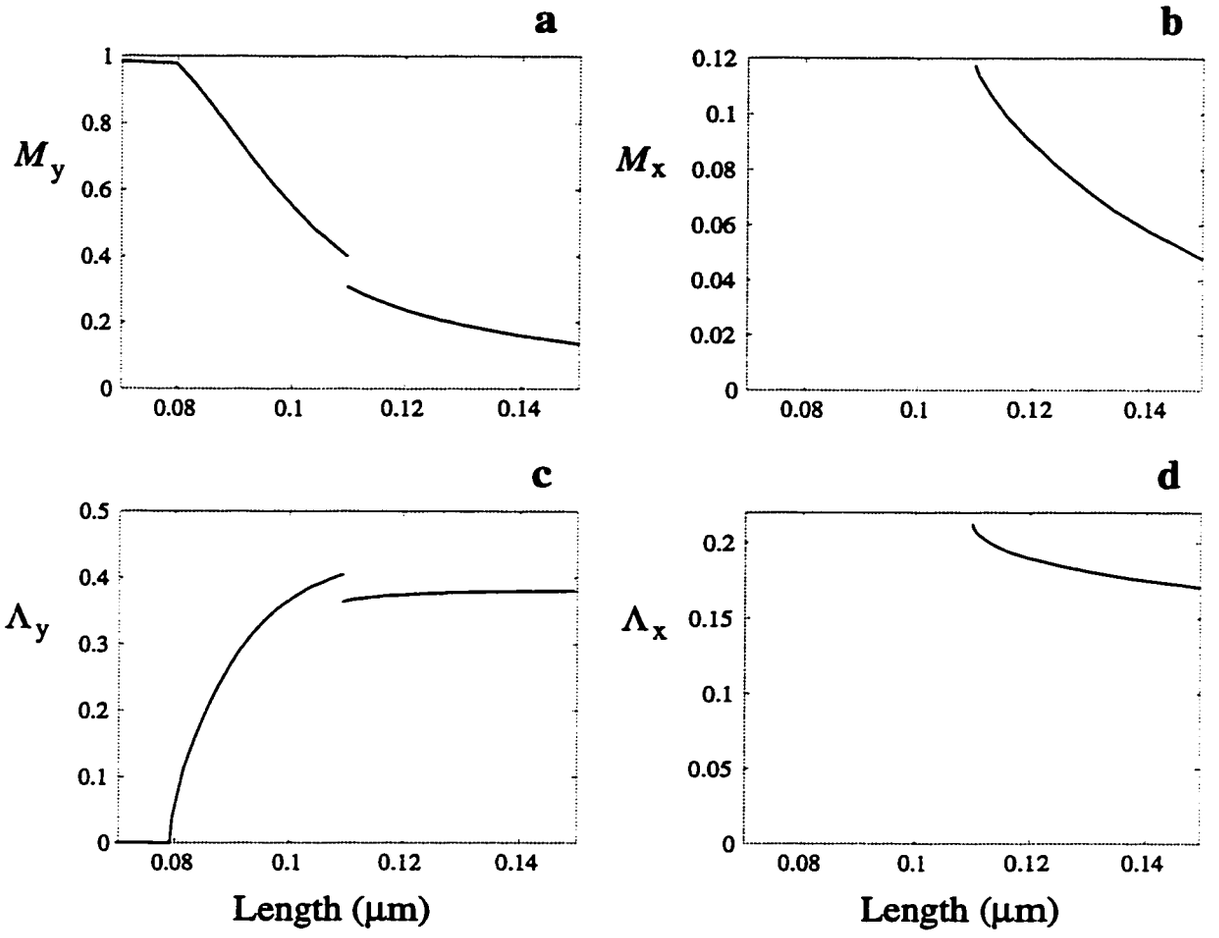

Figure 5.18: Components of normalized volume-average magnetization $\mathbf{M}/M_s$ and normalized volume-average curl $\mathbf{\Lambda}$ for the long-axis curling state. The curling state nucleates at $L = 0.08\mu$m, as indicated by a vertical takeoff for the curl around the intermediate axis (figure c). At $L = 0.11\mu$m, a new state appears. This state begins with a comparatively large z (short axis) component, and then the component decreases with particle size.

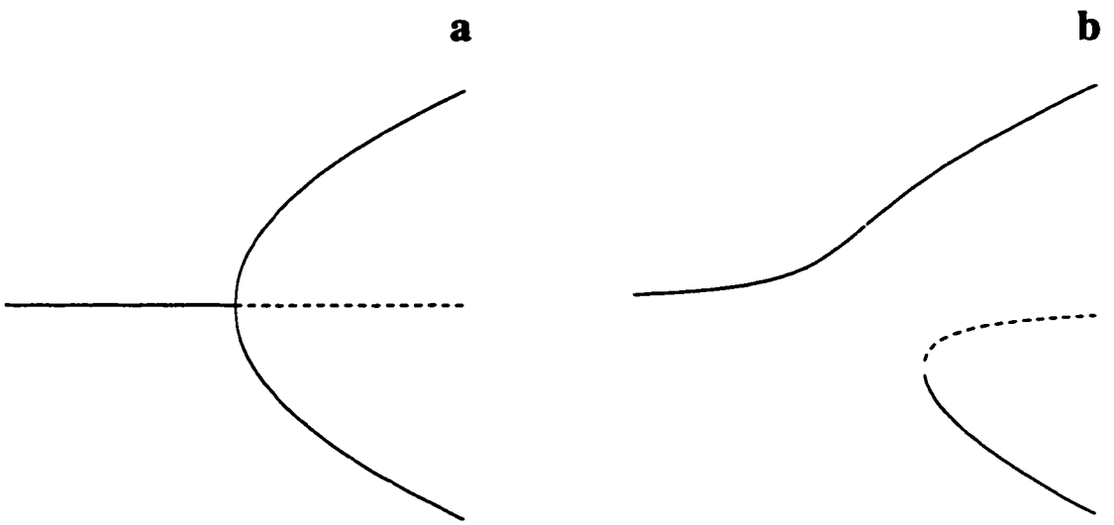

Figure 5.19: Models of bifurcation, after Nicolis and Prigogine [1989]. As the variable on the horizontal axis changes, the variable on the vertical axis has only one possible value at first, but a new state arises at a critical point. (a) Pitchfork bifurcation: two new and symmetric states arise. (b) Bifurcation for broken symmetry: one branch of the bifurcation is selected. The dotted line indicates an unstable state.

same. Since there is no such pair of flower states, nucleation doubles the available states.

This phenomenon is known as bifurcation. An analogous bifurcation in fluid mechanics is the onset of Rayleigh-Bénard convection [Tritton, 1988]. In a highly symmetric configuration as in Figure 5.1 the choices of curl are equally likely, and small fluctuations will determine the choice. This is known as pitchfork bifurcation, and is shown schematically in Figure 5.19a. Many of the curves in the previous section look like one of the branches of a bifurcation, with a vertical initial slope to a component of the curl.

In a real particle, the symmetry between states is usually broken and the bifurcation is more likely to look like Figure 5.19b. As the variable along the horizontal axis (field or particle size) changes, the state follows the upper curve and changes continuously. At a critical point, a pair of stable state and unstable states appear. This is called a limit point bifurcation; examples can be seen in the SD curves in Figure 2.3. In particles where the symmetry is broken, we may see the upper curve and not know there is another branch unless we know there is a bifurcation in the symmetric case.

With each transition involving a new component of curl, the number of distinct remanent states is doubled. I can show that these states are related to each other by symmetry transformations that map the particle onto itself, but the proof requires a significant amount of background material, so I have left it out of this dissertation.

5.7 Summary

In this chapter, I have looked at SD states and nucleation in cuboids and put them in the context of older micromagnetic theory. I showed that the flower state is a SD state that is perturbed by the non-uniform demagnetizing field. The magnetization fits a $H^{-3/2}$ law of approach to saturation, consistent with perturbation forces that

originate in the surface poles $\mathbf{M} \cdot \hat{\mathbf{n}}$.

The nucleation field H_n for the cube has the same dependence on particle size as it does for the sphere, except that the effective demagnetizing factor is smaller. Since the demagnetizing field is destabilizing, this makes nucleation more difficult in the cube.

I also found that (fortunately) the nucleation field does not depend significantly on the grid spacing in the numerical model, even though the transverse demagnetizing fields in the corners increase rapidly with grid size. Since the fields in the corners perturb the SD state, they could plausibly destabilize it - but the SD state is actually more stable in the cube than in the sphere. The nucleation field seems to be determined by the average demagnetizing field, which is smaller than in the cube. The reason the nucleation field does not depend on the local value of the demagnetizing field is that the magnetostatic forces are non-local and the structure of the curling perturbation is also non-local.

In a triaxial cuboid, there are SD states with moments along the axis of intermediate length. No such states occur in ellipsoids of rotation. The states change continuously with particle size, and both the long-axis and intermediate-axis states have a curling mode nucleation at well defined critical sizes. At 0.067μm, a short-axis curling state appears suddenly and then is seen at all larger sizes.

The common feature of nucleation in ellipsoids and cuboids is the appearance of a curl around some axis. I use a normalized volume-average curl $\mathbf{\Lambda}$ for a quantitative measure of the change in magnetization. At 0.11μm, all three curling states (corresponding to the long, intermediate and short axes) develop a new component of curl and a corresponding component in the volume-average magnetization. These quantities appear with a vertical takeoff.

Thus a generalized concept of nucleation can be applied to the initial transition from SD to non-SD states as well as further transitions at larger particle sizes. Each such transition reduces the symmetry of the state and doubles the number of distinct

remanent states, and indicates a reduction in shape control over magnetization.

Chapter 6

HYSTERESIS PROPERTIES ABOVE THE CRITICAL SIZES

Both volume and shape have a strong effect on hysteresis properties and their effects are not easily separated. In the SD size range, the aspect ratio has no effect on M_{rs} but a large effect on H_c, while the volume only affects the hysteresis properties through its role in thermal fluctuations. By contrast, MD models predict that shape only affects H_c through the number of defects a wall intersects, while M_{rs} is determined by a combination of H_c and the shape-dependent factor N. Thus the effect of shape is very different for SD and MD grains. Complicating this picture still further is the strong dependence of the nucleation critical size L_n on aspect ratio. On the other hand, the expression for the nucleation field H_n is a linear superposition of the effects of size, aspect ratio and magnetocrystalline anisotropy.

In addition, other details of the shape besides aspect ratio affect hysteresis properties. As we saw in Chapter 5, a cube has a lower nucleation field than a sphere. Schabes and Bertram [1988] calculated hysteresis loops for cubes with uniaxial magnetocrystalline anisotropy and found that the cubes had larger coercivities than were predicted for the sphere. They attributed this difference to the deflection of the magnetization in the corners of the cube: as the field decreased, the deflection increased. This increase in the degrees of freedom of the state appeared to make the state more stable. Schabes and Bertram [1988] called this effect configurational anisotropy.

A different effect has also been attributed to configurational anisotropy. In a cube of magnetite with easy axes along the body diagonals, Williams and Dunlop [1989]

obtained a curling state with moment in a *hard* direction (perpendicular to a face). They attributed this to configurational anisotropy as well. In a cube, there is clearly a difference between the center of a face and a corner, and one would expect the energy of the curling state to depend on its orientation, with symmetry axes of the cube being likely directions for minima. Indeed, Williams and Dunlop [1989] did not find states with moments in the easy directions. They argued that configurational anisotropy was far stronger than magnetocrystalline anisotropy. However, Newell *et al.* [1993b] and Fabian *et al.* [1996] did find states with moments in the easy directions, and these states had the lowest energy. The difference was in the choice of initial guess. Finally, Enkin and Williams [1994] modeled a cube with uniaxial anisotropy. One of the states they obtained had a moment in the hard direction (perpendicular to the easy axis).

In this chapter, I will attempt to improve our understanding of the effects of shape and volume using the numerical model described in Chapter 4. To isolate shape effects, I neglect the magnetoelastic and magnetocrystalline energies. I call such a material magnetically isotropic; while it may seem unrealistic, it may be a reasonable approximation for amorphous ferromagnets [Aharoni and Jakubovics, 1990].

6.1 The Magnetically Isotropic Sphere and Cube

When studying the effect of some variable, it is useful to look at extreme cases. For shape anisotropy, one extreme is the sphere, because it has no shape anisotropy. If in addition the sphere is magnetically isotropic, the only remaining source of anisotropy is the external field (if there is one).

At absolute zero, the moment of a magnetically isotropic sphere will always be in the direction of the field. When the field crosses zero, the moment will immediately switch to the opposite direction. Thus the sphere will have infinite susceptibility and zero coercivity.

Using a numerical micromagnetic model, Aharoni and Jakubovics [1990] calculated the magnetization curves for magnetically isotropic spheres with sides $9.33L_{ex}$ and $12.4L_{ex}$; for comparison, $L_n = 8.22L_{ex}$ (equation 3.8). As long as the field is not zero, the minimum energy state is well defined. The magnetization is uniform at large fields and the nucleation field is in agreement with nucleation theory (Figure 5.7). Below the nucleation field, the magnetization decreases linearly with the field. As the field crosses zero, the magnetization jumps to a negative value. There is no hysteresis.

Aharoni and Jakubovics [1990] did not consider the effect of thermal fluctuations. Since there is no energy barrier separating different directions of the moment, the particles are superparamagnetic at all sizes. For small particles, the magnetization is given by the Langevin function (equation 2.15). Above $L = L_n$, there are more degrees of freedom, but as a first approximation we may suppose that $M = M_0 L(\mu_0 M_0 HV/k_B T)$ where $M_0(H)$ is the magnetization in the absence of thermal fluctuations. It turns out that for the two particle sizes they model, the curve rises extremely sharply, so the overall curve is well approximated without considering thermal fluctuations.

For comparison with the spheres, I calculated the hysteresis curves for cubes with the same two volumes (Figure 6.1). The field is perpendicular to a face of the cube, so the symmetry constrains the moment to be parallel or antiparallel to the field.

As I showed in Chapter 5, the nucleation field of the cube is displaced by about $0.06M_s$ compared to the sphere. The slope of the $M(H)$ curve is steeper, however, so that the $12.4L_{ex}$ cube has a lower remanence than the sphere of the same volume even though it nucleated at a lower field.

The most dramatic difference between the sphere and the cube is that the cube has hysteresis and the sphere does not. The coercivity of the larger cube is $0.044M_s$; for comparison, the coercivity for a SD magnetite particle is $H_c \approx 0.38|K_1|/\mu_0 M_s \approx 0.016M_s$ (table 2.1).

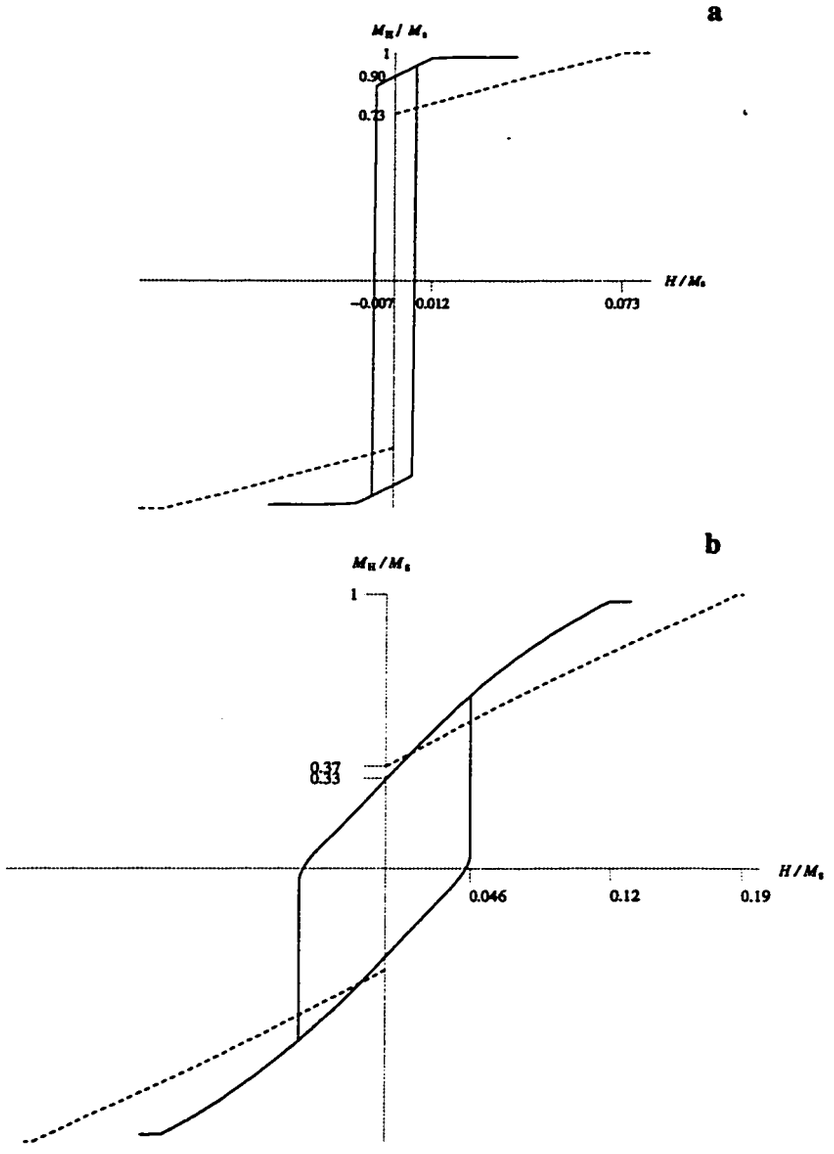

Figure 6.1: Comparison of the magnetization curves for magnetically isotropic cubes and spheres. The field is perpendicular to a face of the cube. In each plot, the solid line is a hysteresis curve for a cube while the dotted line is for a sphere of the same volume [Aharoni and Jakubovics, 1990]. (a) $L = 9.33L_{ex}$ (in magnetite, 0.063μm). (b) $L = 12.44L_{ex}$ (in magnetite, 0.084μm).

Unlike the sphere, the cube has hysteresis properties that depend on the direction of the field (perhaps this is the most appropriate use of the term configurational anisotropy). This is most striking in the SD size range (Figure 6.2). For a field perpendicular to one of the faces, the cube has a coercivity of about $0.2M_s$ - about ten times the SD coercivity for magnetite. For a field at an angle to the symmetry axis, the coercivity is only $0.005M_s$. This suggests that in the latter case the mode of reversal is uniform rotation, against which the shape of the cube is not much of a barrier, while for the field along a symmetry axis the mode of reversal is non-uniform. This result must be viewed with caution, because the curve does not show a smooth approach to the jump (after considerable effort, I was unable to find it). The program may simply be overlooking the uniform reversal mode.

6.2 Hysteresis Curves for the Triaxial Particle

In this section, I look at the effect of adding lower order shape anisotropy by calculating hysteresis curves for the triaxial cuboid ($X = 1.4Y = 1.5Z$). In Figure 6.3, I show a set of curves for a particular field direction $\mathbf{H}||(8,1,4)$ and different particle sizes. These curves show that the change from SD to non-SD behavior is a progression, not a single sharp transition. In large fields, the magnetization initially follows the SD curve, with the moment rotating as the field changes. The larger the particle, the more the curve is displaced downwards relative to the SD curve; but it approaches the SD curve as the field increases. At a well defined field, the slope of the hysteresis curve changes suddenly and the curve diverges from the SD curve.

The outer curve is for $L = 0.07\mu$m: it is still perfectly SD. Between 0.07μm and 0.076μm, nucleation begins and the curve gets narrower. Thus the Stoner-Wohlfarth critical size L_{sw} is in this range. At about 0.08μm, the nucleation field crosses zero, so this is the nucleation critical size L_n.

Up to 0.08μm, the hysteresis curve is quite simple: the state is initially an

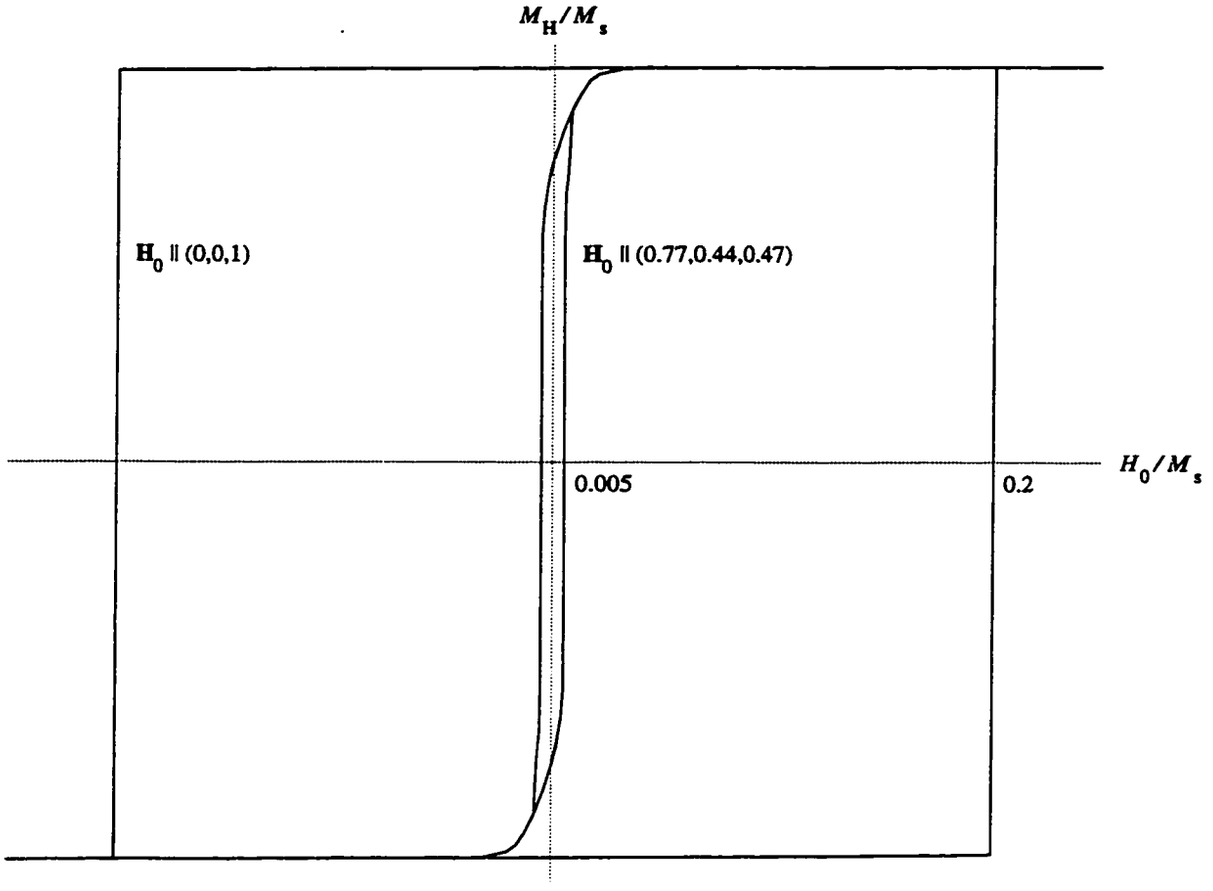

Figure 6.2: Two hysteresis curves for a magnetically isotropic cube in the SD size range ($L = 0.05\mu$m for magnetite). When the field is perpendicular to one of the faces, the coercivity is about $0.2M_s$. For most field directions, it is two orders of magnitude smaller.

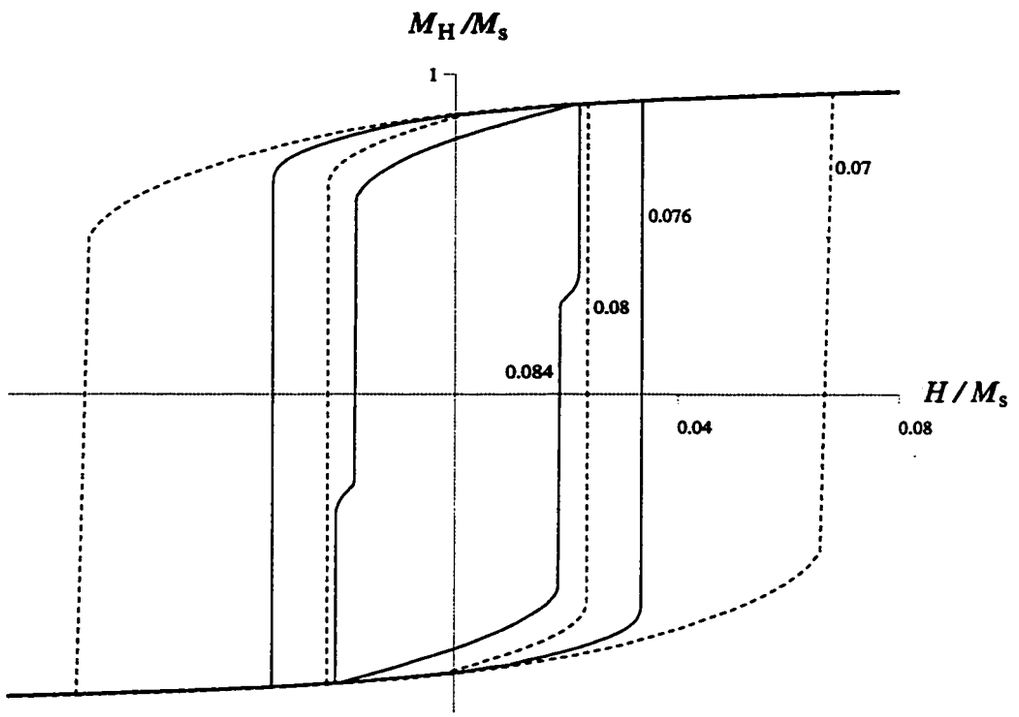

Figure 6.3: A sequence of nested hysteresis curves for triaxial cuboids of varying sizes in a field with direction $\mathbf{H}||(8,1,4)$. The sizes in microns are marked on the curves.

SD (flower) state; nucleation occurs and the slope of the hysteresis curve changes abruptly[1]; the resulting curling state approaches an instability; the moment then reverses.

At $L = 0.084\mu$m, a new phenomenon occurs: when the curling state becomes unstable, the moment jumps to the Z axis (the short axis). If the field is then increased, a first-order reversal curve is obtained (Figure 4.1), and the remanent state is a curling state with moment along the short axis. This state has a lower energy and a moment that is one fifth the moment of the long-axis curling state.

An unusual feature of the short-axis curve in Figure 4.1 is that when the field is continued to positive values, the short-axis curve crosses the main hysteresis loop. The short-axis curling state is more stable than the long-axis curling state. This cannot happen in Stoner-Wohlfarth theory or MD theory, because in both theories the magnetization only depends on one variable (the angle θ or the position of the wall).

Another example of a hysteresis curve is shown in Figure 6.4. For this particle size and field direction, the remanent state has its moment along the short axis.

All of the curves except for the curve for $L = 0.084\mu$m in Figure 6.3 satisfy the conditions for the Wohlfarth relations: there are two symmetrically placed switching fields. By most measures, the hysteresis loops are SD, but the coercivity is as much as a factor of three lower.

6.3 Critical Sizes

In Chapter 3, I derived expressions for three critical sizes - the Stoner-Wohlfarth critical size L_{sw}, the global critical size L_0 and the nucleation critical size L_n. In this

[1] The change in slope is abrupt, but it may be small: at $L = 0.076\mu$m, the nucleation at $H = -0.01M_s$ is not easy to spot - but it can be identified as the meeting point for the stable solution and an unstable solution (Figure 4.2).

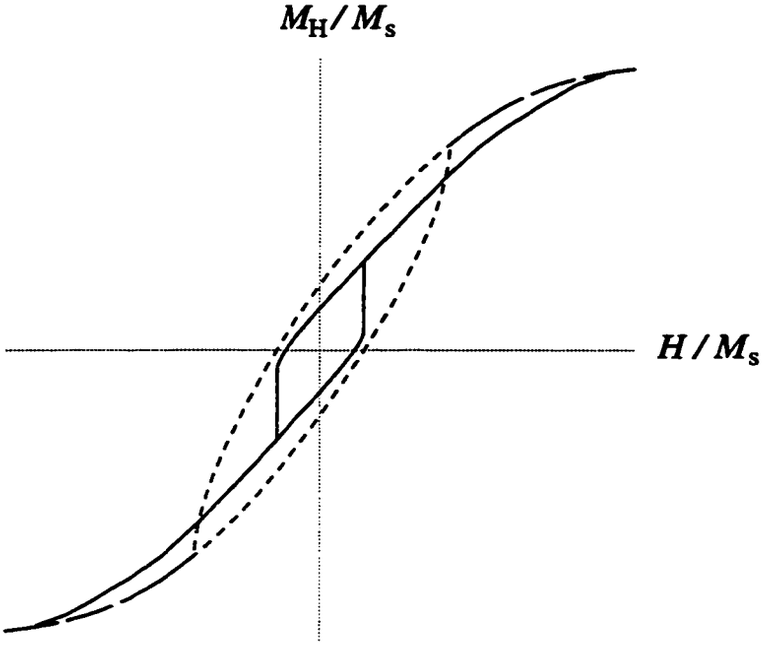

Figure 6.4: A hysteresis curve for a magnetically isotropic triaxial cuboid with size 0.09μm in a field with direction $(0.22, 0.96, 0.19)$. The dashed lines show the SD hysteresis curve for the same field direction.

section I will compare the equations with the results for cuboids.

For the sphere, equations 3.7, 3.8, 3.10 and 3.11 predict that $L_{sw} = L_0 = L_n = (3k)^{1/2} L_{ex}$, where $k = 22.5$ (the demagnetizing factors are $N_a = N_b = 1/3$). In Chapter 5, I showed that the nucleation field is a good fit to the equation

$$\frac{H_n}{M_s} = N_a - \frac{kL_{ex}^2}{L^2}$$

with $N_a = 0.26$. Solving for $H_n = 0$ gives $L_n = (3.8k)^{1/2} L_{ex}$, which is 0.62μm for magnetite. Since I did not find any non-SD states for $L < L_n$, L_0 is probably equal to L_n.

It is more difficult to determine the Stoner-Wohlfarth critical size. Equation 3.7 is obtained by solving $H_n = H_r$, where H_r is the critical field for uniform rotation. For a sphere, $H_r = 0$, but for a cube H_r is nonzero for most field directions and possibly quite large for $\mathbf{H} \parallel (0,0,1)$ (Figure 6.2). I obtained a couple of negative nucleation fields (Figure 5.5), but I did not find nucleation in particles with sizes below 0.06μm.

For an ellipsoid of rotation, the nucleation size L_n increases as $(N_a)^{-1/2}$ (equation 3.8). This is the nucleation size for magnetization aligned with the long axis ; there are no nucleation sizes for the shorter axes, since there is no SD state with a moment along a short axis. This is evident from the symmetry: the only unique direction is the long axis.

For the triaxial cuboid, the principal values of the demagnetizing tensor are $N_{xx} = 0.2557$, $N_{yy} = 0.3596$ and $N_{zz} = 0.3847$. If N_{yy} was equal to N_{zz}, we could compare the nucleation size with that for an ellipsoid using $N_a \equiv N_{xx}$ and $N_b \equiv N_{yy} = N_{zz}$. For a triaxial cuboid, we can make a rough comparison of critical sizes using $N_{yy} \leq N_b \leq N_{zz}$. The predicted nucleation critical size is then $L_n = 0.062/(3N_a)^{1/2} = 0.071\mu$m, which is significantly smaller than the actual critical size of 0.08μm. The prediction for L_{sw} is even further off: $0.058\mu\text{m} \leq L_{sw} \leq 0.060\mu$m, while it is actually above 0.07μm. It is not clear what the reason for the difference is.

Another unexpected result is that the curling states with moments along the

shorter axes do not appear in hysteresis loops until above the critical size for nucleation of the long-axis curling state. Thus even though they appear to be stable in much smaller particles, they are not accessible.

The energy densities of the remanent states for the cuboid are shown in Figure 6.5. The energy densities for the intermediate-axis and long-axis states approach $N_{yy}/2$ and $N_{zz}/2$ in the SD limit, and they increase smoothly through the nucleation points. The intermediate-axis and short-axis states both have higher energies than the long-axis state until the latter has already nucleated. From Chapter 3, the global critical size L_0 is defined as the size below which the SD state has the lowest energy. Since the SD state has already become unstable at the size where the energies cross, the global critical size is equal to L_n (0.08μm). This is consistent with nucleation theory for ellipsoids, which predicts that $L_0 = L_n$ for zero magnetocrystalline anisotropy (equations 3.10 and 3.11).

6.4 Size Dependence of Hysteresis Properties

In Figure 6.6, I show the total moment of the remanent states on a log-log plot. For comparison, I include some results from other micromagnetic simulations. We must be careful in comparing them. The points from Williams and Dunlop [1995] are for cubes with easy axes along the body diagonals; they calculated hysteresis curves for fields in the $\langle 111 \rangle$ and $\langle 100 \rangle$ directions, and argued that these should be upper and lower limits for the volume average remanence $\langle M_H \rangle$. The points from Fabian *et al.* [1996] are for an aspect ratio of 1.52 and they are the magnitude of the volume-average magnetization (as are mine). Thus the contribution to the remanence in the direction of a field will tend to be smaller than shown; the same is true for my results.

Williams and Dunlop [1995] noted that their remanences did not depend strongly on the field direction, and argued that magnetocrystalline anisotropy does not affect the remanence much. Within the size range for which I have made calculations, this

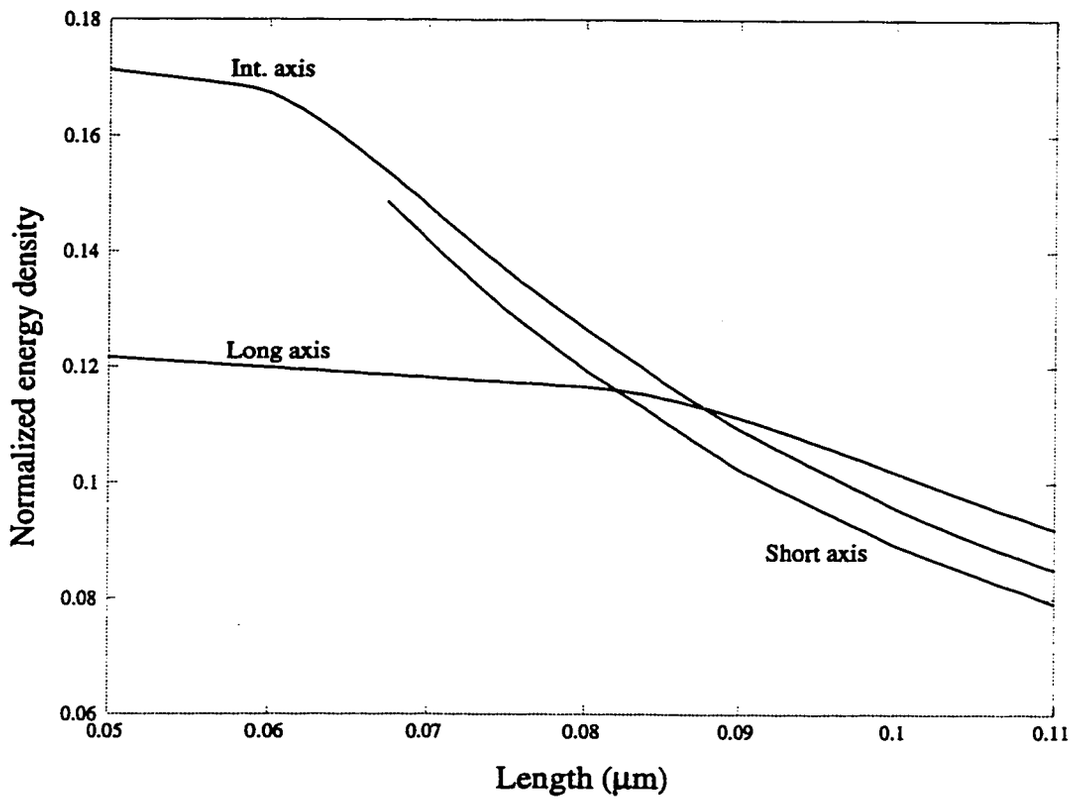

Figure 6.5: The normalized energy density for each stable remanent state of the magnetically isotropic triaxial cuboid. The normalization factor is $(1/2)\mu_0 M_s^2$. The energies for the intermediate and long axis states approach the SD values of $N_{yy}/2$ and $N_{zz}/2$.

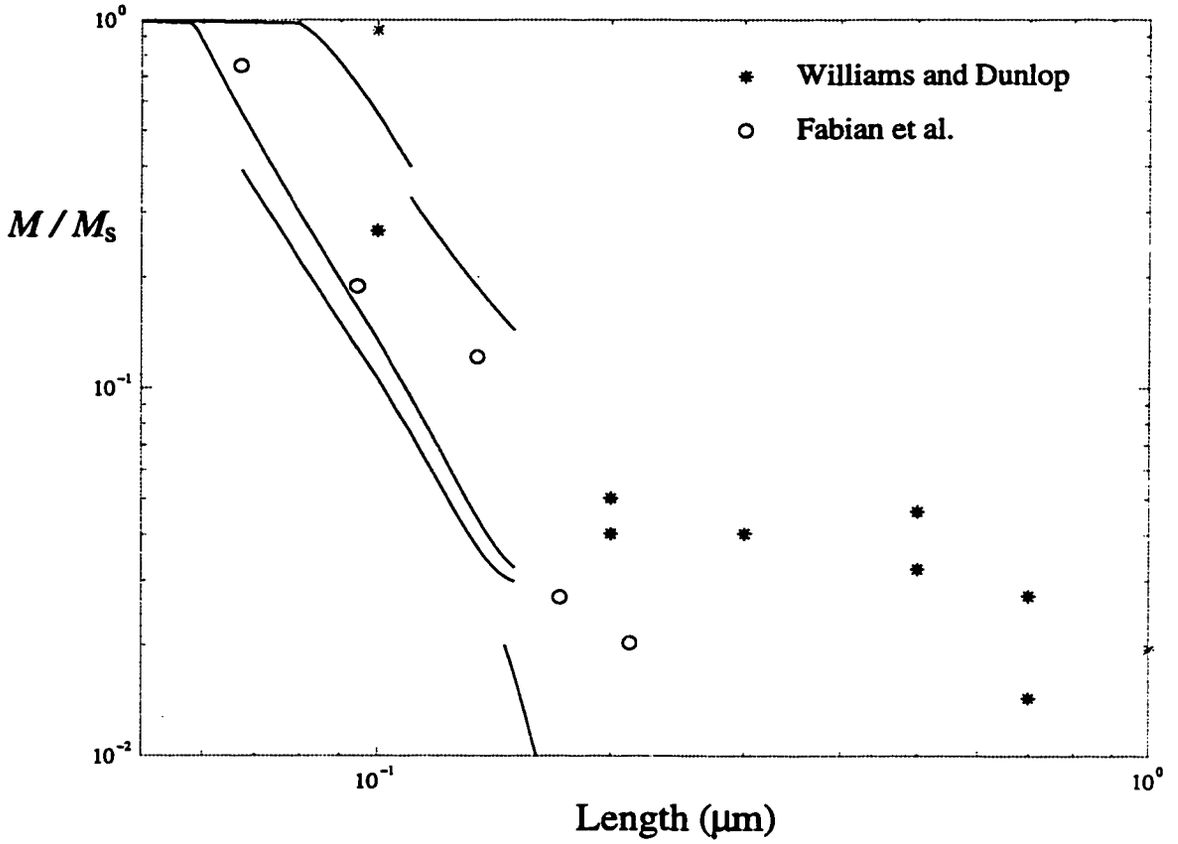

Figure 6.6: The total moment of each remanent state for the magnetically isotropic triaxial cuboid (solid lines). The length scale is based on the constants M_s, A for magnetite, but $K_1 = 0$. For comparison, some results are shown for micromagnetic models of magnetite particles with magnetocrystalline anisotropy included. The asterisks are from Williams and Dunlop [1995]; the circles are from Fabian *et al.* [1996].

seems to be true: the results of Fabian *et al.* [1996] fit between the extremes of my remanences. My remanences decrease with particle size roughly as V^{-1}, so the total moment does not change. This implies that the source region for the remanence is fixed in size. Indeed, the magnetization is aligned with an axis in the center of the particle and then relaxes into the perpendicular plane away from the center, with a scale length L_{ex}. The moment may be concentrated near the center of the top and bottom faces.

Judging by the results of Williams and Dunlop [1995], the decrease of remanence with size slows down considerably as particle size increases. This suggests that, contrary to the claim of Williams and Dunlop [1995], magnetocrystalline anisotropy may dominate the remanence in large particles. I have shown above that shape anisotropy becomes negligible by about 0.15μm, so something must take its place. However, we must be cautious interpreting their results, because some of the solutions may not be stable.

It also appears that without magnetocrystalline anisotropy, both the coercivity and the coercivity of remanence decrease rapidly with particle size. While coercivity in real samples also decreases rapidly with particle size, the coercivity of remanence has only a weak size dependence [Heider *et al.*, 1996]. Again, magnetocrystalline anisotropy may be responsible.

One of the most common proxies for particle size is the plot of M_{rs}/M_s against H_{cr}/H_c, called the Day diagram (Section 1.3). In Figure 6.3, the coercivity decreases from the SD value of $0.067M_s$ to $0.023M_s$ at the nucleation critical size $L_n = 0.08\mu$m, but the hysteresis curve crosses $M_H = 0$ with a large vertical jump, so $H_{cr}/H_c = 1$ over this size range. Of course, the remanence M_{rs}/M_s is also equal to the SD remanence up to the nucleation critical size. Thus there can be a considerable departure from SD hysteresis before the change is apparent on a Day diagram.

6.5 Summary

In this chapter, I looked at some effects of particle shape and size on hysteresis. To learn more about configurational anisotropy, I compared magnetically isotropic spheres and cubes. The shape of the cube gives rise to some hysteresis where there is none in the sphere, but the effect is small for most field directions. When the field is nearly perpendicular to a face of the cube, the coercivity I obtained is much larger, but this may be an artifact because I was unable to demonstrate a smooth approach to vertical of the dM/dH curve. The symmetry of the configuration may make it difficult for the program to find the nucleation point.

I compared the size dependence of remanence for my magnetically isotropic cuboid with the results of Fabian *et al.* [1996] for magnetite particles of a similar elongation. The magnetocrystalline anisotropy in the latter model seems to make little difference. Above $L = 0.2\mu$m, however, Williams and Dunlop [1995] obtain a weaker dependence on particle size. There may be a change in the size dependence as shape anisotropy becomes less dominant in larger particles.

Chapter 7

CONCLUSIONS

The goal of this dissertation was, where possible, to develop hysteresis theories to the point that they could be used for robust interpretations of magnetic measurements. I had some success with SP and SD particles. For larger particles, I tried to identify the robust features of the two main types of hysteresis model, MD and micromagnetic.

Ideally, we would like to have a systematic picture of how magnetization states and hysteresis properties depend on shape, size, composition and so on. Because there is a multidimensional space of such factors, and because it is computationally expensive to run micromagnetic models, it is impractical to simply calculate hysteresis parameters for all combinations. We need to have some framework to guide us. Such a framework is provided by nucleation theory.

In the sections below, I organize my results by the classes of theory (SP, SD, MD and micromagnetic) and then I suggest a few possible implications for paleomagnetism.

7.1 SP and SD Hysteresis Theories

In some systems, such as basaltic glasses [Pick and Tauxe, 1994], limestones [Channell and McCabe, 1994] and soils [Maher and Taylor, 1988], the magnetic particles appear to be primarily superparamagnetic (SP) and single-domain (SD). For such systems, we may be able to use magnetic measurements to extract reliable information about the magnetic particles. In Chapter 2, I developed the theory of SP and SD particles

with this goal in mind.

I showed that the magnetization curve for an ensemble of SP particles does not depend on the symmetry or magnitude of the intrinsic anisotropy, as long as the sample as a whole is isotropic. Furthermore, the magnetization curve depends only on the odd moments of the volume distribution ($\langle V \rangle, \langle V^3 \rangle ...$). The standard deviation and other distribution parameters that depend on even moment are not constrained.

If there is a mixture of SP and SD grains, hysteresis measurements in nonzero field have a non-unique interpretation because both the SP and SD grains contribute. To isolate the SD particles, one can measure changes in remanence. For SD particles with uniaxial anisotropy, I derived analytical expressions for IRM acquisition and for loss of IRM in DC and alternating fields. These expressions should make it easier to model IRM curves in real systems.

I showed that for ensembles of SD particles, both the main hysteresis loop and the IRM acquisition curve have a fixed shape and are scaled by the volume-average anisotropy. This has the surprising consequence that there is no more information contained in the entire hysteresis loop than in a single parameter H_c or H_{cr}.

Thus the information that can be obtained on SP and SD particles is strictly limited. It remains to be seen whether one can use this information to place limits on some important quantities such as the critical size for the SP-SD transition.

The above predictions for SD particles must be modified to take into account thermal fluctuations, which enhance both remanence acquisition and loss and also change the hysteresis curve. The effect of thermal fluctuations can be removed by using a Henkel [1964] plot of IRM acquisition against IRM loss. These plots can be justified by the Wohlfarth [1958] relations, which follow from very general assumptions.

In some recent papers [Gee and Kent, 1995; Channell and McCabe, 1994] there have been claims that for some materials of geological interest the primary remanence carriers are particles with a dominant cubic anisotropy. For samples with $M_{rs}/M_s > 0.5$, this claim seems well founded, although M_{rs}/M_s does depend on the maximum

field used and the algorithm for removing (super)paramagnetic contributions. For the rest of the samples, the arguments are mainly based on Day diagrams and have no theoretical justification. On the Henkel plot, SD particles with cubic anisotropy have a distinctive signature, and such a plot can be used as a robust test of the above claims.

7.2 MD Hysteresis Theories

As I described in Chapter 2, the basic MD model is a two-domain model in which the demagnetizing energy enters as $(1/2)NM^2$, where N is a dimensionless factor that depends only on the geometry. The movement of the wall is determined by the magnetostatic forces and a force due to internal variations in anisotropy. This latter force tends to "pin" the wall away from the magnetostatic minimum and gives rise to hysteresis.

Most models that give the internal energy explicitly solve only for the coercivity - and the internal field approximation is used, which causes the coercivity to be overstated. For the susceptibility, different internal energy models are used that are not obviously related to those for the coercivity. Models that predict both the coercivity and the susceptibility do not solve for them directly using the internal energy. Instead, they use heuristic assumptions that contradict the initial assumption of a dimensionless demagnetizing factor.

I argue in Chapter 2 that when a two-domain model is solved correctly, it has some robust properties. The slopes of the ascending and descending branches of the main loop are always $1/N$, so H_c and M_{rs} have the same temperature dependence (as is indeed observed). It also appears that H_{cr}/H_c is always close to 1, although this conclusion is tentative.

Lamellar domain models may not be applicable to magnetite. Because of its low magnetocrystalline anisotropy, magnetite should have closure domains. In a

two-dimensional model of micron-size magnetite particles, the lowest energy states I obtain are closure domain states, to a good approximation. It is true that many particles do not have closure domains, particularly the magnetite particles in glass ceramics. A major problem for micromagnetics is to determine the conditions for closure domains to occur.

It might seem that there is no point in devoting so much attention to MD hysteresis models when we can now solve three-dimensional micromagnetic models. Such models still have limited resolution, however, and are not always the best choice. In particular, hematite has a large uniaxial anisotropy. This confines the magnetization to the basal plane and makes domain walls very thin. It would be difficult to accurately represent the internal structure of the domain walls in a micromagnetic model of a hematite particle, but a lamellar domain model may work fairly well. The single hematite platelets studied by Halgedahl [1995] are an exciting opportunity to investigate how particles with lamellar domains really behave, and possibly even how domain walls interact.

7.3 Micromagnetics

Numerical micromagnetics offers the promise of greater realism at the expense of a considerable increase in computation time and some difficult numerical problems. The problem that has received the most attention is the accurate calculation of the demagnetizing field. Less attention has been devoted to distinguishing between real minima and saddle points, although it is recognized that minimization routines can be fooled. It has been my experience that a calculated hysteresis curve can change drastically as the step size for the field is decreased, and the curve can end up looking complicated.

I have developed a method that is effective in identifying unstable solutions. This method has two parts: an $M(H)$ curve corresponding to a stable solution is identified

by a smooth approach to vertical before a jump. Often I find this curve after a jump from another branch with larger M. I continue the stable curve back until it meets the unstable one. This is the nucleation point (see below). Having identified the nucleation field, I know the upper branch is unstable and I can prune it.

An unusual feature of this method is that the nucleation field is obtained by backward continuation of the stable branch. To my knowledge, no one has previously thought of reversing the direction of change of the field after a jump, although intuitively one would expect that a jump is an irreversible change in magnetization. This method is also useful for finding physically meaningful remanent states.

The results of numerical micromagnetic modeling are most naturally discussed in the context of nucleation theory, yet the connections between the two have been little discussed and much misunderstood until now. Major contributions of this thesis include extending nucleation theory for ellipsoids to include magnetocrystalline anisotropy, extending nucleation theory to non-ellipsoidal bodies, and developing the relationships between nucleation theory and hysteresis properties.

7.3.1 The SD State

In ellipsoids, the SD state is uniform magnetization. Many authors have claimed that there is no corresponding state in particles of other shapes, because the magnetization is never uniform. On the other hand, the flower state Schabes and Bertram [1988] has nearly uniform magnetization. I showed that for all practical purposed, this is the SD state. It may be thought of as uniform magnetization perturbed by magnetostatic forces concentrated at the surface. The $H^{-1.5}$ approach to saturation is consistent with this interpretation. In addition, as Lederman *et al.* [1994] showed, for most field directions the magnetization curve predicted by Stoner-Wohlfarth theory is a good approximation.

The SD state can be described as a state with zero curl. Numerical models often obtain the flower state and "vortex" states in the same particle, but the flower state

is not stable.

7.3.2 The Nucleation Field

For ellipsoids, I generalized the published expression for the nucleation field to include the effect of magnetocrystalline anisotropy:

$$\frac{H_n}{M_s} = N_a - \frac{kL_{ex}^2}{L^2} - \frac{2\kappa}{\mu_0 M_s^2}$$

In this equation, the effects of shape, size and magnetocrystalline anisotropy are added. It might be possible to gain a systematic knowledge of the dependence of hysteresis properties on these parameters by exploring each of them separately.

In ellipsoids, nucleation is defined as the first departure from uniform magnetization. This definition is not useful for other particle shapes, since the nucleation field would then be infinite. However, I show that there is a more appropriate generalization of nucleation.

I show that in a cuboid, the nucleation field can be precisely identified as the point where a curl appears in the magnetization. Indeed, as a function of field or particle size the volume-average curl has an infinite initial slope. In general, the direction of the curl is parallel to the field ($\nabla \times \mathbf{M} \parallel \mathbf{H}$) even when the field is not aligned with a symmetry axis of the particle. Another consequence of nucleation is a bifurcation: the state with the opposite curl has the same energy. Thus nucleation doubles the number of possible states.

I plotted the nucleation field for a magnetically isotropic cube against $1/L^2$, where L is the cube root of the volume, and it fit a straight line. The line has the same slope as that for nucleation in a sphere, but a smaller intercept. The nucleation field appears to be related to the volume-average demagnetizing field; it does not depend significantly on grid size, although the transverse demagnetizing field in the corners increases rapidly with grid size. This behavior is consistent with the non-local pattern of the curling mode.

7.3.3 Critical Sizes

In the rock magnetic literature, most of the critical size calculations are for what I call the global critical size L_0, below which the SD state is the lowest energy remanent state. This critical size does not have a direct relationship with hysteresis properties. More useful are the Stoner-Wohlfarth critical size L_{sw} and the nucleation critical size L_n. Below L_{sw}, the hysteresis properties are fully SD, while L_n is the upper limit for stability of the SD remanent state.

While rigorous calculations have been made for L_{sw} and L_n, they were never clearly distinguished or compared with each other, and little was said (or known) about their relationship to hysteresis properties. I extended the expressions for the critical sizes to include magnetocrystalline anisotropy:

$$L_{sw} = \left(\frac{k}{N_b}\right)^{1/2} L_{ex}$$

$$L_n = \left(\frac{k}{N_a}\right)^{1/2} \left(1 - \frac{2\kappa}{\mu_0 M_s^2 N_a}\right)^{-1/2} L_{ex}$$

The parameter κ depends on the type of symmetry (uniaxial or cubic), the magnitude and sign of the magnetocrystalline anisotropy constant K_1, and the orientations of the easy axes.

The critical size L_{sw} is weakly dependent on elongation and not at all dependent on magnetocrystalline anisotropy, while L_n is strongly dependent on both. This is important for titanomagnetites, as I describe below.

7.3.4 The Nucleation Field and Hysteresis

Before numerical solutions were feasible, almost nothing was known about what happened after nucleation occurred. Usually, it was assumed either that there was a jump or that the hysteresis curve continued with a slope of $1/N$, where N is the SD demagnetizing factor. The coercivity in the latter case was $H_c = H_n - NM_s$. This

was a very different mechanism for the coercivity than the domain wall pinning of MD theory.

With some hysteresis simulations, I showed that there is a sudden change in slope of the hysteresis curve at nucleation, but the change can be very small at first. With a further change in field, the curve approaches a jump, with the slope dM/dH approaching infinity just before the jump. As particle size increases, the change in slope and the length of the curve after nucleation increases.

For magnetically isotropic particles, the Wohlfarth relations appear hold at least to the nucleation critical size. The assumptions behind the relations break down only when the magnetization starts to jump to a first order reversal branch corresponding to the remanent state with moment along the short axis.

7.4 Possible Implications for Paleomagnetism

7.4.1 Thermoremanent Magnetization

The two main theories for thermoremanent magnetization (TRM) are the SD and MD theories of Néel [1955]. In the SD theory, TRM is acquired by "blocking", a freezing of the equilibrium distribution of moments as particles make the transition from superparamagnetic to single-domain. In the MD theory, TRM is acquired by a hysteresis mechanism. As I pointed out in Chapter 1, we must keep the distinction between these mechanisms clear. In particular, it is misleading to use the term "blocking temperature" for the MD model, because this implies that the acquisition of remanence can be reversed. The essence of hysteresis is irreversibility. Numerous papers have been published on the "anomalous" unblocking temperatures in large particles, but in reality no special mechanism is required.

For extracting a paleointensity from a rock, the modified Thellier-Thellier method is considered the most reliable. For this method to work, the TRM must be acquired by blocking in the correct sense. The temperature at which blocking occurs is deter-

mined by the energy barrier against a transition from one remanent state to another. In the theory of Néel [1955], the transition occurs by uniform rotation. This is expected to occur in the smallest SD particles, but in larger particles the mechanism may be non-uniform rotation [Levi and Merrill, 1978]. Some estimates have been made of the size range for these mechanisms [Dunlop *et al.*, 1994; Enkin and Williams, 1994], but the critical size expressions I have derived can be used to calculate more rigorous bounds as a function of elongation and magnetocrystalline anisotropy.

I showed in Chapter 4 that existing MD models are not self-consistent. A particularly important example is Néel's MD model, which cannot predict a field dependence of TRM without making an assumption that contradicts both observation and the underlying assumption about the demagnetizing factor. A self-consistent MD model for TRM should be developed. In such a model, the intensity of the TRM would depend on both the amplitude and spatial distribution of the wall pinning forces.

BIBLIOGRAPHY

Acton, F. S. (1990). *Numerical Methods That Work*. The Mathematical Association of America, Washington D. C. Updated and revised from the 1970 edition published by Harper & Row. 549 pages.

Aharoni, A. (1959). Some recent developments in micromagnetics at the Weizmann Institute of Science. *J. Appl. Phys.*, **30**, 70S–78S.

Aharoni, A. (1966). Magnetization curling. *Phys. Stat. Sol.*, **16**, 1–42.

Aharoni, A. (1986). Magnetization buckling in a prolate spheroid. *J. Appl. Phys.*, **60**, 1118–1123.

Aharoni, A. (1988). Elongated single-domain ferromagnetic particles. *J. Appl. Phys.*, **63**, 5879–5882.

Aharoni, A. (1989). Single-domain ferromagnetic cylinder. *IEEE Trans. Magnetics*, **25**, 3470–3472.

Aharoni, A. and Jakubovics, J. P. (1986). Cylindrical magnetic domains in small ferromagnetic spheres with uniaxial anisotropy. *Phil. Mag. B*, **53**, 133–145.

Aharoni, A. and Jakubovics, J. P. (1990). Approach to saturation in small isotropic cubes. *J. Magn. Magn. Mat.*, **83**, 451–452.

Aharoni, A. and Shtrikman, S. (1958). Magnetization curve of the infinite cylinder. *Phys. Rev.*, **109**, 1522–1528.

Amar, H. (1958). Magnetization mechanism and domain structure of multidomain particles. *Phys. Rev.*, **111**, 149–153.

Arnold, V. I. (1973). *Ordinary Differential Equations*. MIT Press. Translated and edited by R. A. Silverman. 280 pages.

Asimow, R. M. (1965). The measurement of superparamagnetic particle shapes and size distribution. *Transactions of the Metallurgical Society of AIME*, **233**, 401–409.

Bailey, M. E. and Dunlop, D. J. (1983). Alternating field characteristics of pseudo-single-domain ($2 - 14\mu$m) and multidomain magnetite. *Earth Planet. Sci. Lett.*, **63**, 335–352.

Banerjee, S. K., King, J., and Marvin, J. (1981). A rapid method for magnetic granulometry with applications to environmental studies. *Geophys. Res. Lett.*, **8**, 333–336.

Bergh, H. W. (1970). Paleomagnetism of the Stillwater Complex, Montana. In S. K. Runcorn, editor, *Paleogeophysics*, pages 143–158. Academic.

Berkov, D. V., Ramstöck, K., and Hubert, A. (1993). Solving micromagnetic problems: towards an optimal numerical method. *Phys. Stat. Sol.*, **137**, 207–225.

Bloemendal, J., Barton, C. E., and Radakrishnamurthy, C. (1985). Correlation between Rayleigh loops and frequency-dependent and quadrature susceptibility: application to magnetic granulometry of rocks. *J. Geophys. Res.*, **90**, 8789–8792.

Bol'shakov, A. S. and Shcherbakova, V. V. (1979). Thermomagnetic criterion for determining the domain structure of ferrimagnetics. *Izv. Acad. Sci. U.S.S.R., Phys. solid earth*, pages 111–117.

Boyd, J. R., Fuller, M., and Halgedahl, S. (1984). Domain wall nucleation as a controlling factor in the behaviour of fine magnetic particles in rocks. *J. Geophys. Res.*, **11**, 193–196.

Bozorth, R. M. (1951). *Ferromagnetism*. Van Nostrand, Princeton.

Brown, A. P. and O'Reilly, W. (1996). The magnetic hysteresis properties of ball-milled monodomain titanomagnetite, $Fe_{2.3}Ti_{0.7}O_4$. *Geophys. Res. Lett.*, **23**, 2863–2866.

Brown, Jr., W. F. (1940). Theory of the approach to magnetic saturation. *Phys. Rev.*, **58**, 736–743.

Brown, Jr., W. F. (1945). Virtues and weaknesses of the domain concept. *Rev. Mod. Phys.*, **17**, 15–19.

Brown, Jr., W. F. (1959). Micromagnetics: successor to domain theory? *J. Phys. Radium*, **20**, 101–103.

Brown, Jr., W. F. (1962). *Magnetostatic Principles in Ferromagnetism*. North–Holland, Amsterdam.

Brown, Jr., W. F. (1963). *Micromagnetics*. Interscience, New York. Reprinted by Krieger, New York, 1978.

Brown, Jr., W. F. (1968). The fundamental theorem of fine-ferromagnetic-particle theory. *J. Appl. Phys.*, **39**, 993–994.

Butler, R. F. (1992). *Paleomagnetism: Magnetic Domains to Geologic Terranes*. Blackwell Scientific Publications, Boston.

Butler, R. F. and Banerjee, S. K. (1975). Theoretical single–domain grain size range in magnetite and titanomagnetite. *J. Geophys. Res.*, **80**, 4049–4058.

Channell, J. E. T. and McCabe, C. (1994). Comparison of magnetic hysteresis parameters of unremagnetized and remagnetized limestones. *J. Geophys. Res.*, **99**, 4613–4623.

Chantrell, R. W., O'Grady, K., Bradbury, A., Charles, S. W., and Popplewell, J. (1985). The isothermal remanent magnetization of fine magnetic particles. *J. Phys. D*, **18**, 2505–2517.

Chikazumi, S. (1964). *Physics of Magnetism*. John Wiley and Sons.

Cisowski, S. (1981). Interacting vs. non-interacting single domain behavior in natural and synthetic samples. *Phys. Earth Planet. Inter.*, **26**, 56–62.

Coe, R. S. (1967a). The determination of paleo-intensities of the Earth's magnetic field with emphasis on mechanisms which could cause non-ideal behavior in Thellier's method. *J. Geomagn. Geoelectr.*, **19**, 157–179.

Coe, R. S. (1967b). Paleo-intensities of the Earth's magnetic field determined from Tertiary and Quaternary rocks. *J. Geophys. Res.*, **72**, 3247–3262.

Craik, D. J. and Tebble, R. S. (1965). *Ferromagnetism and Ferromagnetic Domains*, volume 4 of *Series of Monographs on Selected Topics in Solid State Physics*. Elsevier, New York.

Cullity, B. D. (1972). *Introduction to Magnetic Materials*. Addison-Wesley.

Day, R. (1977). TRM and its variation with grain size. In D. J. Dunlop, editor, *Origin of Thermoremanent Magnetization*, volume 1 of *Adv. Earth Planet. Sci.*, pages 1–33. Center for Academic Publications Japan.

Day, R., Fuller, M., and Schmidt, V. A. (1977). Hysteresis properties of titanomagnetites: grain-size and compositional dependence. *Phys. Earth Planet. Inter.*, **13**, 260–267.

Dunlop, D. J. (1973). Superparamagnetic and single-domain threshold sizes in magnetite. *J. Geophys. Res.*, **78**, 1780–1793.

Dunlop, D. J. (1977). The hunting of the 'Psark'. *J. Geomagn. Geoelectr.*, **29**, 293–318.

Dunlop, D. J. (1983a). On the demagnetizing energy and demagnetizing factor of a multidomain ferromagnetic cube. *Geophys. Res. Lett.*, **10**, 79–82.

Dunlop, D. J. (1983b). Viscous magnetization of $0.04 - 100\mu$m magnetites. *Geophys. J. R. astr. Soc.*, **74**, 667–687.

Dunlop, D. J. (1984). A method of determining demagnetizing factor from multidomain hysteresis. *J. Geophys. Res.*, **89**, 553–558.

Dunlop, D. J. and Argyle, K. S. (1991). Separating multidomain and single-domain-like remanences in pseudo-single-domain magnetites ($215 - 540$nm) by low-temperature demagnetization. *J. Geophys. Res.*, **96**, 2007–2017.

Dunlop, D. J. and Waddington, E. D. (1975). The field dependence of thermoremanent magnetization in igneous rocks. *Earth Planet. Sci. Lett.*, **25**, 11–25.

Dunlop, D. J. and West, G. F. (1969). An experimental evaluation of single domain theories. *Rev. Geophys.*, **7**, 709–757.

Dunlop, D. J. and Xu, S. (1994). Theory of partial thermoremanent magnetization in multidomain grains, 1, Repeated identical barriers to wall motion (single coercivity). *J. Geophys. Res.*, **99**, 9005–9023.

Dunlop, D. J., Enkin, R. J., and Tjan, E. (1990). Internal field mapping in single-domain and multidomain grains. *J. Geophys. Res.*, **95**, 4561–4577.

Dunlop, D. J., Newell, A. J., and Enkin, R. J. (1994). Transdomain thermoremanent magnetization. *J. Geophys. Res.*, **99**, 19,741–19,755.

Enkin, R. J. and Dunlop, D. J. (1987). A micromagnetic study of pseudo single-domain remanence in magnetite. *J. Geophys. Res.*, **92**, 12,726–12,740.

Enkin, R. J. and Dunlop, D. J. (1988). The demagnetization temperature necessary to remove viscous remanent magnetization. *Geophys. Res. Lett.*, **15**, 514–517.

Enkin, R. J. and Williams, W. (1994). Three-dimensional micromagnetic analysis of stability in fine magnetic grains. *J. Geophys. Res.*, **99**, 611–618.

Evans, M. E. and McElhinny, M. W. (1969). An investigation of the origin of stable remanence in magnetite-bearing rocks. *J. Geomagn. Geoelectr.*, **4**, 142–146.

Fabian, K., Kirchner, A., Williams, W., Heider, F., Hubert, A., and Leibl, T. (1996). Three-dimensional micromagnetic calculations for magnetite using FFT. *Geophys. J. Inter.*, **124**, 89–104.

Fletcher, E. J. and O'Reilly, W. (1974). Contribution of Fe^{2+} ions to the magnetocrystalline anisotropy constant K_1 of $Fe_{3-x}Ti_xO_4, 0 \leq x \leq 0.55$. *J. Phys. C*, **7**, 171–178.

Fredkin, D. R. and Koehler, T. R. (1987). Numerical micromagnetics by the finite element method. *IEEE Trans. Magnetics*, **23**, 3385–3387.

Fredkin, D. R. and Koehler, T. R. (1988). Numerical micromagnetics of small particles. *IEEE Trans. Magnetics*, **24**, 2362–2367.

Fredkin, D. R. and Koehler, T. R. (1989). Numerical micromagnetics: prolate spheroids. *IEEE Trans. Magnetics*, **25**, 3473–3475.

Fredkin, D. R. and Koehler, T. R. (1990). Hybrid method for computing demagnetizing fields. *IEEE Trans. Magnetics*, **26**, 415–417.

Frost, B. R. and Lindsey, D. H. (1991). Occurrence of iron-titanium oxides in igneous rocks. In D. H. Lindsley, editor, *Oxide Minerals: Petrologic and Magnetic Significance*, volume 25 of *Reviews in Mineralogy*, chapter 12. Mineralogical Society of America, Washington, D. C.

Fukuma, K. and Dunlop, D. J. (1997). Monte carlo simulation of two-dimensional domain structures in magnetite. *J. Geophys. Res.*, **102**, 5135–5143.

Gaunt, P. (1968). The temperature dependence of single domain particle properties. *Phil. Mag.*, **17**, 263–266.

Gee, J. and Kent, D. V. (1995). Magnetic hysteresis in young mid-ocean ridge basalts: dominant cubic anisotropy? *Geophys. Res. Lett.*, **22**, 551–554.

Geiß, C. E., Heider, F., and Soffel, H. C. (1996). Magnetic domain observations on magnetite and titanomaghemite grains ($0.5 - 1.0\mu$m). *Geophys. J. Inter.*, **124**, 75–88.

Geshev, J. and Mikhov, M. (1992). Remanence curves for a disordered system of three- and four-axial fine particles. Henkel-type plots. *J. Magn. Magn. Mat.*, **104–107**, 1569–1570.

Geshev, J., Popov, O., Masheva, V., and Mikhov, M. (1990). Thermomagnetic curves for a disordered system of single-domain particles with cubic anisotropy. *J. Magn. Magn. Mat.*, **92**, 185–190.

Grommé, C. S. and Merrill, R. T. (1965). Paleomagnetism of late Cretaceous granitic plutons in the Sierra Nevada, California: further results. *J. Geophys. Res.*, **70**, 3407–3420.

Halgedahl, S. and Fuller, M. (1980). Magnetic domain observations of nucleation processes in fine particles of intermediate titanomagnetite. *Nature*, **288**, 70–72.

Halgedahl, S. and Fuller, M. (1983). The dependence of magnetic domain structure upon magnetization state with emphasis upon nucleation as a mechanism for pseudo-single-domain behavior. *J. Geophys. Res.*, **88**, 6505–6522.

Halgedahl, S. L. (1991). Magnetic domain patterns observed on synthetic Ti-rich titanomagnetite as a function of temperature and in states of thermoremanent magnetization. *J. Geophys. Res.*, **96**, 3943–3972.

Halgedahl, S. L. (1993). Experiments to investigate the origin of anomalously elevated unblocking temperatures. *J. Geophys. Res.*, **98**, 22,443–22,460.

Halgedahl, S. L. (1995). Bitter patterns versus hysteresis behavior in small single particles of hematite. *J. Geophys. Res.*, **100**, 353–364.

Hargraves, R. B. and Young, W. M. (1969). Source of stable remanent magnetism in Lambertville diabase. *Am. J. Sci.*, **267**, 1161–1177.

Hartmann, U. (1987). Origin of Brown's coercive paradox in perfect ferromagnetic crystals. *Phys. Rev.*, pages 2331–2332.

Hartstra, R. L. (1983). TRM, ARM and Irs of two natural magnetites of MD and PSD grain size. *Geophys. J. R. astr. Soc.*, **73**, 719–737.

Heider, F. and Hoffmann, V. (1992). Magneto-optical Kerr effect on magnetite crystals with externally applied magnetic fields. *Earth Planet. Sci. Lett.*, **108**, 131–138.

Heider, F. and Williams, W. (1988). Note on temperature dependence of exchange constant in magnetite. *Geophys. Res. Lett.*, **15**, 184–187.

Heider, F., Dunlop, D. J., and Sugiura, N. (1987). Magnetic properties of hydrothermally recrystallized magnetite crystals. *Science*, **236**, 1287–1290.

Heider, F., Dunlop, D. J., and Soffel, H. C. (1992). Low-temperature and alternating field demagnetization of saturation remanence and thermoremanence in magnetite grains (0.037μm to 5mm). *J. Geophys. Res.*, **97**, 9371–9381.

Heider, F., Zitzelsberger, A., and Fabian, K. (1996). Magnetic susceptibility and remanent coercive force in grown magnetite crystals from 0.1μm to 6mm. *Phys. Earth Planet. Inter.*, **93**, 239–256.

Henkel, O. (1964). Remanenzverhalten und wechselwirkungen in hartmagnetischen teilchenkollektiven. *phys. stat. sol.*, **7**, 919–929.

Hunt, C. P., Moskowitz, B. M., and Banerjee, S. K. (1995). Magnetic properties of rocks and minerals. In T. J. Ahrens, editor, *Rock physics and phase relations: a handbook of physical constants*, volume 3 of *AGU Reference Shelf*, chapter 3-14. American Geophysical Union, Washington, DC.

Jackson, J. D. (1975). *Classical Electrodynamics*. John Wiley and Sons.

Jeffreys, H. (1962). *The earth: its origin, history and physical constitution*. Cambridge, 4 edition.

Joffe, I. (1969). The temperature dependence of the coercivity of a random array of uniaxial single domain particles. *J. Phys. C*, **2**, 1537–1541.

Joffe, I. and Heuberger, R. (1974). Hysteresis properties of distributions of cubic single-domain ferromagnetic particles. *Phil. Mag.*, **314**, 1051–1059.

Johnson, Jr., C. E. and Brown, Jr., W. F. (1961). Theoretical magnetization curves for particles with cubic anisotropy. *J. Appl. Phys.*, **32**, 243S–244S.

King, J. W., Banerjee, S. K., Marvin, J., and Özdemir, O. (1982). A comparison of different magnetic methods for determining the relative grain size of magnetite in natural materials: some results from lake sediments. *Earth Planet. Sci. Lett.*, **59**, 404–419.

Kirschvink, J. L. and Walker, M. M. (1985). Particle-size considerations for magnetite-based magnetoreceptors. In J. Kirschvink, D. Jones, and B. MacFadden,

editors, *Magnetite Biomineralization and Magnetoreception in Organisms: A New Biomagnetism*. Plenum, New York.

Kittel, C. (1946). Theory of the structure of ferromagnetic domains in films and small particles. *Phys. Rev.*, **70**, 965–971.

Kittel, C. (1949). Physical theory of ferromagnetic domains. *Rev. Mod. Phys.*, **21**, 541–583.

Landau, L. and Lifshitz, E. (1935). On the theory of the dispersion of magnetic permeability in ferromagnetic bodies. In D. ter Haar, editor, *Collected papers of L. D. Landau*, pages 101–114. Pergamon, New York. Originally published in Physik. Z. Sowjetunion, 8, 153, 1935.

Larson, E., Ozima, M., Ozima, M., Nagata, T., and Strangway, D. (1969). Stability of remanent magnetization of igneous rocks. *Geophys. J. R. astr. Soc.*, **17**, 263–292.

Lederman, M., Fredkin, D. R., O'Barr, R., Schultz, S., and Ozaki, M. (1994). Measurement of thermal switching of the magnetization of single domain particles. *J. Appl. Phys.*, **75**, 6217–6222.

Levi, S. (1977). The effect of magnetite particle size on paleointensity determinations of the geomagnetic field. *Phys. Earth Planet. Inter.*, **13**, 245–259.

Levi, S. (1979). The additivity of partial thermal remanent magnetization in magnetite. *Geophys. J. R. astr. Soc.*, **59**, 205–218.

Levi, S. and Merrill, R. T. (1978). Properties of single-domain, pseudo-single-domain, and multidomain magnetite. *J. Geophys. Res.*, **83**, 309–323.

Lifshitz, E. (1944). On the magnetic structure of iron. *J. Phys.*, **8**, 337–346.

Lilley, B. A. (1950). Energies and widths of domain boundaries in ferromagnetics. *Phil. Mag.*, **41**, 792–813.

Lowrie, W. and Fuller, M. (1971). On the alternating field demagnetization characteristics of multidomain thermoremanent magnetization in magnetite. *J. Geophys. Res.*, **76**, 6339–6349.

Maher, B. A. and Taylor, R. M. (1988). Formation of ultrafine-grained magnetite in soils. *Nature*, **336**, 368–370.

Mansuripur, M. and Giles, R. (1988). Demagnetizing field computation for dynamic simulation of the magnetization reversal process. *IEEE Trans. Magnetics*, **24**, 2326–2328.

Mattis, D. C. (1988). *The Theory of Magnetism I: Statics and Dynamics*. Springer-Verlag, New York.

McCabe, C. and Elmore, R. D. (1989). The occurrence and origin of late Paleozoic remagnetization in the sedimentary rocks of North America. *Rev. Geophys.*, **27**, 471–494.

McClelland, E. and Shcherbakov, V. P. (1995). Metastability of domain state in multidomain magnetite: consequences for remanence acquisition. *J. Geophys. Res.*, **100**, 3841–3857.

McClelland, E. and Sugiura, N. (1987). A kinematic model of TRM acquisition in multidomain magnetite. *Phys. Earth Planet. Inter.*, **46**, 9–23.

McClelland, E., Muxworthy, A. R., and Thomas, R. M. (1996). Magnetic properties of the stable fraction of remanence in large multidomain (MD) magnetite grains: single-domain or MD? *Geophys. Res. Lett.*, **23**, 2831–2834.

McElhinny, M. W., McFadden, P. L., and Merrill, R. T. (1996). The time-averaged paleomagnetic field 0-5 Ma. *J. Geophys. Res.*, **101**, 25,007–25,027.

Merrill, R. T. (1977). The demagnetization field of multidomain grains. *J. Geomagn. Geoelectr.*, **29**, 285–292.

Merrill, R. T., McElhinny, M. W., and McFadden, P. L. (1996). *The Magnetic Field of the Earth: Paleomagnetism, the Core, and the Deep Mantle*. Academic, San Diego.

Metcalf, M. and Fuller, M. (1987). Domain observations of titanomagnetites from room temperature to curie point and the nature of thermo-remanent magnetism in fine particles. *Nature*, **321**, 847–849.

Metcalf, M. and Fuller, M. (1988). Domain observations of titanomagnetites during hysteresis at elevated temperatures and thermal cycling. *Phys. Earth Planet. Inter.*, **46**, 120–126.

Moon, T. and Merrill, R. T. (1984). The magnetic moments of non-uniformly magnetized grains. *Phys. Earth Planet. Inter.*, **34**, 186–194.

Moon, T. S. and Merrill, R. T. (1985). Nucleation theory and domain states in multidomain magnetic material. *Phys. Earth Planet. Inter.*, **37**, 214–222.

Morgan, G. E. and Smith, P. P. K. (1981). Transmission electron microscope and rock magnetic investigations of remanence carriers in a Precambrian metadolerite. *Earth Planet. Sci. Lett.*, **53**, 226–240.

Morrish, A. H. (1966). *The Physical Principles of Magnetism*. John Wiley & Sons.

Moskowitz, B. M. (1987). Towards resolving the inconsistencies in characteristic physical properties of synthetic titanomaghemites. *Phys. Earth Planet. Inter.*, **46**, 173–183.

Moskowitz, B. M. and Halgedahl, S. L. (1987). Theoretical temperature and grain-size dependence of domain state in x = 0.6 titanomagnetite. *J. Geophys. Res.*, **92**, 10,667–10,682.

Néel, L. (1948). La loi d'approche en a : H et une nouvelle théorie de la dureté magnétique. *J. Phys. Rad.*, **9**, 184–192. Translated in Nicholas Kurti, editor, *Selected Works of Louis Néel*, Gordon and Breach, New York, pagés 161–169.

Néel, L. (1949). Théorie du trainage magnétique des ferromagnétiques en grains fins avec application aux terres cuites. *Ann. Géophys.*, **5**, 99–136. Translated in Nicholas Kurti, editor, *Selected Works of Louis Néel*, Gordon and Breach, New York, pages 407–427.

Néel, L. (1955). Some theoretical aspects of rock magnetism. *Adv. Phys.*, **4**, 191–243.

Newell, A. J., Dunlop, D. J., and Enkin, R. J. (1990). Temperature dependence of critical sizes, wall widths and moments in two-domain magnetite grains. *Phys. Earth Planet. Inter.*, **65**, 165–176.

Newell, A. J., Williams, W., and Dunlop, D. J. (1993a). A generalization of the demagnetizing tensor for nonuniform magnetization. *J. Geophys. Res.*, **98**, 9551–9556.

Newell, A. J., Dunlop, D. J., and Williams, W. (1993b). A two-dimensional micromagnetic model of magnetizations and fields in magnetite. *J. Geophys. Res.*, **98**, 9533–9550.

Nicolis, G. and Prigogine, I. (1989). *Exploring Complexity*. W.H. Freeman and Company, New York. 313 pages.

Opdyke, N. D. and Channell, J. E. T. (1996). *Magnetic Stratigraphy*. Academic Press, San Diego.

O'Reilly, W. (1984). *Rock and mineral magnetism.* Blackie and Son, Glasgow.

Özdemir, O. and Dunlop, D. J. (1993). Magnetic domain structures on a natural single crystal of magnetite. *Geophys. Res. Lett.*, **20**, 1835–1838.

Özdemir, O., Xu, S., and Dunlop, D. J. (1995). Closure domains in magnetite. *J. Geophys. Res.*, **100**, 2193–2209.

Parry, L. G. (1965). Magnetic properties of dispersed magnetite powders. *Phil. Mag.*, **11**, 303–312.

Pick, T. and Tauxe, L. (1994). Characteristics of magnetite in submarine basaltic glass. *Geophys. J. Inter.*, **119**, 116–128.

Pokhil, T. G. and Moskowitz, B. M. (1997). Magnetic domains and domain walls in pseudo-single-domain magnetite studied with magnetic force microscopy. Preprint.

Powell, M. J. D. (1977). Restart procedures for the conjugate gradient method. *Mathematical programming*, **12**, 241–254.

Press, W., Teukolsky, S., Vetterling, W., and Flannery, B. (1992). *Numerical Recipes in FORTRAN: the art of scientific computing.* Cambridge.

Ramstöck, K., Leibl, T., and Hubert, A. (1994). Optimizing stray field computations in finite-element micromagnetics. *J. Magn. Magn. Mat.*, **135**, 97–110.

Sahu, S. and Moskowitz, B. M. (1995). Thermal dependence of magnetocrystalline anisotropy and magnetostriction constants of single crystal $Fe_{2.4}Ti_{0.61}O_4$. *Geophys. Res. Lett.*, pages 449–452.

Schabes, M. E. (1991). Micromagnetic theory of non-uniform magnetization processes in magnetic recording particles. *J. Magn. Magn. Mat.*, **95**, 249–288.

Schabes, M. E. and Bertram, H. N. (1988). Magnetization processes in ferromagnetic cubes. *J. Appl. Phys.*, **64**, 1347–1357.

Schmidt, V. A. (1976). The variation of the blocking temperature in models of thermoremanence (TRM). *Earth Planet. Sci. Lett.*, **29**, 146–154.

Shaw, J. (1974). A new method of determining the magnitude of the palaeomagnetic field: application to five historic lavas and five archaeological samples. *Geophys. J. R. astr. Soc.*, **39**, 133–141.

Shtrikman, S. and Treves, D. (1960). On the resolution of Brown's paradox. *J. Appl. Phys.*, **31**, 72S–73S.

Shtrikman, S. and Treves, D. (1963). Micromagnetics. In G. T. Rado and H. Suhl, editors, *Spin Arrangements and Crystal Structure, Domains, and Micromagnetics*, volume 3 of *Magnetism*, chapter 8. Academic.

Smith, G. and Merrill, R. T. (1982). The determination of the internal magnetic field in magnetic grains. *J. Geophys. Res.*, **87**, 9419–9423.

Smith, P. J. (1967). The intensity of the Tertiary geomagnetic field. *Geophys. J. R. astr. Soc.*, **12**, 239–258.

Smith, P. P. K. (1980). The application of Lorentz electron microscopy to the study of rock magnetism. In T. Mulvey, editor, *Electron microscopy and analysis, 1979*, 52, pages 125–128. Institute of Physics, Bristol.

Soffel, H., Aumüller, C., Hoffmann, V., and Appel, E. (1990). Three-dimensional domain observations of magnetite and titanomagnetites using the dried colloid SEM method. *Phys. Earth Planet. Inter.*, **65**, 43–53.

Stacey, F. D. (1963). The physical theory of rock magnetism. *Advan. Phys.*, **12**, 45–133.

Stacey, F. D. and Banerjee, S. K. (1974). *The Physical Basis of Rock Magnetism*. Elsevier, New York.

Stewart, K. H. (1954). *Ferromagnetic Domains*. Cambridge.

Stoner, E. C. and Wohlfarth, E. P. (1947). A mechanism of magnetic hysteresis in heterogeneous alloys. *Phil. Trans. Roy. Soc. London*, **A240**, 599–642.

Strangway, D. W., Larson, E. E., and Goldstein, M. (1968). A possible cause of high magnetic stability in volcanic rocks. *J. Geophys. Res.*, **73**, 3787–3795.

Syono, Y. (1965). Magnetocrystalline anisotropy and magnetostriction of Fe_3O_4 – Fe_2TiO_4 series - with special application to rock magnetism -. *Jpn. J. Geophys.*, **4**, 71–143.

Tauxe, L. (1993). Sedimentary records of relative paleointensity of the geomagnetic field: theory and practice. *Rev. Geophys.*, **31**, 319–354.

Tauxe, L., Mullender, T. A. T., and Pick, T. (1996). Potbellies, wasp-waists, and superparamagnetism in magnetic hysteresis. *J. Geophys. Res.*, **101**, 571–583.

Thellier, E. and Thellier, O. (1959). Sur l'intensité du champ magnétique terrestre dans le passé historique et géologique. *Ann. Géophys.*, **15**, 285–376.

Thompson, R. and Oldfield, F. (1986). *Environmental Magnetism*. Allen and Unwin, Winchester.

Trauble, H. (1969). The influence of crystal defects on magnetization processes in ferromagnetic single crystal. In A. E. Berkowitz and E. Kneller, editors, *Magnetism and Metallurgy*. Academic, San Diego.

Tritton, D. H. (1988). *Physical Fluid Dynamics*. Oxford. 519 pages.

Tucker, P. and O'Reilly, W. (1980). The acquisition of thermoremanent magnetization by multidomain single-crystal titanomagnetite. *Geophys. J. R. astr. Soc.*, **60**, 21–36.

Van der Voo, R. (1993). *Paleomagnetism of the Atlantic, Tethys and Iapetus Oceans*. Cambridge.

Verhoogen, J. (1959). The origin of thermoremanent magnetization. *J. Geophys. Res.*, **64**, 2441–2449.

Walker, M., Chantrell, R. W., O'Grady, K., and Charles, S. W. (1988). The isothermal remanence of fine particle systems. In D. Givord, editor, *Proceedings of the International Conference on Magnetism: ICM 88, Paris, France, July 25-29, 1988*, Journal de physique. Colloque ; 1988, C8, pages 1819–1820.

Walker, M., Mayo, P. I., O'Grady, K., Charles, S. W., and Chantrell, R. W. (1993a). The magnetic properties of single-domain particles with cubic anisotropy: I. Hysteresis loops. *Journal of Physics: Condensed Matter*, **5**, 2779–2792.

Walker, M., Mayo, P. I., O'Grady, K., Charles, S. W., and Chantrell, R. W. (1993b). The magnetic properties of single-domain particles with cubic anisotropy: II. Remanence curves. *Journal of Physics: Condensed Matter*, **5**, 2793–2808.

Williams, W. and Dunlop, D. J. (1989). Three-dimensional micromagnetic modelling of ferromagnetic domain structure. *Nature*, **337**, 634–637.

Williams, W. and Dunlop, D. J. (1990). Some effects of grain shape and varying external magnetic fields on the magnetic structure of small grains of magnetite. *Phys. Earth Planet. Inter.*, **65**, 1–14.

Williams, W. and Dunlop, D. J. (1995). Simulation of magnetic hysteresis in pseudo-single-domain grains of magnetite. *J. Geophys. Res.*, **100**, 3859–3871.

Williams, W., Enkin, R. J., and Milne, G. (1992). Magnetic domain wall visibility in Bitter pattern imaging. *J. Geophys. Res.*, **97**, 17,433–17,438.

Wohlfarth, E. P. (1958). Relations between different modes of acquisition of the remanent magnetization of ferromagnetic particles. *J. Appl. Phys.*, **29**, 595–596.

Worm, H. U. and Markert, H. (1987a). Magnetic hysteresis properties of fine particle titanomagnetites precipitated in a silicate matrix. *Phys. Earth Planet. Inter.*, **46**, 84–92.

Worm, H. U. and Markert, H. (1987b). The preparation of dispersed titanomagnetite particles by the glass-ceramic method. *Phys. Earth Planet. Inter.*, **46**, 263–269.

Worm, H. U., Ryan, P. J., and Banerjee, S. K. (1991). Domain size, closure domains, and the importance of magnetostriction in magnetite. *Earth Planet. Sci. Lett.*, **102**, 71–78.

Wu, Y. T., Fuller, M., and Schmidt, V. A. (1974). Microanalysis of N.R.M. in a granodiorite intrusion. *Earth Planet. Sci. Lett.*, **23**, 274–285.

Xu, S. and Dunlop, D. J. (1994). Theory of partial thermoremanent magnetization in multidomain grains, 2, Effect of microcoercivity distribution and comparison with experiment. *J. Geophys. Res.*, **99**, 9025–9033.

Xu, S. and Dunlop, D. J. (1995). Toward a better understanding of the lowrie-fuller test. *J. Geophys. Res.*, **100**, 22,533–22,542.

Xu, S. and Merrill, R. T. (1987). The demagnetizing factors in multidomain grains. *J. Geophys. Res.*, **92**, 10,657–10,665.

Xu, S. and Merrill, R. T. (1989). Microstress and microcoercivity in multidomain grains. *J. Geophys. Res.*, **94**, 10,627–10,636.

Xu, S. and Merrill, R. T. (1990). Toward a better understanding of magnetic screening in multidomain grains. *J. Geomagn. Geoelectr.*, **42**, 637–652.

Xu, S., Dunlop, D. J., and Newell, A. J. (1994). Micromagnetic modeling of two-dimensional domain structures in magnetite. *J. Geophys. Res.*, **99**, 9035–9044.

Xu, W., Geissman, J. W., der Voo, R. V., and Peacor, D. R. (1997). Electron microscopy of iron oxides and implications for the origin of magnetizations and rock magnetic properties of Banded Series rock of the Stillwater Complex, Montana. *J. Geophys. Res.*, **102**, 12,139–12,157.

Ye, J. and Merrill, R. T. (1995). Residual stress and domain structure. *J. Geophys. Res.*, **100**, 9995–10,002.

Ye, J., Newell, A. J., and Merrill, R. T. (1994). A re-evaluation of magnetocrystalline anisotropy and magnetostriction constants. *Geophys. Res. Lett.*, pages 25–28.

Yuan, S. W. and Bertram, H. N. (1992). Fast adaptive algorithms for micromagnetics. *IEEE Trans. Magnetics*, **28**, 2031–2036.

Zitzelsberger, A. and Schmidbauer, E. (1996). Magnetic properties of synthetic milled and annealed titanomagnetite ($Fe_{2.3}Ti_{0.7}O_4$) particles $1 - 125\mu$m in diameter and analysis of their microcrystalline structure. *Geophys. Res. Lett.*, **23**, 2855–2858.

Appendix A

SD CALCULATIONS USING LAGRANGE MULTIPLIERS

In this appendix I describe a polynomial method for solving for the magnetization in SD particles. This method can be applied to any particle with triaxial anisotropy, whether the origin of the anisotropy is magnetocrystalline, magnetoelastic or magnetostatic. It calculates all the stationary points, including saddle points and maxima, and classifies them.

A.1 Calculating Stationary Points

For calculating a hysteresis curve, it is convenient to express the applied field as $\mathbf{H} = H\mathbf{h}$, where H is the magnitude of the field and $\mathbf{h}$ is the unit vector in the direction of the field. The normalized energy density is

$$\eta \equiv \frac{E}{\mu_0 M_s^2 V} = \frac{1}{2}\hat{\mathbf{m}} \cdot \mathsf{N} \cdot \hat{\mathbf{m}} - H\mathbf{h} \cdot \hat{\mathbf{m}} \tag{A.1}$$

where $\hat{\mathbf{m}}$ is the unit vector in the direction of the magnetization. We choose the coordinates so that N is diagonal and the diagonal components are $N_1 \geq N_2 \geq N_3$.

The magnetization of a stationary state is a minimum of the energy η on the surface $\Phi(\alpha, \beta, \gamma) \equiv \alpha^2 + \beta^2 + \gamma^2 = 1$. The derivatives $(\partial\Phi/\partial\alpha, \partial\Phi/\partial\beta, \partial\Phi/\partial\gamma)$ are never zero simultaneously, so we can use the method of Lagrange multipliers. The stationary points satisfy $\partial(\eta + \lambda\Phi/2)/\partial\hat{\mathbf{m}} = 0$ and $\hat{\mathbf{m}} \cdot \hat{\mathbf{m}} = 1$, or

$$N_1\alpha - Hh_1 + \lambda\alpha = 0 \tag{A.2}$$

$$N_2\beta - Hh_2 + \lambda\beta = 0 \tag{A.3}$$

$$N_3\gamma - Hh_3 + \lambda\gamma = 0 \tag{A.4}$$

$$\alpha^2 + \beta^2 + \gamma^2 = 1 \tag{A.5}$$

For $H = 0$, the solutions are $\hat{\mathbf{m}} = (\pm 1, 0, 0)$ (maxima), $\hat{\mathbf{m}} = (0, \pm 1, 0)$ (saddle points) and $\hat{\mathbf{m}} = (0, 0, \pm 1)$ (minima). For $H \neq 0$, substituting the first three equations in the third gives

$$H^2 \left[\frac{h_1^2}{(N_1 + \lambda)^2} + \frac{h_2^2}{(N_2 + \lambda)^2} + \frac{h_3^2}{(N_3 + \lambda)^2} \right] = 1 \tag{A.6}$$

Rearranging, we get a polynomial

$$\sum_{i=0}^{6} p_i \lambda^i = 0 \tag{A.7}$$

where (using $h_1^2 + h_2^2 + h_3^2 = 1$)

$$\begin{aligned}
p_0 &= N_1^2 N_2^2 N_3^2 - H^2 \left[h_1^2 N_2^2 N_3^2 + h_2^2 N_1^2 N_3^2 + h_3^2 N_1^2 N_2^2 \right] \\
p_1 &= 2 N_1 N_2 N_3 (N_1 N_2 + N_2 N_3 + N_3 N_1) \\
&\quad - H^2 \left[h_1^2 N_2 N_3 (N_2 + N_3) + h_2^2 N_1 N_3 (N_1 + N_3) + h_3^2 N_1 N_2 (N_1 + N_2) \right] \\
p_2 &= N_1^2 N_2^2 + N_2^2 N_3^2 + N_3^2 N_1^2 + 4 tr(\mathsf{N}) N_1 N_2 N_3 \\
&\quad - H^2 \left[h_1^2 (N_2^2 + N_3^2 + 4 N_2 N_3) + h_2^2 (N_1^2 + N_3^2 + 4 N_1 N_3) + h_3^2 (N_1^2 + N_2^2 + 4 N_1 N_2) \right] \\
p_3 &= tr(\mathsf{N}) (tr(\mathsf{N})^2 - N_1^2 - N_2^2 - N_3^2) + 2 N_1 N_2 N_3 \\
&\quad - 2 H^2 \left[tr(\mathsf{N}) - h_1^2 N_1 - h_2^2 N_2 - h_3^2 N_3 \right] \\
p_4 &= 2 tr(\mathsf{N})^2 - 2 (N_1^2 + N_2^2 + N_3^2) - H^2 \\
p_5 &= 2 tr(\mathsf{N}) \\
p_6 &= 1
\end{aligned}$$

where $tr(\mathsf{N}) \equiv N_1 + N_2 + N_3$ is the trace of the tensor N. If N is a pure demagnetizing tensor, $tr(\mathsf{N}) = 0$.

I solve for the roots of the polynomial using the MATLAB routine ROOTS, which creates a companion matrix for the polynomial and solves for the eigenvalues. The type of solution is determined by the closest axis: $(\pm 1, 0, 0)$ for a maximum, $0, \pm 1, 0)$

for a saddle point, $(0,0,\pm 1)$ for a minimum. The stationary points should satisfy the following theorem for a differentiable mapping on a sphere [Arnold, 1973, page 262]:

$$\#(minima) - \#(saddlepoints) + \#(maxima) = 2 \tag{A.8}$$

A.2 Using Perturbation Theory to Calculate Susceptibility

Second-Order Anisotropy (Uniaxial or Triaxial)

Let us assume that N is diagonal and $N_1 \geq N_2 > N_3$, so in zero field the remanent states are $\hat{\mathbf{m}} = \pm\hat{z}$. Consider the $+\hat{z}$ remanent state. Now suppose a small field $\mathbf{H} = \epsilon\mathbf{J}$ ($\epsilon \ll 1$) is applied. This will rotate the magnetization vector. The new perpendicular components are $\alpha = \epsilon u$ and $\beta = \epsilon v$, while $\gamma = \sqrt{1-\alpha^2-\beta^2} = 1 - O(\epsilon^2)$. The equations for the new stationary state are

$$\begin{aligned} (N_1+\lambda)\epsilon u &= \epsilon J_1 \\ (N_2+\lambda)\epsilon v &= \epsilon J_2 \\ N_3+\lambda &= \epsilon J_3 \end{aligned}$$

Thus

$$\lambda = -N_3 + O(\epsilon)$$

so

$$\begin{aligned} u &= \frac{J_1}{N_1 - N_3} + O(\epsilon) \\ v &= \frac{J_2}{N_2 - N_3} + O(\epsilon) \end{aligned}$$

and the initial susceptibility tensor is

$$(\chi_0)_{ij} = \left.\frac{d\alpha_i}{dH_j}\right|_{H_h \to 0} = \begin{pmatrix} (N_1-N_3)^{-1} & 0 & 0 \\ 0 & (N_2-N_3)^{-1} & 0 \\ 0 & 0 & 0 \end{pmatrix} \tag{A.9}$$

The average susceptibility for an isotropic distribution of orientations is

$$\langle \chi_0 \rangle = \frac{1}{3}\left[\frac{1}{N_1 - N_3} + \frac{1}{N_2 - N_3}\right] \tag{A.10}$$

If $N_1 = N_2$ (as in an ellipsoid of rotation) and $N \equiv N_1 - N_3$, $\langle \chi_0 \rangle = 2/3N$. For magnetocrystalline anisotropy, $\langle \chi_0 \rangle = \mu_0 M_s^2/3K_1$.

Cubic Anisotropy

The above linearized equations can also be obtained by expanding the energy to second order in u and v and keeping terms up to second order. This approach can also be used for cubic particles if we expand to second order about the minimum energy.

At first sight, it would seem more difficult to calculate the average susceptibility for particles with cubic anisotropy, because the remanent state can be in any of six or eight easy directions, depending on the sign of K_1. If, however, the sample is demagnetized, and if we consider each particle separately and choose the coordinates so the remanent state points in the $+\hat{\mathbf{z}}$ direction, then the applied field is equally likely to be in any direction relative to this axis. Thus we can average the susceptibility by integrating over all field directions in the same way as for uniaxial anisotropy.

If $K_1 > 0$ and the x, y, z directions are the $\langle 100 \rangle$ crystallographic directions, the z direction is still an easy axis. To second order,

$$K_1\left[\alpha^2\beta^2 + \beta^2\gamma^2 + \gamma^2\alpha^2\right] = \epsilon^2 K_1\left[u^2 + v^2\right] + O(\epsilon^4) \tag{A.11}$$

Thus, as for uniaxial anisotropy, $\langle \chi_0 \rangle = \mu_0 M_s^2/3K_1$.

If $K_1 < 0$, the easy axes are the $\langle 111 \rangle$ directions. If we choose the z axis in the $(1,1,1)$ direction, we must choose the x and y axes in perpendicular directions, for example $(1,-1,0)$ and $(1,1,-2)$. If a, b, c are the direction cosines in the x, y, z directions, then

$$\alpha = a/\sqrt{2} + b/\sqrt{6} + c/\sqrt{3}$$

$$\begin{aligned}\beta &= -a/\sqrt{2} + b/\sqrt{6} + c/\sqrt{3} \\ \gamma &= -2b/\sqrt{6} + c/\sqrt{3}\end{aligned}$$

Then

$$\alpha^2\beta^2 + \beta^2\gamma^2 + \gamma^2\alpha^2 = \frac{a^4}{4} + \frac{b^4}{4} + \frac{c^4}{4} + \frac{a^2b^2}{4} + \sqrt{2}a^2bc + \frac{\sqrt{2}b^3c}{3}$$

If we eliminate c using $c^2 = 1 - a^2 - b^2$ and substitute $a = \epsilon u, b = \epsilon v$, then (ignoring constant terms)

$$K_1\left[\alpha^2\beta^2 + \beta^2\gamma^2 + \gamma^2\alpha^2\right] = \epsilon^2\left(-\frac{2K_1}{3}\right)\left[u^2 + v^2\right] + O(\epsilon^3) \qquad \text{(A.12)}$$

Thus the effective uniaxial anisotropy is $-2K_1/3$, so $\langle\chi_0\rangle = \mu_0 M_s^2/2K_1$. This can also be derived using small-angle expansions of the energy [Chikazumi, 1964, page 138].

For uniaxial particles, the susceptibility of the saturation remanent state is the same as the susceptibility of the demagnetized state, because the demagnetizing tensor is symmetric and the field directions are still averaged over half the unit sphere. For cubic particles, the susceptibility for the saturation remanent state will be lower than the susceptibility for the demagnetized state because the field directions are more restricted.

VITA

NAME: Andrew James Newell

EDUCATION:

1987	BSc, University of Toronto
1990	MSc, University of Toronto

AWARDS:

1987	E.F. Burton Fellowship (University of Toronto)
1996	Johnston Fellowship (University of Washington)

PUBLICATIONS:

Newell, A. J., D. J. Dunlop, and W. Williams (1993). A two-dimensional micromagnetic model of magnetizations and fields in magnetite. *Journal of Geophysical Research* **98**, 9533-9549.

Newell, A. J., W. Williams, and D. J. Dunlop (1993). A generalization of the demagnetizing tensor for nonuniform magnetization. *Journal of Geophysical Research* **98**, 9551-9555.

Ye, J., A. J. Newell, and R. T. Merrill (1994). A re-evaluation of magnetocrystalline anisotropy and magnetostriction constants. *Geophysical Research Letters* **21**, 25-28.

Xu, S., D. J. Dunlop, and A. J. Newell (1994). Micromagnetic modelling of two-dimensional domain structures in magnetite. *Journal of Geophysical Research* **99**, 9035-9044.

Dunlop, D. J., A. J. Newell, and R. J. Enkin (1994). Transdomain thermoremanent magnetization. *Journal of Geophysical Research* **99**, 19,741-19,755.

SELECTED TITLES OF TALKS:

Newell, A. J. and R. T. Merrill (AGU, Fall 1995). A theoretical model of remanence loss across the Verwey transition.

Newell, A. J. (Hysteresis Modeling and Micromagnetics Workshop, 1996). The method of strain suppression and its application to magnetostriction.